学　位　論　文　（要約）

Study of Zn finger proteins and the homeodomain protein Otx2 in early *Xenopus* eye development

（ツメガエルの眼の初期発生に関わる Zn フィンガー蛋白質と
ホメオドメイン蛋白質 Otx2 に関する研究）

平成 29 年 7 月　博士（理学）申請

東京大学大学院理学系研究科

生物科学専攻

佐　藤　夢　子

Contents

Abstract

During early *Xenopus* development, the neuroectoderm acquires regional identities along the anteroposterior axis and develop into brain, eye, and so on. In this process, various region-specific transcription factors (TFs) have been shown to play roles in the specification and differentiation of these organs. However, whether other TFs are involved in this process, how those TFs interact and regulate each other, and how TF activity is modulated by post-transcriptional modifications remain to be elucidated. In this thesis, I addressed these three subjects by focusing on two uncharacterized zinc finger (Znf) genes and the homeobox gene *otx2*, which are expressed in the anterior neuroectoderm (ANE).

In Chapter I, I investigated the roles of two uncharacterized Znf proteins, XXXX and YYYY, in eye formation, in concert with Otx2. I chose XXXX and YYYY as candidate regulators of early eye development based on a systematic expression pattern database using a *Xenopus* ANE (ANE) cDNA library. I first showed that both proteins were localized in the nucleus, suggesting their functions as TFs. At the early neurula stage, *xxxx* and *yyyy* were expressed in the ectodermal sensory layer, and their expression domains were gradually restricted to the eye field and the neural fold as development proceeds. Gain-of- and loss-of-function experiments using *Xenopus* embryos suggested that XXXX and YYYY are involved in eye development by regulating the expression of eye marker genes at the early neurula stage. In addition, I found that XXXX and YYYY

physically interact with Otx2 as assayed by co-immunoprecipitation (Co-IP) analysis. Reporter analysis suggested that XXXX enhances the transrepression activity of Otx2 for posterior genes, whereas YYYY inhibits the transactivation activity of Otx2 for anterior genes. These data suggest that XXXX and YYYY function as regulators of Otx2 in a distinct manner to execute eye development.

In Chapter II, I investigated the role of modifications on Otx2, and demonstrated that both exogenous and endogenous Otx2 are phosphorylated at multiple sites in *Xenopus* embryos. I identified three possible cyclin-dependent kinase (Cdk) sites and one possible Akt site, and analysed biological activities of phosphomimetic (4E) and non-phosphorylatable mutants (4A) of Otx2 for those four sites. In the neuroectoderm, the 4E, but not the 4A mutant downregulated the Cdk inhibitor gene *p27xic1*, and promoted cell proliferation, possibly forming a positive feedback loop consisting of Cdk, Otx2, and p27xic1 for cell proliferation. In addition, the 4A mutant downregulated the expression of the hindbrain marker gene *gbx2* for anteroposterior patterning. In contrast, the 4A mutant functioned as an activator on its own and upregulated the expression of eye marker genes, and later enlarged the eyes. Consistent with these results, the interaction of Otx2 with the corepressor Tle1 is suggested to be phosphorylation-dependent. Finally, I found that XXXX enhances the repression activity by Otx2 through phosphorylation-dependent interaction of Otx2 with XXXX. These data suggest that the ternary complex of Otx2, XXXX and Tle1 is formed upon Otx2 phosphorylation for repressing target genes in the ANE.

Taken together, I propose a molecular mechanism in which transcriptional activator and repressor activities of Otx2 are regulated not only by its interaction with the corepressor Tle1 as well as the partner TFs XXXX and YYYY, but also by its phosphorylation states. Thus, Otx2 could coordinate cell proliferation and differentiation during neural patterning and early eye development in *Xenopus*.

Abbreviations

AD, activation domain

ANE, anterior neuroectoderm

BTB, bric-a-brac, tramtrack, broad-complex

Cdks, cyclin dependent kinases

ChIP, chromatin immunoprecipitation

CNS, conserved non-coding sequence

Co-IP, co-immunoprecipitation

CRM, cis-regulatory module

EFTFs, eye field specific transcription factors

λPP, λ protein phosphatase

MAPK, mitogen-activated protein kinase

PH3, Phospho-Histone H3

RPE, retinal pigment epithelium

TFs, transcription factors

NLS, nuclear localization signal

WISH, whole mount in situ hybridization

Znf, zinc finger

Gene names and gene symbols

Official gene name (gene symbol):	synonymous gene symbol
goosecoid homeobox (*gsc*)	*gsc*, *Xgsc*, *goosecoid*, *gsc-a*, *gsc-b*
Meis homeobox 3 (*meis3*)	*XMeis3*, *mrg2*, *meis3-a*, *meis3-b*
orthodenticle homeobox 2 (*otx2*)	*Xotx2*, *otx-2*, *Xotx-2*, *otxA*, *otx2-a*, *otx-b*
cyclin-dependent kinase inhibitor xic1 (*cdknx*)	*Xic-1*, *Xic1*, *p27XIC1*, *p28*
paired box 2 (*pax2*)	*XPax2*, *XPax-2*, *pax-2*, *pax2-a*, *pax2-b*
paired box 6 (*pax6*)	*XLPAX6*, *xpax6*, *pax-6*, *an2*, *mgda*, *wagr*, *pax6-a*, *pax6-b*
retina and anterior neural fold homeobox (*rax*)	*rx1*, *Xrx1*, *Xrax*, *Rx2A*, *rx*, *rx1a*, *rax-a*, *rax1*, Xrx1A, *rax-b*, *rx-1*
SIX homeobox 3 (*six3*)	*XSix3*, *hpe2*, *six3-1*, *six3-b*
SRY-box 2 (*sox2*)	*XLSOX-2*, *Sox-2*, *XSox2*, *Xsox-2*, *anop3*, *mcops3*
T-box 3 (*tbx3*)	*xtbx3*, *Xltbx3*, *tbx3-a*, *tbx3-b*
transducin like enhancer of split 1 (*tle1*)	*grg1*, *xgrg1*, *esg*, *esg1*
XXXX (*xxxx*)	
YYYY (*yyyy*)	

General introduction

Detailed molecular mechanisms in establishing the vertebrate basic body plan have been elucidated by analyses of various signaling molecules, intracellular signal transducers, and transcription factors (TFs) (De Robertis et al., 2000; Niehrs, 2004). Among these factors, TFs directly regulate various genes that are involved in tissue-specific gene cascade or gene regulatory networks during development, so I have been interested in how TFs design outputs of gene expressions to drive a tissue-specific program in cellular and developmental regulatory processes. Recently, comprehensive analyses such as RNA-seq and ChIP-seq provide the information about tissue-specific gene expression profiles and TF-binding genomic loci, but how TFs are coordinately regulated to exert their transcriptional activities by physical and functional interactions with other partner TFs and transcriptional cofactors (coactivators and corepressors) or by posttranslational modifications still needs to be elucidated by focusing on individual TFs.

Xenopus laevis and *X. tropicalis* are useful model systems for molecular embryological studies, because large numbers of easily manipulated embryos can be obtained, and gain-of- and loss-of function analyses have been established. Especially, using *X. laevis* embryos, many region- and tissue-specific TFs have been identified, such as the organizer genes, which are specifically expressed in the Spemann and Mangold

organizer (also called the gastrula organizer), including *goosecoid* (*gsc*), *lim1* (the same as *lhx1*), and *otx2*, and the neural genes including *otx2*, *rax*, *pax2*, and *gbx2*. From the extensive analyses of these TFs, we have learned about molecular mechanisms of early vertebrate development (Andoniadou and Martinez-Barbera, 2013; Lake and Kao, 2003; Yasuoka and Taira, 2018) Compared to the study of the gastrula organizer and early neural patterning, it remains elusive how the early development of the brain and eye is regulated at the level of TFs.

In this thesis, I focused on region- and tissue-specific TFs that are expressed during neural patterning and eye formation, and addressed two subjects; (i) analysis of two uncharacterized Znf genes, *xxxx* and *yyyy* isolated from the systematic expression pattern screening of an anterior neuroectoderm (ANE) cDNA library (Takahashi et al., 2005), (ii) analysis of the regulatory mechanism of transcriptional activities of the homeodomain TF Otx2 through posttranslational modifications in early development.

Chapter I

Analysis of C2H2-type zinc finger proteins, XXXX and YYYY, for eye development

1.1 Introduction

During early eye development in vertebrates, a part of the anterior neural plate is fated to the eye field that will form eye structures, such as eye vesicles including the retina and optic stalks at later stages. Subsequently, sequential processes progress for eye formation: splitting the eye field, the formation of the optic vesicle and the optic cup, and lens induction (Graw, 2010; Zuber, 2010) (Fig. 1). There are many reports for later eye development in vertebrate such as the specification of the optic vesicle and stalk, retina differentiation and lens placode formation. However, the molecular mechanism to specify the eye field, which is one of the earliest event in eye development, is not fully understood, though a rough genetic cascade has been proposed (Zuber et al., 2003).

The homeobox gene, *otx2* is reportedly involved in early eye formation in *Xenopus*. In the neuroectoderm, *otx2* starts to be expressed in the anterior domain which gives rise to the forebrain and midbrain, and plays an essential role in anteroposterior patterning by preventing Meis3 and Gbx2-mediated caudalization (Agoston and Schulte, 2009; Katahira et al., 2000) (Fig. 2A). In early eye formation, Otx2 is involved in the specification of the eye field by upregulating an eye field-specific gene, *rax*, in the center of the *otx2*-expressing domain at the gastrula stage (Danno et al., 2008). In turn, Rax downregulates *otx2* to discriminate the eye field from the diencephalon (Zuber, 2010). Subsequently, eye field specific transcription factors (EFTFs) including *pax6*, which are essential for eye field specification, are expressed in the center of the region where *otx2* is expressed (Fig.2A,B). In *Xenopus*, a gene cascade of TFs starting from *otx2* and *tbx3*

through *rax* to *pax6* is reported to define the eye field, and this region starts to express other downstream eye-specific genes, *six3*, *lhx2*, *tll*, and *six6* (Zuber et al., 2003) (Fig. 2C), suggesting that Otx2 functions at the top of the hierarchy in ocular morphogenesis. Although the genetic relationship of Otx2 with other EFTFs in the early eye gene cascade has been proposed, it remains elusive how individual TFs interact with each other to exert their functions in this cascade.

以下、Chapter I の詳細については、5 年以内に雑誌で刊行予定のため、非公開。

Chapter II

Modulation of the homeodomain protein Otx2 activity in cell proliferation, anteroposterior patterning and eye formation by phosphorylation states

2.1 Introduction

As described in Chapter I, I found several bands of Otx2 in western blotting (Fig. 10A,B), and Dr. Sudou, a previous member in our laboratory, also noticed that multiple bands of overexpressed Otx2 in *Xenopus* embryos migrate more slowly than an in vitro translated product, suggesting a post-translational modification of Otx2. Similarly, a few previous studies using western blotting showed multiple bands of exogenous mouse Otx2 in transfected cultured cells (Mallamaci et al., 1996) and endogenous Otx2 in mouse embryos (Boyl et al., 2001), but post-translational modification of Otx2 has remained to be characterized.

otx2 is required for the formation of the anterior portion of the head and eye development. In early eye development, Otx2 upregulates an eye field-specific gene, *rax*, in the center of the *otx2*-expressing domain at the gastrula, and subsequently this region starts to express other downstream EFTFs including *pax6* (Zuber, 2010). In later eye development, *otx2* restarts to be expressed in the developing optic vesicle (Martinez-Morales et al., 2001; Viczian et al., 2003), and is involved in the specification of presumptive neural retina (*pax6*-positive cells) from the optic stalk (*pax2*-positive cells) in mice (Martinez-Morales et al., 2001) (Fig. 13). After the retinal specification, *otx2* expression becomes restricted to postmitotic retinal progenitors, and determines bipolar cell fate (Brzezinski and Reh, 2015). Thus, the knowledge of the role of Otx2 for head and eye formation is being accumulated.

Otx2 has both transactivation and transrepression activities for the regulation of downstream target genes. Otx2 has a transactivation domain in the C-terminal region (Gammill and Sive, 2001), and directly upregulates a cement gland marker *xcg1* in *Xenopus* (Gammill and Sive, 1997). Otx2 also has a repression domain with a motif of SIWSPAS, which belongs to the engrailed homology region 1 (eh1) (Heimbucher et al., 2007). This domain is conserved in vertebrate Otx family proteins, and interacts with the corepressor TLE/Groucho (Heimbucher et al., 2007). With this domain, Otx2 functions as a repressor that inhibits the posterior gene *gbx2* to form the midbrain-hindbrain boundary (MHB) (Nakamura et al., 2005). Furthermore, genome wide analysis of chromatin immunoprecipitation (ChIP) sequencing using *X. tropicalis* gastrula embryos has shown that Otx2 cooperates with the transcriptional activator Lim1/Lhx1 to bind specific cis-regulatory modules (CRMs) to activate anterior genes in the head organizer, whereas Otx2 cooperates with the repressor Goosecoid (Gsc) to inhibit non-head organizer genes (Yasuoka et al., 2014). Thus, both the transactivation and transrepression activities of Otx2 are important for regionalization and tissue patterning and function during embryogenesis.

Recently, several reports have shown that Otx2 directly influences both cell proliferation and differentiation. In mice, aberrant expression of Otx2 in the hindbrain induces the ectopic proliferation of neural progenitor cells (Wortham et al., 2012), and overexpression of Otx2 causes proliferation of dopaminergic progenitors in the ventral mesencephalon (Omodei et al., 2008; Vernay et al., 2005). In addition, in a

medulloblastoma cell line, Otx2 upregulates cell cycle-positive regulator genes, such as *cyclin D3*, and downregulates cell cycle-negative regulator genes including *p27* and differentiation-specific genes, such as *neuroD* (Bunt et al., 2012). Thus, Otx2 is likely to be involved in both proliferation and differentiation. However, the molecular mechanism of how Otx2 coordinates cell proliferation and differentiation remains unknown.

Here, I show that Otx2 is phosphorylated, which confers transrepression activity, otherwise functioning as a transactivator on its own. Functional analyses using phosphomimetic or non-phosphorylatable Otx2 mutants suggest that phosphorylated Otx2 represses the Cdk inhibitor gene *p27xic1* and the posterior gene *gbx2* for promoting cell proliferation and anteriorizing the neuroectoderm, respectively, whereas unphosphorylated Otx2 enhances the formation of the eye field and later the retina in the place of the optic stalk. Additionally, I have shown that XXXX or Tle1 interacts with the phosphorylated mutant of Otx2 and potentiates the repression activity of Otx2. These functional and biological data suggest that phosphorylated Otx2 interacts with partner proteins including XXXX and Tle1 to form a repressive complex, leading to the downregulation of repressed target genes of Otx2, such as cell cycle inhibitor genes and posterior genes. Thus, my data provide a new possibility that Otx2 exerts its versatile functions with cell proliferation- and differentiation-orientated activities through its post-translational regulation.

2.2 Results

Phosphorylation of exogenous Otx2

Using western blotting analysis of N-terminally Myc-tagged full length (Myc-Otx2FL) and several deletion mutants of Otx2 constructed by previous members of our laboratory (Ms. Hosono, Mr. Minami, and Mr. Okada), we showed that modification mainly occurs in the region of amino acid positions 96-184 (Fig. 14A). The amino acid sequence from position 96 to 184 indicated possible phosphorylation sites for Cdk (cyclin-dependent kinase; S^*/T^*-P or S^*/T^*-P-X-R/K; *, phosphorylatable residues), MAPK (mitogen-activated kinase), casein kinase (S^*/T^*-X_{0-2}-D/E/S^p_{1-3}; S^p, primary phosphorylatable serine residue), and Akt kinase (R/K-X_2-S*/T*) (Fig. 14B). Notably, mouse Otx2 reportedly possesses an Akt phosphorylation site at S115 (the corresponding site of *Xenopus laevis* Otx2 is T115; see Fig. 15), according to the database for the prediction of phosphorylation sites (see Materials and Methods). I first took over this work from previous members, and tried to identify modification sites of Otx2 by the examination of four serine residues (S116, S132, S153, S158) and one threonine (T115) by introducing point mutations. Because we found the suitable conditions in SDS-PAGE to separate the shifted bands of modified Otx2 by using Myc-Otx2ΔAD constructs, and that modification of Otx2 mainly occurs around the repression domain, we used Myc-Otx2ΔAD constructs in the following experiments. Replacement of a single serine with alanine revealed that S116A, S132A and S158A constructs eliminated the uppermost

band and increased the lower bands, compared with the wild type (WT), T115A and S153A construct (Fig. 14C). Furthermore, a triple alanine mutant of Myc-Otx2ΔAD for S116, S132 and S158 (named ΔAD-3A) showed no slowly migrating bands (Fig. 14D; lane 3). These data suggest that S116, S132 and S158, which have the S-P consensus motif for Cdk and MAPK, are responsible for multiple shifted bands (up to seven bands by combinations of three sites) of Myc-Otx2. To examine this hypothesis, embryonic lysates expressing Myc-Otx2 constructs were treated with λ-protein phosphatase (λ-PP). As shown in Fig. 14D (upper panel), λ-PP treatment removed all of the modified bands of Myc-Otx2ΔAD (lanes 1, 2) and did not change the band of ΔAD-3A itself (lanes 3, 4), suggesting that slowly migrating bands of Myc-Otx2ΔAD were caused by phosphorylation at S116, S132 and S158. The same experiment was performed with full-length Myc-Otx2 (FL), showing a similar result, in which all modified bands of Myc-Otx2FL were removed by λ-PP treatment except for a weak shifted band (Fig. 14D, lower panel). Consistently, Myc-Otx2FL-3A had only a single weak shifted band, and this band was not removed with λ-PP (Fig. 14D, lower panel; orange arrowheads), suggesting another distinct modification site around the activation domain.

I next asked whether T115 of *Xenopus* Otx2 is an Akt phosphorylation site, although I did not detect a shifted band in Otx2 mutant 3A (ΔAD-3A) in western blotting (see Fig. 14D, upper panel; lanes 3, 4). In addition, there was no difference in band positions between ΔAD-3A (remaining T115) and ΔAD-4A (alanine mutation at T115 in addition to 3A) regardless of λ-PP (Fig. 14D, upper panel; lanes 3-6). However, it was still

possible that phosphorylation at T115 may not have caused band shift in ΔAD-3A in western blotting, or may have been inhibited by alanine mutations at the three sites including S116 next to T115. Therefore, I performed IP-western assays using anti-Phospho-Akt Substrate antibody, which recognizes the R-X-X-S^p/T^p motif (S^p/T^p, phosphorylated residues). Myc-Otx2ΔAD in embryonic lysates was immunoprecipitated with anti-Myc antibody and then was subjected to western blotting with anti-Phospho-Akt Substrate antibody. The result showed that a band was detected with mutant ΔAD-3A but not with ΔAD-4A (Fig.14E, upper panel, lanes 2, 3), suggesting T115 as an Akt site. Reasons why no clear band was detected in WT (lane 1) might be (i) phospho-Akt signals were dispersed in several shifted bands caused by phosphorylation at other sites, and (ii) phosphorylation at T115 was inhibited by phosphorylation at S116 or the other sites. Thus, I identified four possible phosphorylation sites for Akt (T115) and Cdk/MAPK (S116, S132 and S158) in Otx2, and these sites are well conserved in vertebrate Otx2 as well as an Otx2 paralog, Otx5/Crx (Fig. 15).

Phosphorylation of endogenous Otx2

It is important to show whether endogenous Otx2 is phosphorylated, but no antibodies against phosphorylated sites of Otx2 are available. As far as I know, there is no report on detecting phosphorylation of TFs expressed region-specifically and endogenously in

Xenopus embryos, like Otx2, as evidenced by band shift in western blotting, possibly due to their limited amounts in the whole embryo. Therefore, I first estimated sensitivity of detection using a diluted series of *otx2* mRNA injected into *Xenopus* embryos. As shown in Fig. 16A, modified bands of full-length Otx2 without Myc-tag (Otx2FL) was clearly detected when *otx2FL* mRNAs were exogenously injected with greater than 200 pg per embryo. Based on an RNA-seq data from *X. tropicalis* (Owens et al., 2016), the amount of *otx2* mRNA was estimated to be the order of 1 pg per embryo at the neurula stage. I therefore predicted that endogenous Otx2 can be detected by western blotting with more than 200 *X. tropicalis* embryos. As expected, I successfully detected multiple bands of the endogenous Otx2 protein immunoprecipitated from lysates of approximately 800 *X. laevis* neurula embryos in total, and the upper bands were reduced by λ-PP treatment (Fig. 16B, left). Similarly, shifted bands of exogenous Otx2FL were detected, and those were abolished by λ-PP treatment (Fig. 16B, right). Thus, endogenous Otx2 is actually phosphorylated, though the intensities of phosphorylated bands of endogenous Otx2 appeared to be lower than those of exogenous Otx2.

Phosphorylation of Otx2 depends on Cdk activity

Because S116, S132 and S158 sites have the S-P motif (Fig. 14B), I speculated that MAPK or cyclin/Cdk complexes may phosphorylate Otx2. To examine this, I tested the effect of MAPK on Otx2 modifications. Overexpression of the constitutively active form of MAPKK, MAPKK* (Kosako et al., 1993), did not strongly affect the modified band patterns of Myc-Otx2ΔAD even with the high-dose injection of MAPKK* (Fig. 17A). In addition, Mr. Minami, a previous member, tested the blastocoel injection of a chemical inhibitor for MAPK, U0126, and reduced the activation form of MAPK, in the embryonic lysate, but this did not affect the modified band patterns of Myc-Otx2ΔAD (data not shown). These data suggest that Otx2 does not respond to MAPKK and its downstream kinases.

I next tried to hyperactivate endogenous Cdk activity in *Xenopus* embryos by overexpression of stable mutants of cyclin B1 (cyclin B1* for Cdk1) and cyclin A1 (cyclin A1* for Cdk1 and Cdk2), both of which lack the destruction box (Geley et al., 2001; Yamano et al., 2004). Hyperactivation of Cdks by mRNA injection for HA-cyclin B1* or HA-cyclin A1* in the *Xenopus* embryo was verified by cell-cycle arrest of mRNA-injected blastomeres (Fig. 17B, white asterisks). Under these conditions, modifications of Myc-Otx2ΔAD were dramatically enhanced (Fig. 17C,D), and these modified bands

were almost removed by λ-PP treatment (Fig. 17C,D). These data suggest that Cdk is involved in phosphorylation of Otx2.

If Otx2 is phosphorylated by cyclin/Cdks, a preference of cyclin B/Cdk and cyclin A/Cdks for Otx2 phosphorylation might emerge. To examine this, I constructed double alanine mutants (2A) for S116, S132 and S158 in ΔAD, in which only one site is responsible for Otx2 phosphorylation (Fig. 18A). The intensity of uppermost bands of S132 (S116A/S158A) and S116 (S132A/S158A) constructs, but not that of S158 (S116A/S132A), was increased by HA-cyclin B1* expression (Fig. 18B), whereas all modified bands were enhanced by HA-cyclin A1* expression (Fig, 18C), with an additional modified band (white arrowheads). These data suggest that S116 and S132 have a preference for both cyclin B/Cdk and cyclin A/Cdks, and that S158 has it for cyclin A/Cdks, if Otx2 is directly phosphorylated by cyclin/Cdks.

To further examine Cdk-dependent phosphorylation of Otx2, I overexpressed the Cdk inhibitor p27xic1 in the embryo (Vernon, 2003). I first verified cleavage arrest by *p27xic1* mRNA injection (Fig. 19A left; white asterisks) as reported (Ohnuma et al., 1999). When a mixture of *p27xic1* and *Myc-Otx2ΔAD* mRNAs were injected at the 2-cell stage, modified bands of Myc-Otx2ΔAD were reduced, but a weak band still remained, which might be due to phosphorylation occurring prior to the accumulation of p27xic1 protein translated from injected mRNA (Fig. 19A, right; lanes 1, 2). Therefore, I first injected *p27xic1* mRNA alone at the 2-cell stage, then Myc-Otx2ΔAD mRNA was injected into the cleavage-arrested blastomeres at the 32-cell stage equivalent. As

shown in Fig. 19A (right; lanes 3, 4), p27xic1 completely abolished modified bands of Myc-Otx2ΔAD, suggesting that phosphorylation of Otx2 depends on Cdk activity. These data also imply that the reduction of modified Otx2 by p27xic1 expression was probably not caused by dephosphorylation, because, once Otx2 was phosphorylated at the 2- to 32-cell stages (lane 2), it appeared to be stable until the late blastula stage when western blotting was performed (compare lanes 2 and 4). Because phosphorylation of Otx2 appears to start very early, I examined developmental changes of phosphorylation levels using Myc-Otx2ΔAD (Fig. 19B). The wild type (WT) and alanine mutants of a single serine at S132 (S132A) and S158 (S158A), and of 6 serines at S122, S123, S132, S153, S158, and S161 (6A) in Myc-Otx2ΔAD constructs were analyzed from stages 5 to 10.5, as indicated. Note that the 6A construct has S116, which is a phosphorylation site. The data showed that modification of Otx2ΔAD was already detected at the 16-cell stage (stage 5), gradually increased until the early gastrula stage (stage 10.5), and reached almost a plateau at stage 10.5 onwards (Fig. 19B). In addition, mutation at S132 (S132A and 6A constructs) reduced phosphorylation levels compared to S158 mutation, indicating that S132 and S116 are more efficiently phosphorylated than S158 during cleavage stages. Increase of phosphorylation levels until stage 9 correlates well with the cleavage cycle, supporting again the possibility that Otx2 is a substrate of cyclin/Cdks.

Taken together, Otx2 has four possible phosphorylatable sites, and I referred to T115 as A-site (putative Akt site) and S116, S132 and S158 as C-sites (putative Cdk sites) in the following experiments.

Otx2 mutants 4A and 4E have distinct functions in eye formation

To ask whether known Otx2 activities are affected by phosphorylation states, I overexpressed phosphomimetic or non-phosphorylatable mutants and analysed eye phenotypes, which have been well-documented for Otx2 functions (Martinez-Morales et al., 2001; Nishihara et al., 2012). A phosphomimetic mutant, Otx2-4E, was made by replacing A-site (T115) and three C-sites (S116, S132 and S158) with glutamate in Otx2FL. Non-phosphorylatable mutants, named Otx2-T115A, -3A and -4A, were similarly made by replacing A-site, C-sites or all four sites with alanine, respectively. Each Otx2 construct was expressed unilaterally in the anterior neuroectoderm (ANE), which includes the eye field, and the phenotypes were scored at stages 38-42. I categorized abnormal eye phenotypes into three types compared with the normal looking phenotype (Fig. 20A-D). Expression of Otx2-WT, -4E -T115A, or -3A caused small/trace eye and ventral defect phenotypes in a dose-dependent manner (Fig. 20E), in which stronger phenotypes appeared to be obtained by expression of Otx2-WT, -4E, -3A, and -T115A in order. By contrast, only Otx2-4A caused enlarged eye phenotypes, which

have not previously been reported by expressing any other Otx2 mutants in *Xenopus* (Andreazzoli et al., 1997; Isaacs et al., 1999). Notably, either Otx2-T115A or -3A did not enlarge, but rather reduced eye sizes (Fig. 20E), indicating that mutations at both A-site and C-sites are necessary for the activity of Otx2-4A. Quantitative analysis for the area of the eye vesicle showed that the eye size in Otx2-4A expressing embryos was enlarged by approximately 1.3 times, whereas that in Otx2-4E expressing embryos was reduced by approximately 0.5 times, compared with control (Fig. 20F). Section examination for the enlarged eye phenotype by Otx2-4A showed that the retinal tissue was expanded ventrally with the reduction of the retinal pigment epithelium (Fig. 20H,H'; arrowheads) compared with the control (Fig. 20G,G'). These results clearly demonstrated that Otx2-4A has different activities in eye formation compared to the other mutants, and imply that exogenous Otx2-WT functions as phosphorylated forms, because WT exhibits similar activities to 4E (Fig. 20E).

To further examine whether all C-site mutations are required for the activity of Otx2-4A, I constructed triple alanine mutants of Otx2 (named A2A constructs), in which only one of C-sites (S116, S132 or S158) is intact, referred to as A2A-S116, -S132, or -S158, respectively. As shown in Fig. 20I, A2A-S116 and A2A-S132 both caused small/trace

and ventral defect eye phenotypes. By contrast, A2A-S158 caused enlarged eye phenotype in a dose dependent manner, though the fraction of enlarged eye phenotypes by A2A-S158 was lower than that of Otx2-4A. This data indicates that mutations at T115, S116, and S132 are essential for enlarged eye phenotypes.

I next examined the early effect of Otx2-4A and -4E by focusing on the eye field marker genes, *rax* and *pax6*. Overexpression of Otx2-4A increased the expression of *rax* compared with the uninjected side (Fig. 21D), whereas Otx2-WT and -4E as well as the globin control did not affect (Fig. 21A-C). The expansion of *rax* expression by Otx2-4A may be a reason for enlarged phenotypes. Similarly, Otx2-4A enhanced the expression of *pax6* compared with the uninjected side (Fig. 21H) and globin injected control (Fig. 21E), whereas Otx2-4E showed no effect (Fig. 21G). The effect of Otx2-WT on *pax6* was complicated; Otx2-WT expanded *pax6* expression but partially reduced it (Fig. 21F), possibly due to a combination of various phosphorylation states. These data suggest the possibility that unphosphorylated Otx2, as mimicked by Otx2-4A, promotes eye field formation. The enlarged eye phenotypes with aberrant ventral eye structures (see Fig. 20H,H') raised another possibility that Otx2-4A converts the presumptive optic stalk to the retina. Therefore, I examined the expression of *pax2*, *six3* and *pax6* in the late neurula, in which *pax2* is expressed in the optic stalk (OS) and MHB (Fig. 21I), whereas *six3* is expressed in the optic vesicle (OV) and telencephalon (Te) (Fig. 21M), and *pax6* is expressed in the OV and diencephalon (Di) side by side with different WISH intensities (Fig. 21Q). Overexpression of Otx2-WT, -4E, and -4A all

inhibited *pax2* expression in the OS (Fig. 21J-L), while Otx2-WT or -4E, but not -4A caused posterior shift of *pax2* expression in the MHB (open arrowheads). The reduction of *pax2* in the OS by Otx2-WT, -4E, and -4A (Fig. 21J-L) are well consistent with the aberrant eye morphology at the tailbud stage on the ventral side where the OS is formed (see Fig. 20C,E). Regarding *six3* expression, Otx2-WT, -4E, and -4A expanded in the OV (Fig. 21N-P), and Otx2-4A appeared to be most effective for this expansion (Fig. 21P). As for *pax6* expression, Otx2-WT, -4E, and -4A differently affected. WT reduced OV but expanded Di *pax6* expression (Fig. 21R,R'; black dashed lines, Di; white dashed lines, OV); and Otx2-4E slightly reduced the OV expression similar to WT (Fig. 21S,S'), consistent with their small/trace eye phenotypes (see Fig. 20B,E). Opposite to them, Otx2-4A expanded the OV *pax6* expression (Fig. 21T,T'), consistent with its enlarged eye phenotypes (see Fig. 20D,E). These data demonstrated that Otx2-4E and -4A have different activities in eye formation. This raised the next question whether Otx2-4E and -4A have different activities in cell proliferation and anteroposterior patterning, which have been reported for Otx2 functions (Pilo et al., 2001; Acampora et al., 2000).

Otx2-4E stimulates cell proliferation

To investigate the effect of Otx2 on cell proliferation, Otx2-WT, -4E or -4A was expressed in the dorsoanterior region of the embryo, and then immunostaining was

performed with anti-PH3 (phospho-Histone H3) antibody as a mitosis marker. The numbers of PH3-positive nuclei were counted in eGFP-positive and negative areas for quantitative analysis as shown in Fig. 22A-C. The data showed that the ratio of the number of PH3-positive nuclei in injected versus uninjected areas was 1.27 ± 0.07 (mean ± s.e.m.) and 1.38 ± 0.05 in Otx2-WT and -4E expressing embryos, respectively, whereas that was 0.727 ± 0.062 in Otx2-4A expressing embryos. These ratios significantly differed from the control (0.944 ± 0.014) (Fig. 22D), suggesting that Otx2-WT and -4E both stimulate cell proliferation whereas Otx2-4A reduces it. To confirm this, I counted the number of nuclei stained by DAPI (Fig. 22E-G). Quantitative analysis showed that the ratio of cell number in injected versus uninjected areas was 1.08 ± 0.061 and 1.13 ± 0.02 in Otx2-WT and -4E expressing embryos, respectively, whereas that was 0.894 ± 0.019 in Otx2-4A expressing embryos. The ratios in 4E and 4A embryos differed from the control (1.02 ± 0.04) (Fig. 22H). Thus, these data suggest that Otx2-4E and -4A exhibited opposite effects on cell proliferation: Otx2-4E stimulates but -4A reduces proliferation.

To gain in vivo relevance of the Otx2 function in cell proliferation, I next performed loss-of-function experiments using antisense morpholino oligos (MOs) for *otx2* and its paralog *otx5*. Previous study using MO-injection in *X. tropicalis* embryos has shown that Otx2 and its paralogue Otx5, which are expressed in the ANE, have functional redundancy in head development (Yasuoka et al., 2014). *X. tropicalis* is a diploid species closely related to the tetraploid species *X. laevis* and suitable for MO knockdown experiments, and all three C-sites of Otx2 are conserved in Otx5. MOs together with FITC dextran as a tracer were injected into one blastomere at the 4-cell stage of *X. tropicalis* embryos; followed by PH3 immunostaining and DAPI staining at early neural stage. The numbers of stained nuclei were counted and compared between injected and uninjected areas. As shown in Fig. 23, the number of PH3-positive nuclei was almost unchanged in the ANE injected with standard control MO (A,A',A",C), whereas it significantly decreased in the region injected with *otx2*/*otx5*-MOs (B,B',B",C). Consistent with this, the number of nuclei decreased in the *otx2*/*otx5*-MOs injected area (Fig. 23E,E',E",F), but not affected in the control MO-injected area (Fig. 23D,D',D'',F). These data indicate that Otx2 and Otx5 are required for cell proliferation in the ANE, and this in vivo data is consistent with the enhancement of cell proliferation by exogenous Otx2-WT and -4E (see Fig. 22D,H). This may also suggest that the reduction of cell proliferation by Otx2-4A is caused by dominant-negative action of Otx2-4A against endogenous phosphorylated Otx2 that stimulates cell proliferation, and the unphosphorylated form of Otx2 cannot take its place.

To ask how Otx2 stimulates proliferation, I focused on *p27xic1* because Otx2 reportedly inhibits the *p27* gene (Bunt et al., 2012). Analysis of our ChIP-seq data using *X. tropicalis* gastrula embryos (Yasuoka et al., 2014) showed co-occupancy of Otx2 and Tle1 to several potential CRMs near *p27xic1* (Fig. 24A), suggesting that *p27xic1* is a direct target gene of Otx2. Using mRNA injection, Otx2-WT, -4E, or -4A with n*β*-gal as a tracer was unilaterally expressed, and the expression of *p27xic1* was examined by WISH. Expression of Otx2-WT and -4E, but not -4A, downregulated *p27xic1*, compared with globin-injected negative control and on the uninjected side (Fig. 24B-E), consistent with the stimulation of cell proliferation by Otx2-4E (see Fig. 22D,H).

To assess the gain-of- and loss-of-function data shown above, the expression domains of *otx2* and *p27xic1* and the distribution of PH3-positive cells in the early neurula were examined using sagittal hemisections. The data showed that the *otx2* expressing region did not overlap with that of *p27xic1* (Fig. 24F,G), and has more mitotic cells than the posterior region (Fig. 24H), consistent with the involvement of *otx2* in cell proliferation in the ANE. These data suggest the existence of a positive feedback loop involving Otx2, Cdk, and p27xic in the regulation of cell proliferation (Fig. 24I).

Activities of Otx2-4E and -4A for anteroposterior patterning

In the neural plate, Otx2 is involved in anteroposterior patterning by directly inhibiting posterior genes, which are suggested to include *gbx2* and *meis2* (Yasuoka et al., 2014),

and by directly activating anterior genes such as *xcg1* (Gammill and Sive, 1997) and *rax* (Danno et al., 2008). I first examined *gbx2* by ectopically expressing Otx2-WT, -4E or -4A, in the posterior neuroectoderm. Both Otx2-WT and -4E downregulated the expression of *gbx2* (Fig. 25B,C,C'; blue arrowheads) compared with the uninjected side and globin-injected control (Fig. 25A,A'). This activity explains the posterior shift of *pax2* expression in the MHB by Otx2-WT and -4E (see Fig. 21J,K). Conversely, Otx2-4A did not downregulate *gbx2* expression (Fig. 25D,D'; white arrowheads), suggesting the possibility that only phosphorylated Otx2 has the ability to inhibit posteriorization.

xcg1 is expressed in the cement gland, which is the anterior most organ (Fig. 25E). Ectopic expression of Otx2-WT, -4E and -4A all upregulated *xcg1* (Fig. 25F,G,H; magenta arrowheads), and this activation was observed in the ventrolateral ectoderm, but not in the neuroectoderm as reported (Gammill and Sive, 1997). To assess whether the ectopic upregulation of *xcg1* by the Otx2 mutants requires their transactivation activity, I made transactivation domain-deleted constructs of 4E (ΔAD-4E) and 4A (ΔAD-4A). Neither ΔAD-4E nor ΔAD-4A upregulated *xcg1* (Fig. 25I,J), indicating that the transactivation domain of Otx2-4E and -4A is required for their activation of *xcg1*. These data suggest that Otx2 has transactivation activity regardless of its phosphorylation states.

The above data suggest that the difference in function between Otx2-4E and -4A is repression activity. To further examine whether phosphorylation states affect the repression and activation activity of Otx2, I performed luciferase reporter assays. I first examined the response of the silencer of *meis3*, a posterior gene, which is expected to be repressed by Otx2. The *meis3*-D2 silencer (Yasuoka et al., 2014) was inserted upstream of the SV40 promoter in the reporter construct, and this reporter alone showed a high level of luciferase activity in the animal pole region. Under this condition, reporter activity was significantly repressed by Otx2-WT and -4E, but not by -4A (Fig. 25K). I next tested combinatorial repressive activity of Otx2 with the interacting partner Gsc and the corepressor Tle1, which form the repression complex for negative target genes of Otx2 (Yasuoka et al., 2014). Repression of the *meis3-D2* reporter by Gsc and Tle1 was enhanced by co-expression of Otx2-WT, and this enhancement was also observed with Otx2-4A (Fig. 25L), suggesting that neither phosphorylation of Otx2 is required for nor unphosphorylated Otx2 interferes with the formation of a ternary repression complex. Because Otx2-4A and Tle1 did not repress the reporter (Fig. 25L), repression activity by a combination of Otx2-4A, Gsc, and Tle1 is probably due to recruitment of Tle1 to Gsc. Although Otx2-4A does not interfere with complex formation, Otx2-4A may weaken repression activity of the complex as implied in Fig. 25M (compare Otx2-4A with Otx2-4E).

I next examined an activated target gene of Otx2, *rax*, using the reporter gene SOP-FLASH, which has 8 tandemly repeated *rax* enhancer elements binding for Otx2 and

Sox2 (Danno et al., 2008). The data showed that both Otx2-4E and -4A exerted transactivation activity (Fig. 25N), similarly to activation of the *xcg1* gene by Otx2-4E and -4A (see Fig. 25G,H). Because Sox2 is expressed in the neuroectoderm (Mizuseki et al., 1998) and has a transactivation domain (Nowling et al., 2000), a combination of Sox2 and Otx2 may function as activator regardless of phosphorylation states of Otx2. Because Otx2-4E did not upregulate the endogenous *rax* gene (see Fig. 21C), activation of the *rax* reporter by Otx2-4E may be due to the "boosted CRM" by 8 tandem repeats. Taken together, it is suggested that phosphorylation of Otx2 is required for its repression activity, but does not affect transactivation activity itself.

Otx2-4E, but not -4A interacts with Tle1

To investigate how phosphorylated Otx2 functions as a gene repressor, I tested the association with other repressor factors. The eh1 repression domain of Otx2 reportedly interacts with TLE/Groucho (Heimbucher et al., 2007). Therefore, I tested the physical interaction between Otx2 mutants and HA-tagged Tle1 by Co-IP assays (Fig. 25O). A co-immunoprecipitated band of HA-Tle1 was detected with Myc-Otx2-4E as well as Myc-Otx2-WT (magenta arrowheads), but barely with Myc-Otx2-4A, consistent with the data that neither Otx2-4A alone nor co-expression with Tle1 exerted repressive activity for *meis3-D2* luciferase reporter (see Fig. 25K,L). The reason why the intensity of the co-immunoprecipitated Tle1 band with WT was weaker than that of 4E (Fig. 25O) is possibly due to partial phosphorylation of WT. These data suggest that phosphorylation

of Otx2 is required for the interaction with Tle1 to exert its own repression activity. The phosphorylation-dependent interaction of eh1 domains with TLE has not previously been reported.

Otx2-4E but not -4A interacts with XXXX

Fig. 26 の結果については、5 年以内に雑誌で刊行予定のため、非公開。

2.3 Discussion

Repressor activity of Otx2 conferred by post-translational modification

In this study, I have shown that Otx2 exists in two distinct states, phosphorylated and unphosphorylated states. Using phosphomimetic and non-phosphorylatable constructs of Otx2, I demonstrated that phosphorylated Otx2 can function as both repressor and activator, whereas non-phosphorylated Otx2 can function solely as an activator. To date, only a few TFs have been reported to be converted between being an activator and a repressor by post-translational modification. The SoxE group of TFs including Sox9 are converted by SUMOylation from an activator to a repressor by displacing CBP/p300 and recruiting Tle4/Grg4 (Lee et al., 2012). Another case is Pax2, transactivation of which is enhanced through JNK kinase-mediated phosphorylation in the activation domain by blocking TLE/Groucho (Cai et al., 2003). Thus, I have shown the third case, in which phosphorylation of Otx2 enables it to function as a repressor through the interaction with Tle1 and XXXX (Fig. 27), opposite to the case of Pax2.

It is noted that Otx2 has a novel eh1 domain with a Cdk site (SIWSPASISP; underlined is a possible Cdk site), which is only present in the Otx family proteins (Otx1,

Otx2, and Otx5/Crx) as well as a few other TFs (Copley, 2005). The eh1 domain is present in many metazoan TFs (Copley, 2005) and known to interact with TLE family proteins through the conserved C-terminal WD40 repeat domain (Heimbucher et al., 2007; Pickles et al., 2002). Because some WD40 domains of ubiquitin ligases and phosphatases, such as β-Trcp and Cdc4, are known to interact with a phosphorylated serine residue in their substrates (Yaffe and Elia, 2001), it is possible that one of the WD40 repeats of TLE may interact with the eh1 domain with a phosphorylated site in Otx2.

Role of cyclin/Cdk-dependent phosphorylation of TFs

From my observations, I propose a positive-feedback-loop model for Otx2 functions in cell proliferation (Fig. 24I). In this model, in a proliferative state, Otx2 is phosphorylated by elevated Cdk activity, and phosphorylated Otx2 becomes to repress *p27xic1*, which, in turn, derepresses cyclin/Cdk activity to enhance phosphorylation of Otx2, thereby forming a positive feedback loop (Fig. 24I, left). When the cell cycle is arrested, cyclin/Cdk activity decreases and hence phosphorylated Otx2 decreases, causing derepression of p27 expression to repress Cdk, keeping unphosphorylation state of Otx2 (Fig. 24I, right). Thus, the phosphorylated and unphosphorylated states of Otx2 can be

toggled by the cell cycle. However, it is not known how the phosphorylated state of Otx2 is changed to the unphosphorylated state. There are two possibilities: (i) dephosphorylation of Otx2 by phosphatase, and (ii) degradation of phosphorylated Otx2. I did not observe any difference in instability of the Otx2-4E mutant compared to -4A by western blotting, which does not support the second possibility, and denies a phosphorylation dependent degradation. A putative PEST sequence, an indicator of rapidly degraded protein, is present in the *Xenopus* Otx2 protein (Mori et al., 1994; Williams and Holland, 1998), and Otx2 may have a short half-life. Therefore, unphosphorylated Otx2 could be generated through the rapid turn-over of Otx2 regardless of its phosphorylation state.

I have shown that endogenous Otx2 is phosphorylated, but its phosphorylation levels were much lower than those of exogenous Otx2 (Fig. 16B). This difference might be caused by the timing of protein production and the number of proliferating cells where phosphorylation of Otx2 supposedly occurs. For exogenous Otx2, mRNA was injected into the animal pole region at 2- or 4-cell stages, and translated in the presumptive ectoderm from early cleavage stages, and the translation product is phosphorylated until the blastula stage (Fig. 19B) by Cdk1 activity, which oscillates with a period of ~30 minutes during the cleavage cycle (Hörmanseder et al., 2013). By contrast, in the in

vivo situation, *otx2* starts to be transcribed in the dorsal endoderm and mesoderm at the late blastula stage and in the dorsal ectoderm at the early gastrula stage (Sudou et al., 2012), and then the endogenous Otx2 protein accumulates in the head organizer and the ANE, and the proliferation rates in these regions dramatically decrease especially in the head organizer (Fig. 24H). Therefore, even if phosphorylation levels of endogenous Otx2 in proliferating cells are high, the average phosphorylation level of major non-proliferating and minor proliferating cell populations in a gastrula or neurula embryo is much lower than those of exogenous Otx2.

I have proposed a positive feedback loop involving Cdk-dependent phosphorylation of Otx2 for cell proliferation (Fig. 24I). Similar feedback loops involving other TFs are also reported, but the regulatory mode is different from Otx2. That is, TFs are switched "on" or "off" by Cdk-dependent phosphorylation to promote cell cycle progression. An example for regulation by an "on" switch is FOXM1. FOXM1 is activated by the phosphorylation of the N-terminal inhibitory domain by cyclin/Cdk to upregulate cyclin B and cdc25B, thereby forming a positive feedback loop for cell proliferation (Park et al., 2008; Major et al., 2004). An example for an "off" switch is FOXO. FOXO upregulates the Cdk inhibitor genes *p27kip1* and *p21WAF1*, but, upon phosphorylation by cyclin/Cdk, undergoes nuclear export, which virtually switches off the function of FOXO, leading to cell proliferation (Schuff et al., 2010; Liu et al., 2008; Stahl et al., 2002). In the case of Otx2, Cdk-dependent phosphorylation confers repressor activity to Otx2

for repressing *p27xic*, otherwise it functions as an activator on its own as mentioned above, differing from simple switch on or off regulations.

Regarding tissue specification and differentiation, Cdk-dependent phosphorylation generally negatively regulates activity of TFs that directly activate differentiation genes. For example, the phosphorylation of the myogenic TF MyoD by cyclin/Cdk leads to its degradation to prevent muscle differentiation (Kitzmann et al., 1999). During neurogenesis, the Cdk-dependent phosphorylation of Ngn2 (neurogenin 2) inhibits its neural differentiation activity (Ali et al., 2011; Hindley et al., 2012). In these cases, Cdk-dependent phosphorylation of the TFs switches off their functions. Taken together, phosphorylation of TFs by cyclin/Cdks either promotes cell cycle progression (e.g., FOXM1 and FOXO) or inhibits tissue differentiation (e.g., MyoD and Ngn2). In contrast, Cdk-dependent phosphorylation does not simply inhibit the function of Otx2 in differentiation, but at the same time converts it to function in proliferation. Thus, this study has shown a new category of TFs, in which post-translational modification of a single TF converts from a differentiation- to proliferation-orientated role.

Repression activity by phosphorylated Otx2 and XXXX

It is not well understood how Otx2 properly functions as an activator or a repressor for its target genes. An answer to this question was reported (Yasuoka et al., 2014), showing that Otx2 functions as an activator together with Lim1 and also as a repressor

together with Gsc, suggesting that the combination with partner proteins determines transcriptional activity of Otx2. This combinatorial regulation may dominate over phosphorylation states because the Otx2-4A construct, which does not have repression activity by itself (Fig. 25K), still exert repressive activity together with Gsc for repressing the *meis3-D2-luc* reporter (Fig. 25L,M). However, it should be noted that *gsc* is not expressed, in the neural plate, and it is not known yet what is a partner protein of Otx2 for repressing *meis3* and *gbx2*. In this study, I demonstrate a possible partner TF of Otx2 in the neural plate, XXXX.

How does Otx2 coordinate its activator and repressor functions for development?

Based on these lines of evidence together with other observations, I propose a model for Otx2 functions (Fig. 27). In this model, during cell cycle progression (in proliferation), Otx2 is phosphorylated by cyclin/Cdk and Akt upon growth stimulation, and phosphorylated Otx2 is able to interact with Tle1 and XXXX to repress *p27xic1*, and, in turn, derepresses cyclin/Cdk activity, thereby forming a positive feedback loop (Fig. 27, upper). In the ectoderm, phosphorylated Otx2 also represses posterior genes (*gbx2* and *meis3*) and activates anterior genes (*xcg1*, *rax*) to establish anteroposterior patterning. When growth stimuli are reduced, and the cell cycle is arrested, unphosphorylated Otx2

functions as an activator for anterior development (cement gland formation and retinal differentiation) (Fig. 27, lower). Thus, Otx2 has ability to orchestrate cell proliferation and differentiation through changing its phosphorylation states. This model is consistent with the expression patterns of related genes. The ANE (future forebrain and midbrain), which expresses *otx2* as well as *cyclin* and *cdk* genes (Fig. 24F) (Vernon and Philpott, 2003), exhibits high mitotic rate with no expression of *p27xic1* (Fig. 24G,H). By sharp contrast, the posterior neuroectoderm, which expresses no *otx2* but *cyclin* and *cdk* to a lesser extent (Fig. 24F) (Vernon and Philpott, 2003), exhibits low mitotic rate with the expression of *p27xic1* (Fig. 24G,H). However, at the tailbud stages (stages 20-40), the developing retina expresses both *otx2* (Wang and Harris, 2005; Viczian et al., 2003) and *p27xic1* (Ohnuma et al., 1999). It was reported that, in developing retinal cells, *otx2* is transcribed, but not translated during the early to mid-retinal neurogenesis (stages 33, 37), and Otx2 protein was only detectable from late retinal neurogenesis (stage 38) in bipolar cells (Decembrini et al., 2006). Therefore, the absence of the Otx2 protein at the early to mid-retinal neurogenesis in the developing retina may explain colocalization of *otx2* and *p27xic1* mRNAs (Decembrini et al., 2006).

Notably, both Otx2-4E and -4A upregulate *xcg1* (Fig. 25G,H), and this activity needs the activation domain (Fig. 25I,J), implying that phosphorylated Otx2 retains transactivation activity, consistent with reporter analysis (Fig. 25N), and that Otx2 can directly upregulate *xcg1* as has been shown (Gammill and Sive, 1997). During cement gland formation, *xcg1* appears to be expressed in both proliferating and non-proliferating cells because the expression of *xcg1* starts at the gastrula stage in the anterior-most ectoderm at the dorsoventral border (Gammill and Sive, 1997; Gammill and Sive, 2001), and continues during neurula stages beyond stage 18, at which cell proliferation is undetectable (Saka and Smith, 2001). This observation is consistent with the data that Otx2-4E and 4A both activate *xcg1* expression, supporting the model that activator activity of Otx2 is unchanged by phosphorylation.

In eye formation, it was reported that expression of a repressor form of Otx2 (Otx2-EnR) by mRNA injection in *Xenopus* embryos results in small eye or eyeless phenotype (Isaacs et al., 1999), and that expression of another type of repressor form, EnR-Otx2, in chick eyes by electroporation caused pigmentation defects of the retinal pigment epithelium and the reduction of *pax6* (Nishihara et al., 2012). These activities of repressor forms of Otx2 are similar to that of Otx2-4E in *Xenopus* embryos (Fig. 20E and Fig. 21R,S), consistent with the repressor activity of Otx2-4E (Fig. 25K). In contrast with Otx2-4E, Otx2-4A expanded the expression of *rax* at early neurula stage (Fig. 21D) without stimulating cell proliferation (Fig. 22D,H); at later stages, Otx2-4A expanded the expression of *pax6* (retina) but inhibited *pax2* (optic stalk) on the ventral side, leading to

ventral expansion of the retina. These data suggest that Otx2-4A can expand the eye field, and subsequently alter patterning of the neural retina and optic stalk. In other words, enlarged eye phenotypes by Otx2-4A is caused by changes in patterning, not by proliferation. Our data is reminiscent of the previous report on the function of Otx2 for *Xenopus* retina formation, in which an activator type of Otx2 (Otx2-VP16) promotes the bipolar cell fate without stimulating retinal proliferation (Viczian et al., 2003), supporting the possibility that unphosphorylated Otx2 acts mainly as an activator in retina formation.

Several heterozygous Otx2 mutations in human were reportedly linked with severe ocular malformation. For example, point mutations of P133T, P134A, and P134R, which occur near one of the four putative phosphorylation sites, S132, found in our study (see Fig. 15), are associated with microphthalmia, anophthalmia, sclerocornea and retinal detachment (Beby and Lamonerie, 2013). It is not certain whether these mutations actually affect phosphorylation of Otx2, and if it affects the interaction with putative binding partners of Otx2, but it is possible to speculate that ocular defects in human are caused by the alteration of phosphorylation states of Otx2.

In summary, I demonstrated that Otx2 undergoes phosphorylation *in vivo*, and that phosphomimetic and non-phosphorylatable mutants of Otx2 exhibit distinct activities in cell proliferation, patterning and differentiation in *Xenopus* embryos. *In vivo* analysis

of the phosphorylation sites, such as a mutated gene knock-in approach, is now awaited to explore the role of phosphorylated Otx2 in embryonic development.

General Discussion

To understand the molecular mechanisms of gene regulation during development, it is important to elucidate not only genome-wide binding profiles of individual transcription factors (TFs) to cis-regulatory modules (CRMs) near target genes together with their loss-of- and gain-of-function data, but also the regulation of individual TFs at the protein level, such as the combinatorial interplay among TFs and their binding partners or cofactors as well as the post-translational modification of TFs. In this thesis, I investigated the molecular mechanism of how transcriptional activities of Otx2 are regulated by the combination with XXXX and YYYY, and by its phosphorylation states in developmental processes, such as the patterning of neuroectoderm and early eye formation in *Xenopus*.

I started this study by investing two uncharacterized genes, *xxxx* and *yyyy*, which are expressed in the anterior neuroectoderm (ANE), and found that these two genes are involved in the gene cascade for eye development at positions downstream of Otx2. This finding led me to hypothesize functional and physical interactions of XXXX and YYYY with Otx2. In Chapter I, I found that XXXX enhances the gene repression activity of Otx2, whereas YYYY inhibits the gene activation activity of Otx2. From the data of WISH and RNA-seq, *xxxx* and *yyyy* are maternally expressed in the animal pole (Fig. 6), in which *otx2* is not expressed (Sudou et al., 2012), suggesting the possibility that XXXX and YYYY associate with other TFs rather than Otx2. Such TF could be a maternally expressed gene, *otx1*, because the possible phosphorylation sites are conserved

between Otx1 and Otx2 (Fig. 15). In chapter II, I focused on post-translational modifications of Otx2, and found that the modification is phosphorylation. Then, I investigated the role of phosphorylation at the three possible Cdk sites and one possible Akt site by using phosphomimetic and non-phosphorylatable mutants of Otx2. Although these data in this thesis obtained from overexpression approach, the differences of the activities between phosphomimetic or non-phosphorylatable Otx2 were clearly shown, thereby reasonably speculating in vivo functions of phosphorylated and unphosphorylated Otx2 proteins. It would now be necessary to carry out knock-in experiments with a phosphomimetic or non-phosphorylatable *otx2* gene for obtaining in vivo relevance data, but those are not feasible at this moment, in the *Xenopus* system. In near future, it may be possible to examine this by CRISPR-Cas9-mediated generation of knock-in and knock-out approaches.

My data suggest that phosphorylation of Otx2 confers repression activities of Otx2, otherwise functioning as a transactivator on its own. Importantly, the interaction of Otx2 with Tle1 and XXXX is dependent on the phosphorylation of Otx2 (Fig. 25O and 26A). By contrast, Otx2 expressed in the head organizer does not require phosphorylation for interacting with Goosecoid to repress target genes (Fig. 25L,M). Thus, the data in my thesis suggest various regulatory modes of Otx2, which are summarized in Fig. 28. To repress Otx2-target genes (Fig. 28A), Otx2 takes two modes, phosphorylation-dependent and -independent transrepression activity: (i) In the anterior neuroectoderm, where cell proliferation rate is high (see Fig. 24H), Otx2 requires

Cdk/cyclin-dependent phosphorylation to interact with Tle1 and XXXX, thereby linking cell proliferation and Otx2-mediated repression of target genes including p27 (see Fig. 22D,H and 24D); and (ii) in the head organizer, where cell proliferation rate is low (see Fig. 24H), Otx2 does not require phosphorylation to repress its repressed target genes. Thus, phosphorylation-dependent regulation of Otx2 takes place in proliferative cells in the ANE, and the possible four phosphorylation sites (A-site and 3 C-sites) are evolutionarily conserved in vertebrates but only A-site and S132 are conserved in the echinoderm sea urchin, only S132 is conserved in the amphioxus, and no site seems to be conserved in the sea anemone *Nematostella* (Fig. 29), implying that this regulatory system might have started to be evolved in the common ancestor of deuterostomes and have been established in the common ancestor of vertebrates, whereas the amphioxus lost A-site. This evolutionary scenario of the Otx2 regulatory system might be related to the evolutionary development of the ANE in the chordate lineage.

For activated target genes (Fig. 28B), Otx2 could upregulate them regardless of its phosphorylation stage in the case of the cement gland (Fig. 25G,H), but, in the neuroectoderm, phosphorylated Otx2 may tend to be recruited in a repression complex by interacting with XXXX, thereby reducing the contribution of Otx2 to activation of target genes. In the head organizer, Otx2 requires a partner TF like Lim1 to activate target genes, because Otx2 alone does not confer the organizer activity when expressed alone in the ventral region (Yasuoka et al., 2014). The third regulatory mode of Otx2 is shown in Fig. 28C, in which YYYY inhibit Otx2 transactivation activity, but whether

YYYY inhibits binding of Otx2 to a coactivator (p300) or CRMs of target genes remains to be elucidated.

Thus, post-translational regulation of Otx2 repressor activity (Chapter II) in addition to combinatorial regulations with partner TFs (Chapter I) may allow Otx2 to play versatile roles during development. As exemplified by Otx2, other TFs could be modulated by post-translational modifications including phosphorylation, ubiquitination, methylation, and so on, and by combinations of partner TFs as well as coactivators or repressors, thereby generating the diversity of multiple outputs in gene regulation for cellular and developmental processes. Further elucidation of how TFs are regulated at various levels is necessary to understand the general principal of gene regulatory networks during development including cell proliferation, patterning, and differentiation.

Conclusion

The thesis study has shown that XXXX and YYYY are involved in eye development in *Xenopus*, and both interact with Otx2 to modulate transcriptional activities of Otx2. I also have shown that Otx2 undergoes phosphorylation *in vivo*, and that phosphomimetic and non-phosphorylatable mutants of Otx2 exhibit distinct activities in cell proliferation, patterning, and differentiation in *Xenopus* embryos. Based on these findings, the combinatorial regulation with XXXX and YYYY, and post-translational regulation of Otx2 bring a proper gene expression of Otx2 for cell proliferation, the specification of the eye field and the patterning of neuroectoderm.

Experimental procedures

cDNA cloning, sequence analysis, and constructs

EST clones of *xxxx* (clone name XXXX) and *yyyy* (YYYY) in *X. laevis* were previously reported (Takahashi et al., 2005). Dr. Mamada PCR-amplified the full-length cDNA for *yyyy* and a 3'-portion of the *xxxx* and cloned them into the pCSf107-mT vector, which contains SP6 terminator sequences downstream of the SV40 polyadenylation signal (Mii and Taira, 2009). The 5'-portion of *xxxx* (2078 bp) was purchased from Open Biosystems (IMAGE 5065565) and cloned into the 3'-portion of the *xxxx* at BamHI/AflII sites of pCSf107-mT to reconstruct the full-length cDNA *xxxx.S* (accession number XM_018249724). The coding sequences (CDSs) of XXXX [amino acid numbers, 1-1136] and YYYY [1-545] were PCR-cloned into the pCSf107mT, pCSf107_Venus_mT (for Venus constructs), pCSf107_MTmT (Myc constructs) and pCSf107_4HAmT (HA constructs) vectors (Shibano et al., 2015). PCR fragments of deleted CDSs of XXXX (BTB domain [1-581]), ZF domain [582-1136]) were cloned into the pCSf107-Venus_mT. Predicted domain search was done using Pfam (http://www.sanger.ac.uk/Software/Pfam/). Point mutants and deletion constructs of Otx2 were made by using PCR-mediated methods. PCR fragments of Otx2 mutants were cloned into the pCSf107mT, pCSf107_MTmT and pCSf107_4HAmT vectors. To construct the stable mutant of cyclin B1, pGEX-GST-ΔN106cyclin B1 (Iwabuchi et al.,

2002) was re-cloned into pCSf107_HAmT. To construct the stable mutant of cyclin A1, pGEM-Δcyclin A (deletion of 55 amino acids from the N terminus of the protein) gifted by Dr. Furuno (Hiroshima University) was re-cloned into pCSf107_HAmT. All constructs made in this study are listed in Table. 1.

Xenopus *embryo and microinjection*

Xenopus laevis and *Xenopus tropicalis* embryos were obtained by artificial fertilization, dejellied, and incubated in 0.1x Steinberg's solution (Peng, 1991). Embryos were staged according to the normal table of Nieuwkoop and Faber (Nieuwkoop and Faber, 1967). Microinjection of mRNA or antisense morpholino oligos (MOs) were done with a fine glass capillary and a pneumatic pressure injector IM300 (Narishige) in 3% Ficoll in 1x Modified Bath's solution (Peng, 1991). Injected embryos were kept in 3% Ficoll in 1x Modified Bath's solution for 2–3 h, transferred into 0.1x Steinberg's solution containing 50 μg/ml gentamicin sulfate, and incubated until embryos reached the appropriate stages. For mRNA synthesis, pCSf107mT constructs, which possess 4x SP6 terminators, were transcribed with SP6 polymerase (mMESSAGE mMACHINE SP6 kit, Ambion). mRNAs were injected into one or two dorsal blastomeres of 2- or 4-cell stage embryos. Nuclear *β-galactosidase* (*nβ-gal*) mRNA (50-100 pg/embryo) or *eGFP* mRNA (250 pg/embryo) was co-injected for lineage tracing. Antisense and standard control MOs were dissolved in water and injected into a dorsal blastomere at 4-cell stages in *X. tropicalis* embryos. FITC-dextran (5 ng/embryo) was coinjected for lineage

tracing in MO-injected experiments. MOs against sequences near the start codon of *xxxx* and *yyyy* were obtained from Gene Tools: zbtb11-MO, 5'-ccaggtagctctcctcgttagacat-3'; yyyy-MO, 5'-cctcgctcttggtggaagtcattgt-3' (antisense ATG codons are underlined). Standard control MO (control-MO) targeting a beta-globin intron was used as a negative control: 5'-cctcttacctcagttacaatttata-3'. Sequences and specificities of antisense MOs for *X. tropicalis otx2* and *otx5* were described previously (Yasuoka et al., 2014).

Observation of subcellular localization of Venus-fused XXXX constructs and YYYY by confocal microscopy

mRNA for Venus-XXXX constructs or -YYYY was injected into one blastomere at the 4-cell stage. Injected gastrula embryos were fixed in MEMFA (0.1 M MOPS, pH 7.4, 2 mM EGTA, 1 mM $MgSO_4$, 3.7% formaldehyde) for 1 hour, followed by removing the vitelline membrane, and washed three times with MEM (0.1 M MOPS, pH 7.4, 2 mM EGTA, 1 mM $MgSO_4$). Confocal microscopic analyses were performed with LSM 710 (Zeiss).

Whole-mount in situ hybridization (WISH)

WISH was performed according to Harland (Harland, 1991) with BM purple (Roche) as a substrate. Antisense *xxxx* and *yyyy* probes were transcribed with T7 RNA polymerase from BamHI-linearized pCSf107-*xxxx*-T and pCSf107-*yyyy*-T plasmids. Other antisense RNA probes were transcribed from linearized plasmids as described in Table. 2.

Western blot analysis

Lysates were prepared from embryos (stages 10-10.5 otherwise mentioned) that had been injected with mRNA into both blastomeres in the animal pole region at the 2-cell stage. SDS-polyacrylamide gel electrophoresis (PAGE) was carried out with 7.5-10% polyacrylamide gels for detecting the bands of XXXX and YYYY, and with 12-12.5% polyacrylamide gels for detecting modified bands of Otx2. Western blotting was performed essentially as described (Shibano et al., 2015), using anti-Myc (9E10, 1:10000 dilution), anti-HA (12CA5, 1:10000), anti-GFP IRDye 800 conjugated (Rockland Immunochemicals Inc., 600-132-215, 1:5000), anti-Otx2 (Sudou et al., 2012, 1:2500), and anti-p44/42 MAP kinase and anti-phospho-p44/42 MAP kinase (CST inc., 1:2500) antibodies. For secondary antibodies, 'Goat anti-Mouse IgG (H+L) Highly Cross-Adsorbed Secondary Antibody and Alexa Fluor 680' (Invitrogen, A21058, 1:7500) and anti-rabbit IRDye® 800 conjugated antibodies (Rockland, 611-132-122, 1:5000) were

used for detecting with the Odyssey Infrared Imaging system (LI-COR Biosciences)., and Peroxidase AffiniPure F(ab')$_2$ Fragment Goat Anti-Rabbit IgG F(ab')$_2$, Fragment Specific (Jackson Immuno Research inc., 111-036-047, 1:5000) was used for detecting with enhanced chemiluminescence (Amersham ECL prime) (GE Healthcare, RPN2236).

Co-immunoprecipitation assay

mRNAs were injected into the animal pole region of 2-cell stage *X. laevis* embryos. Injected embryos were cultured at 14-21°C until the gastrula stages (stages 10.5-11), homogenized in 500 μl lysis buffer (50 mM Tris-HCl, pH 8.0, 5 mM EDTA, 100 mM NaCl, 10% glycerol, 8 mM DTT, 40 μg/ml leupeptin, 20 μg/ml aprotinin, 1 mM PMSF) containing 0.1% NP40. The lysate was centrifuged at 13,000 rpm (16,000 xg) for 20 minutes at 4°C, and the 400 μl supernatant was transferred into a new tube. The supernatant was incubated with anti-Myc or anti-HA antibody at 4°C for more than 2 hours. Thereafter, 20 μl of protein G/protein A Sepharose beads (Merck IP05) were added and incubated more than 2 hours. Subsequently, the Sepharose bead were washed six times with lysis buffer. Bound proteins were eluted by boiling in 2×SDS sample buffer, separated by SDS-PAGE (7.5% gel, 10% gel or 12.5% gel), and analysed by western blotting with anti-Myc or anti-HA or anti-GFP antibodies.

Luciferase reporter assays

Embryos were injected SOP-FLASH, pGL4p-*meis3*-D2-luc, or pGL4.23-*wnt8*-U1-luc reporter with mRNAs into two dorsal animal blastomeres at the 2- or 4-cell stage. Five pools of three injected embryos were assayed for luciferase activity at stage 10.5 for pGL4p-*meis3*-D2-luc reporter or pGL4.23-*wnt8*-luc reporter, and at stage 12 for SOP-FLASH assay.

In vitro translation and protein phosphatase treatment

In vitro translation was performed using the TNT SP6 Quick-Coupled Transcription/Translation System (Promega) as described (Yamamoto et al., 2003). For λ-protein phosphatase (λ-PP) treatment, embryonic lysate was incubated in 1× λ-PP buffer with 1 μl of λ-PP (NEB) at 37 °C for 1 hour, and analysed by western blotting.

Immunoprecipitation (IP) assays for putative phosphorylated Akt sites and the detection of endogenous Otx2 protein

Possible Akt sites of Otx2 were searched for the database PhosphoSitePlus, (www.phosphosite.org/). Immunoprecipitates with anti-Myc antibody were boiled in

2×SDS sample buffer, and analysed by western blotting with anti-Phospho-Akt Substrate antibody (CST inc., 110B7E). To detect the endogenous Otx2, we modified the preparation of embryonic lysate. *Xenopus* neurula embryos (approximately 800 embryos) were homogenized with 2.5 μl lysis buffer A (50 mM Tris-Cl, pH 8.0, 10% glycerol, 0.1%NP-40, 40 μ g/ml aprotinin, 20 μg/ml leupeptin, 1 mM PMSF) plus 400 mM NaCl per embryo, and homogenates were centrifuged at 4°C for 1hr at 13,000 rpm (16,000 xg). Supernatants were diluted four times with buffer A, and centrifuged at 4°C for 1hr at 13,000 rpm. Eleven ml of Lysate were incubated with 5 μg of the anti-Otx2 antibody (Sudou et al., 2012) and 25 μl of protein A-agarose beads (Roche). The Sepharose beads were washed six times with lysis buffer. The resulting immunoprecipitates were solubilizing by boiling in 2×SDS sample buffer, and analysed by SDS-PAGE with a 15% polyacrylamide gel and western blotting with anti-Otx2 antibody (Abcam, ab21990, 1:2000 dilution).

Quantitation of the eye size in tailbud stage embryos

Embryos injected for phenotypic analysis were reared until stages 38-42 and fixed with

MEMFA for 1 hour. Experiments were carried out with at least three clutches. The lengths of semi-major and semi-minor axes of the eye vesicle were measured, and the eye size were calculated by the formula for the area of an ellipse.

Immunostaining for PH3 and DAPI nuclear staining

mRNA or MO with eGFP mRNA or FITC dextran, respectively, as a lineage tracer was injected into one blastomere at the 4-cell stage. Injected gastrula or neurula embryos were fixed with MEMFA for 1 hour, during which the vitelline membrane was manually removed, dehydrated with methanol, and stored at -20°C. Fixed embryos were rehydrated sequentially in 75% and 50% methanol, 25% methanol/75% TBT (25 mM Tris-Cl, pH 7.4, 137 mM NaCl, 2.7 mM KCl, 0.2% BSA, 0.1% TritonX-100), then TBT, and blocked with TBTS (10% lamb serum in TBT) at room temperature for 1 hour. Treated embryos were incubated overnight at 4°C with rabbit Anti-phospho-Histone H3 (Ser10) Antibody (Millipore, 1:500 dilution), and washed 6 times with TBT. Embryos were incubated over 3 hours at room temperature with goat Alexa Fluor 555-conjugated anti-rabbit IgG antibody (Molecular Probes, 1:500 dilution) as secondary antibody. Nuclei were stained with 400 ng/ ml DAPI. Confocal microscopic analysis was performed with LSM 710 (Zeiss). Embryos with a lineage tracer in the ANE were selected for counting PH3- or DAPI-positive nuclei in an area (0.44 mm^2) in the ANE on the injected or uninjected side. The effect was scored by dividing the number of nuclei

on the injected side with that on the uninjected side. The statistical significance (*P*-value) was calculated using Student's *t*-test after a one-way analysis of variance (ANOVA). Eexperiments were carried out with four or three clutches for mRNA or MO injection experiments, respectively.

Tables and Figures

Table. 1. The list of plasmid constructs

Plasmid names	Cloning sites	Vectors	Comments
pCSf107_XXXX_T	*Bam*HI, *Xba*I	pCSf107_mT	aa 1-1136 (Full length: FL); XXXX.S (*X. laevis*), XM_018249724
pCSf107_Myc-XXXX_T	*Bam*HI, *Asc*I	pCSf107_MycmT	Replaced pCSf107-XXXX_T
pCSf107_HA-XXXX_T	*Bam*HI, *Asc*I	pCSf107_HAmT	Replaced pCSf107-XXXX_T
pCSf107_Venus-XXXX_T	*Bam*HI, *Xba*I	pCSf107_venus-mT	
pCSf107_Venus-BTB_T	*Bam*HI, *Xba*I	pCSf107_venus-mT	aa 1-581 (N-terminal BTB domain)
pCSf107_Venus-ZF_T	*Bam*HI, *Xho*I	pCSf107_venus-mT	aa 582-1136 (C-terminal Zinc fingers)
pCSf107_Venus-NLS-BTB_T	*Bam*HI, *Sac*II	pCSf107_Venus-NLS-mT	Replaced pCSf107_Venus-BTB_T
pCSf107_YYYY_T	*Bam*HI, *Xba*I	pCSf107_mT	aa 1-545 (Full length: FL); YYYY.L (*X. laevis*),
pCSf107_Venus-YYYY_T	*Bam*HI, *Xba*I	pCSf107_venus-mT	
pCSf107_XXXX-ATG-eGFP_T	*Bam*HI, *Xba*I	pCSf107_mcs2-eGFP-C2mT	
pCSf107_YYYY-ATG-eGFP_T	*Bam*HI, *Xba*I	pCSf107_mcs2-eGFP-C2mT	
pCSf107_MycOtx2FL_T	*Bam*HI, *Xba*I	pCSf107_MTmT	aa 1-288 (Full length: FL); Otx2.S (*X. laevis*), NP_001084160
pCSf107_MycOtx2FL-K87Q_T	*Bam*HI, *Xba*I	pCSf107_MTmT	
pCSf107_MycOtx2FL-K87E_T	*Bam*HI, *Xba*I	pCSf107_MTmT	
pCSf107_MycOtx2HD_T	*Bam*HI, *Xba*I	pCSf107_MTmT	aa 1-96 (constructed by Ms. Hosono)
pCSf107_MycOtx2ΔAD_T	*Bam*HI, *Xba*I	pCSf107_MTmT	aa 1-184 (constructed by Ms. Hosono)

pCSf107_MycOtx2AD_T	*Bam*HI, *Xba*I	pCSf107_MTmT	aa 185-288 (constructed by Ms.Hosono)
pCSf107_MycOtx2ΔRD_T	*Bam*HI, *Xba*I	pCSf107_MTmT	aa 1-96/185-288 (constructed by Ms. Hosono)
pCSf107_MycOtx2ΔAD-T115A_T	*Bam*HI, *Xba*I	pCSf107_MTmT	
pCSf107_MycOtx2ΔAD-S116A_T	*Bam*HI, *Xba*I	pCSf107_MTmT	
pCSf107_MycOtx2ΔAD-S122A_T	*Bam*HI, *Xba*I	pCSf107_MTmT	(constructed by Mr. Minami)
pCSf107_MycOtx2ΔAD-S123A_T	*Bam*HI, *Xba*I	pCSf107_MTmT	(constructed by Mr. Minami)
pCSf107_MycOtx2ΔAD-S132A_T	*Bam*HI, *Xba*I	pCSf107_MTmT	(constructed by Mr. Minami)
pCSf107_MycOtx2ΔAD-S153A_T	*Bam*HI, *Xba*I	pCSf107_MTmT	(constructed by Mr. Minami)
pCSf107_MycOtx2ΔAD-S158A_T	*Bam*HI, *Xba*I	pCSf107_MTmT	(constructed by Mr. Minami)
pCSf107_MycOtx2ΔAD-S161A_T	*Bam*HI, *Xba*I	pCSf107_MTmT	(constructed by Mr. Minami)
pCSf107_MycOtx2ΔAD-3A_T	*Bam*HI, *Xba*I	pCSf107_MTmT	S116A, S132A, S158A
pCSf107_MycOtx2ΔAD-4A_T	*Bam*HI, *Xba*I	pCSf107_MTmT	T115A, S116A, S132A, S158A
pCSf107_MycOtx2ΔAD-2A(S158)_T	*Bam*HI, *Xba*I	pCSf107_MTmT	S116A, S132A
pCSf107_MycOtx2ΔAD-2A(S132)_T	*Bam*HI, *Xba*I	pCSf107_MTmT	S116A, S158A
pCSf107_MycOtx2ΔAD-2A(S116)_T	*Bam*HI, *Xba*I	pCSf107_MTmT	S132A, S158A
pCSf107_Otx2-WT_T	*Bam*HI, *Xba*I	pCSf107_mT	Wild type: WT
pCSf107_Otx2-4E_T	*Bam*HI, *Xba*I	pCSf107_mT	T115E, S116D, S132E, S158E
pCSf107_Otx2-T115A_T	*Bam*HI, *Xba*I	pCSf107_mT	
pCSf107_Otx2-3A_T	*Bam*HI, *Xba*I	pCSf107_mT	S116A, S132A, S158A
pCSf107_Otx2-4A_T	*Bam*HI, *Xba*I	pCSf107_mT	T115A, S116A, S132A, S158A
pCSf107_Otx2-A2A(S116)_T	*Bam*HI, *Xba*I	pCSf107_mT	T115A, S132A, S158A
pCSf107_Otx2-A2A(S132)_T	*Bam*HI, *Xba*I	pCSf107_mT	T115A, S116A, S158A
pCSf107_Otx2-A2A(S158)_T	*Bam*HI, *Xba*I	pCSf107_mT	T115A, S116A, S132A
pCSf107_Otx2ΔAD-4A_T	*Bam*HI, *Xba*I	pCSf107_mT	
pCSf107_Otx2ΔAD-4E_T	*Bam*HI, *Xba*I	pCSf107_mT	
pCSf107_HA-cyclin A1*_T	*Bam*HI, *Xho*I	pCSf107_4HAmT	Replaced Δcyclin A1 (from Dr. N. Furuno)
pCSf107_HA-cyclin B1*_T	*Bam*HI, *EcoR*I	pCSf107_4HAmT	Replaced GST-ΔN106cyclin B1 (Iwabuchi et al., 2002)
pCSf107_p27xic1_T	*Bam*HI, *Xho*I	pCSf107_mT	

pCSf107_HATLE1_T	*Age*I, *Xba*I	pCSf107_4HAmT	Replaced pCSf107-TLE1
pCS2+Gsc	*Nco*I, *Sal*II	pCS2+	
pCSf107_pax6_T	*Sfu*I, *Not*I	pCSf107_mT	replaced pCS105-pax6

Note: the postfix "_T" indicates the presence of SP6/T7 terminators at the end of the transcribed region.

Table. 2. The list of cutting sites and RNA polymerases for the in vitro transcription of anti-sense RNA probe.

Plasmid names	Cutting sites	RNA polymerase
pCSf107_XXXX_T	*BamHI*I	T7
pCSf107_YYYY_T	*BamHI*I	T7
pCSf107_p27xic1_T	*BamHI*I	T7
pCS2+_Sox2	*Hind*III	T7
pCSf107_Otx2-WT_T	*BamHI*I	T7
pBS SK(-)gbx2	*EcoR*I	T3
pCS107BSX_rax	*Xho*I	SP6
pCSf107_pax6_T	*Sal*I	T7
pDH105(CS2)_XSix3		T7
BS4A 3(X pax2-2a)	*EcoR*I	T3
pBSK_xcg1	*NotI*I	T3

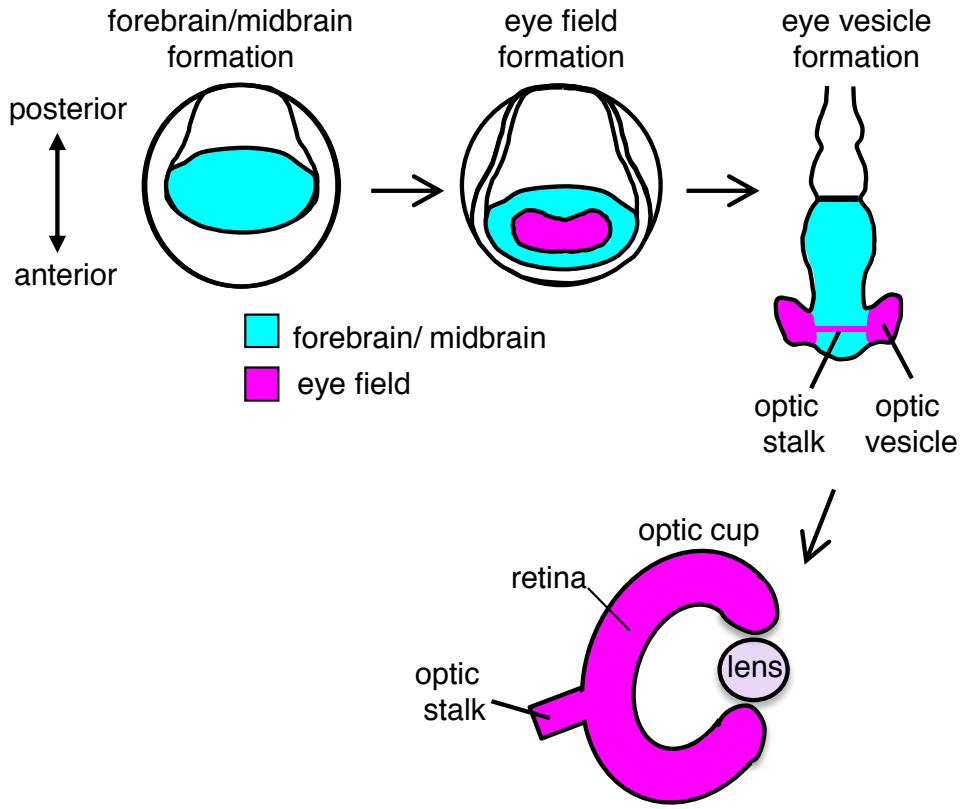

Fig. 1. Developmental processes of vertebrate eye.

In the neurula embryo, the neural plate is divided into the presumptive forebrain-midbrain region and hindbrain region, respectively, in terms of the anteroposterior position. As the first step of vertebrate eye development, the eye field, in which the eyes will be formed is specified in the center of the forebrain. The eye field is gradually separated into two bilateral regions to give rise to the optic vesicles, and subsequently the optic cup and retina are formed.

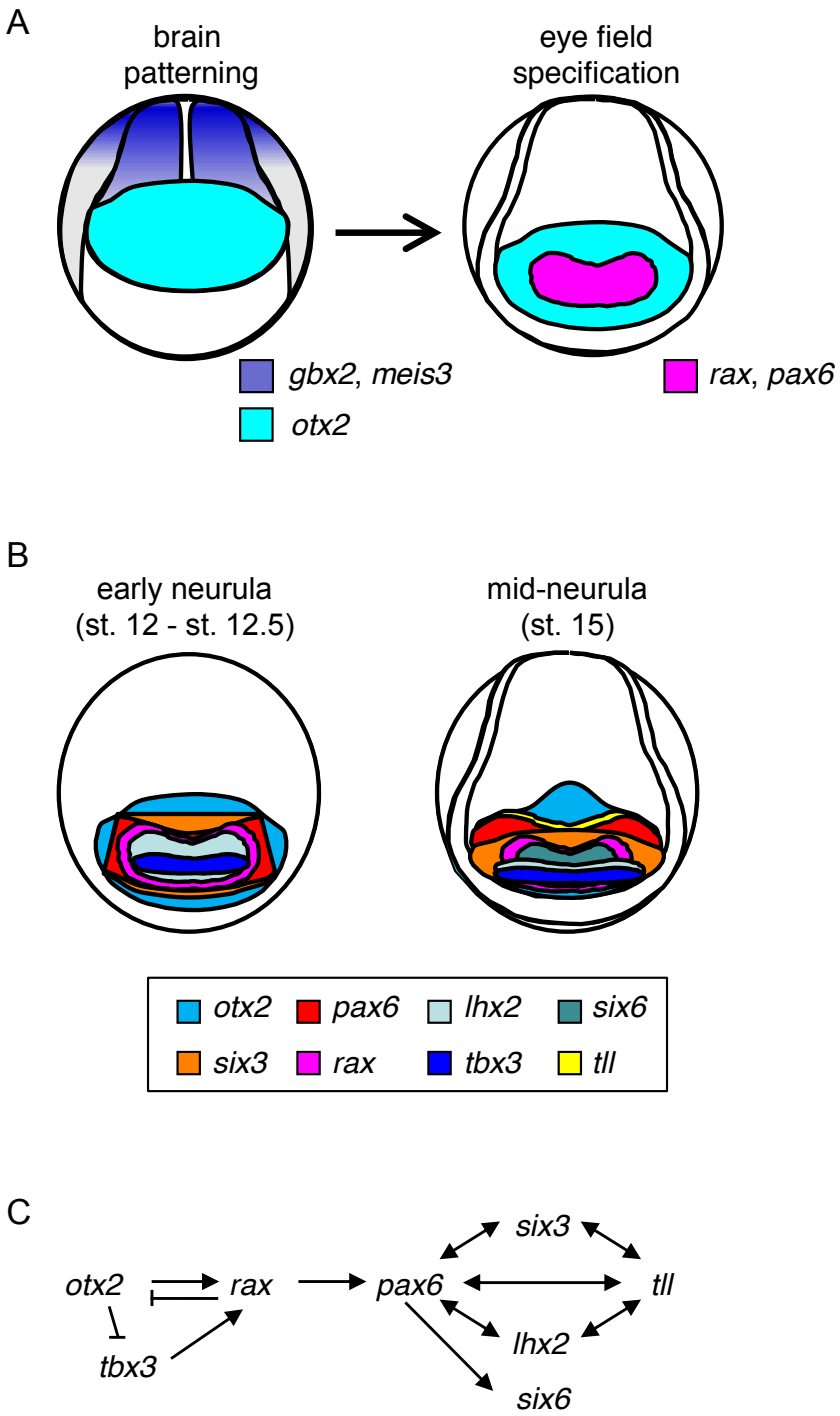

Fig. 2. A model of eye field formation in the anterior neural plate.

(A) Expression patterns of TFs *otx2* (forebrain and midbrain, light blue), *gbx2* and *meis3* (hindbrain, blue), *rax* and *pax6* (eye field, magenta) in early *Xenopus* neurula embryos. For the anteroposterior patterning in the neuroectoderm, *otx2* is expressed in the forebrain and midbrain, and *gbx2* and *meis3* are expressed in the hindbrain. During late gastrulation, EFTF genes, *rax* and *pax6*, are expressed in the center of the region where *otx2* is expressed. (B) A schematic model of gene expression patterns of known EFTFs in early neurula (stages 12-12.5, left) and mid-neurula (stage 15, right) embryos. (C) A gene cascade of eye field specification. In the early step of eye field specification, *otx2* upregulates the expression of *rax* and subsequently the expression of *pax6* is activated, and *otx2* represses the expression of *tbx3*. During mid-step for eye field specification, *rax* in turn represses *otx2*, forming a negative feedback loop between *otx2* and *rax*. In addition, the expression of other EFTFs (*six3*, *lhx2*, *six6*, and *tll*) downstream of *pax6* starts to be expressed.

Fig. 3〜Fig. 12については、5年以内に雑誌で刊行予定のため、非公開。

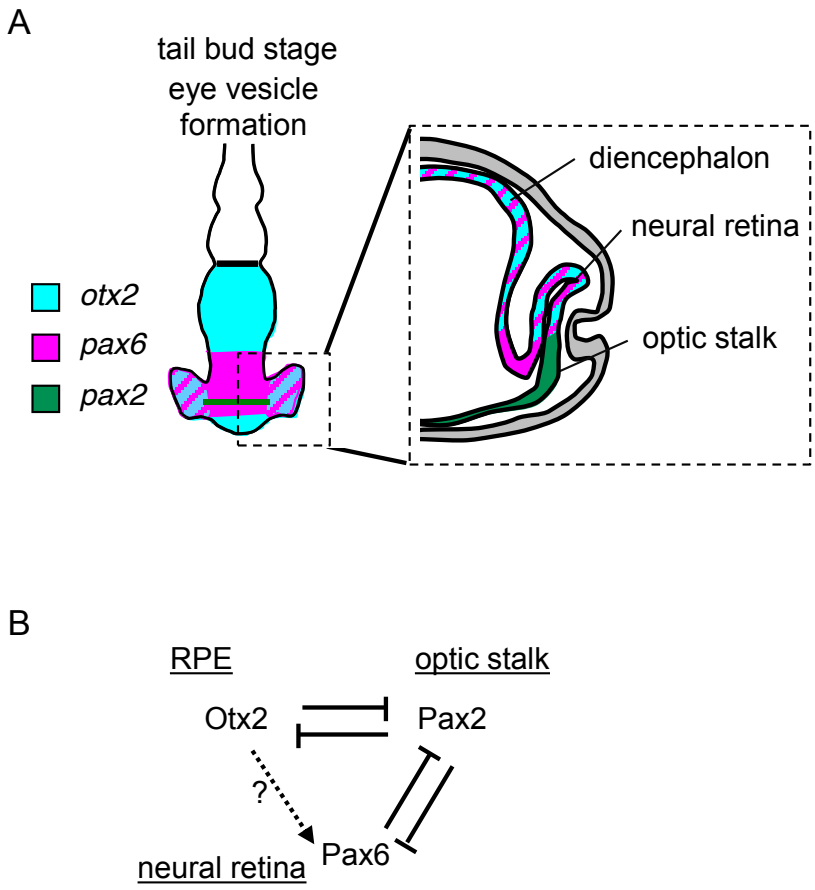

Fig. 13. Expression patterns and gene interactions involved in the patterning of eye vesicle.

(A) Expression patterns of *otx2*, *pax6* and *pax2* in the diencephalon, neural retina and optic stalk. (B) A model for gene interactions for the establishment of the territories of eye vesicle. The reciprocal repression of Otx2 and Pax2 determines the segregation of RPE (the retinal pigment epithelium)/OS (optic stalk), and the similar mechanism is proposed for Pax2 and Pax6 interaction in the establishment of RPE/NR (neural retina). It remains to be elucidated whether Otx2 contributes to the direct regulation of *pax6*.

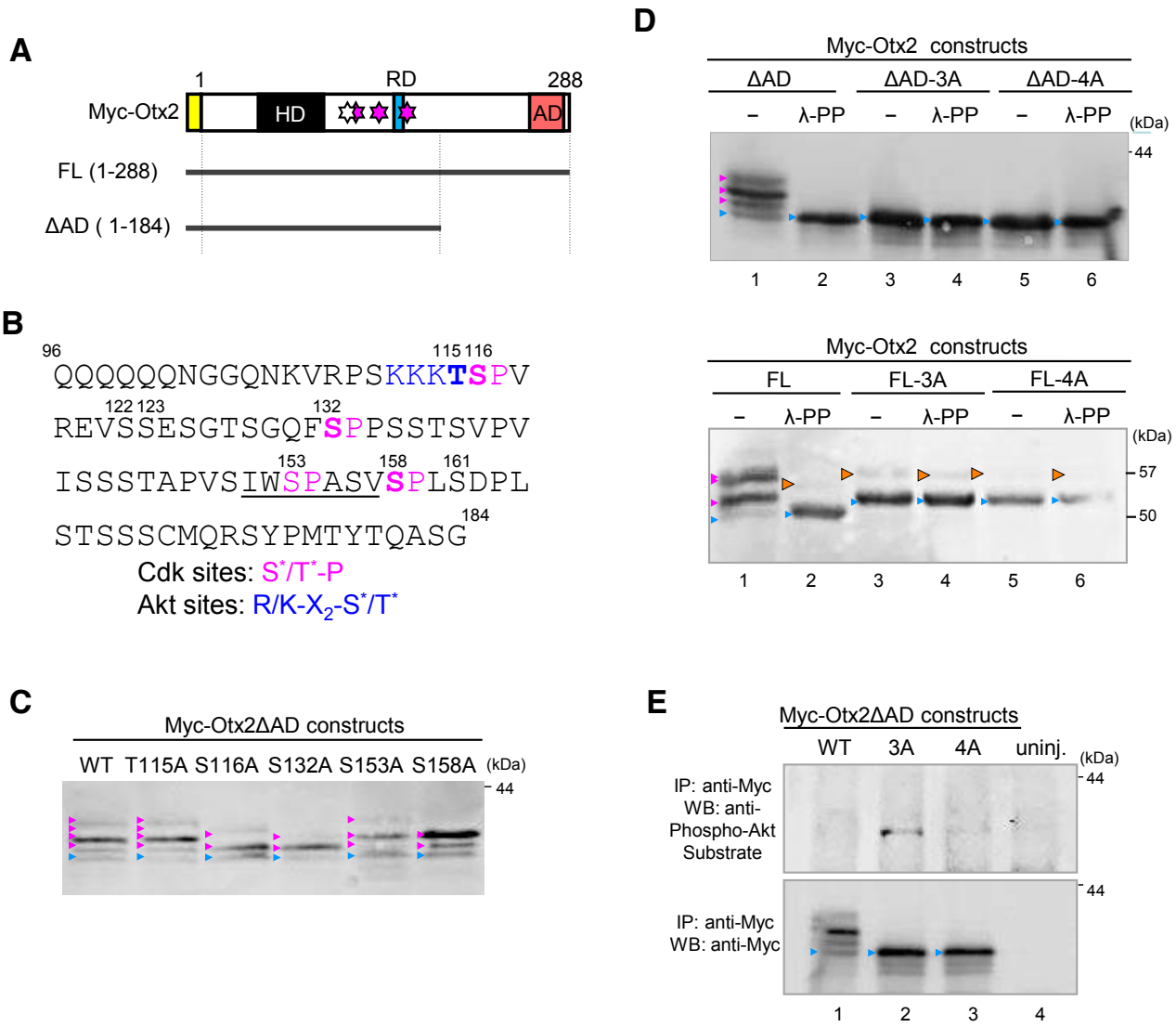

Fig. 14. Exogenous Otx2 is phosphorylated.

(A) Schematic structures of Myc-Otx2 and deletion constructs. The homeodomain (HD), repression domain (RD) and activation domain (AD) are indicated. A Myc-tag at the N-terminus is indicated as a yellow box. White star, Akt site; pink stars, Cdk sites. The regions of Otx2 constructs are indicated by thick lines and positions of amino acid residues are indicated in parentheses. (B) Amino acid sequences around the repression domain. Colored cases indicate the consensus motif for Cdks (magenta) and Akt kinase (blue). Bold cases indicate modified serine and threonine residues that were suggested in the experimental process (T115, S116, S132 and S158). Under line, the eh1 motif of the repression domain. Consensus motifs for Cdk and Akt are indicated at the bottom. *, phosphorylated serine/threonine residues. (C) Western blotting of Myc-Otx2ΔAD constructs, WT and alanine mutants at T115 (T115A), S116 (S116A), S132 (S132A), S153 (S153A) and S158 (S158A). (D) Western blotting of Myc-Otx2ΔAD (upper) and Myc-Otx2FL constructs (lower), WT, 3A and 4A with or without λ-protein phosphatase (λ-PP) treatment. (E) IP-western assay. Myc-Otx2ΔAD was immunoprecipitated with anti-Myc antibody, and subjected to western blotting with the anti-Phospho-Akt substrate antibody (upper) or anti-Myc antibody (lower). 3A, alanine mutant at S116, S132 and S158; 4A, alanine mutant at T115, S116, S132 and S158; uninj., uninjected control; orange arrowheads, bands resistant to λ-PP. FL, full length; WT, wild type; blue arrowheads, nascent proteins; magenta arrowheads, modified proteins. Size markers (kDa) are indicated on the right of panels (C,D,E).

Fig. 15. Alignment of amino acid sequences of Otx2 and Otx5/Crx among vertebrates.

Abbreviations of species are *Xenopus laevis* (Xl), *Xenopus tropicalis* (Xt), *Danio rerio* (Dr), *Gallus gallus* (Gg), *Mus musculus* (Mm) and *Homo sapiens* (Hs). Protein sequences were obtained from the NCBI database: Xl_Otx2.L (NP_001084955), Xl_Otx5.L (NP_001081916), Xt_Otx2 (NP_001016177), Xt_Otx5 (NP_001016021), Dr_Otx2 (NP_571326), Dr_Otx5 (NP_851848), Gg_Otx2 (NP_989851), Gg_Otx5 (NP_001288716), Mm_Otx2 (NP_001273412), Mm_Crx (NP_031796), Hs_Otx2 (NP_001257453), Hs_Crx (AAH53672). Boxes coloured in green, homeodomain; blue, SIWSPAS motif; yellow, repeated Otx tail motif; red, Otx2 mutation sites (P133 and P134) that were reportedly associated with human ocular malformation. Blue or magenta letters, consensus motifs for Akt and Cdks. Bold cases, putative phosphorylation sites of Otx2 as shown in this study.

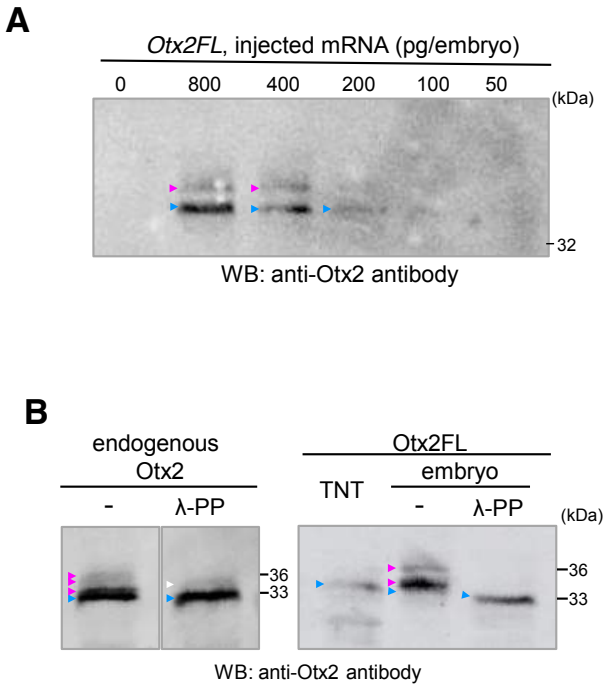

Fig. 16. The detection limit of Otx2FL and phosphorylation of endogenous Otx2 by western blotting.

(A) Embryos were injected with *Otx2FL* mRNA at various doses as indicated. Modified bands of Otx2FL was clearly detected when *Otx2FL* mRNAs were exogenously injected with greater than 400 pg per embryo, but not less than 200 per embryo. Embryonic lysate of 0.42 embryo equivalent was loaded per lane. (B) Western blotting of endogenous Otx2 (left panel) and exogenous Otx2FL construct (right panel) with or without λ-PP treatment. Otx2FL and endogenous Otx2 was detected with anti-Otx2 antibodies (A,B). Blue arrowheads, nascent proteins; magenta arrowheads, modified proteins.

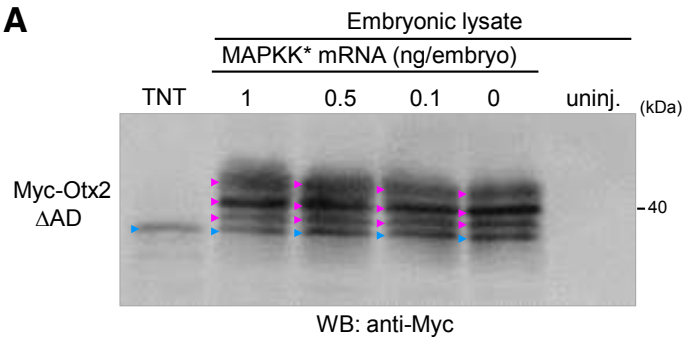

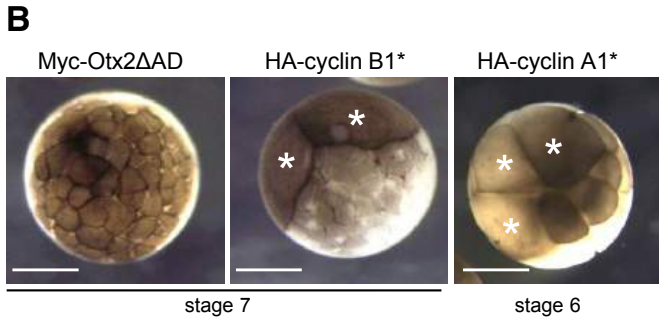

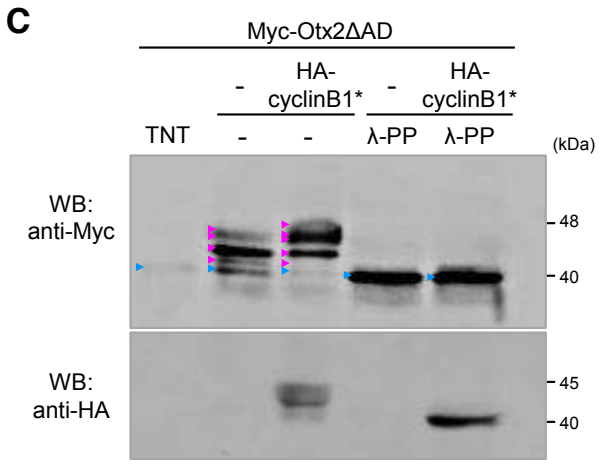

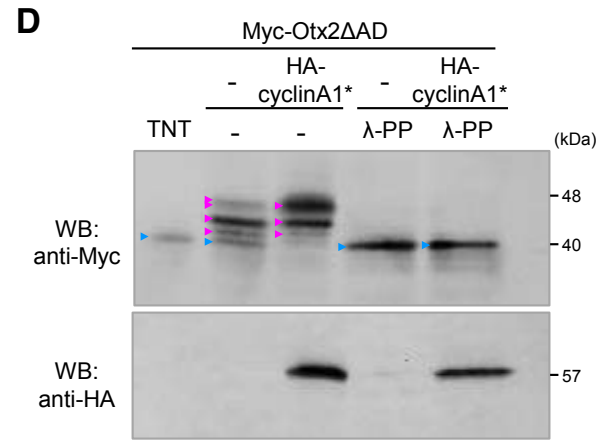

Fig. 17. Effects of MAPK and Cdk on modifications of exogenous Otx2.

(A) No effect of constitutively active mutant of MAPKK (MAPKK*) on modifications of Otx2. Western blotting of Myc-Otx2ΔAD co-expressed with MAPKK*. The amounts of injected *MAPKK*** mRNA were as indicated. mRNAs were injected into the animal pole region of both blastomeres at the 2-cell stage. (B) Phenotypes of Myc-Otx2ΔAD, HA-cyclin B1* (stable mutants of cyclin B1), and HA-cyclin A1* (stable mutants of cyclin A1) overexpressing embryos. Embryos were observed at the early blastula stage (animal pole view). (C,D) Western blotting of Myc-Otx2ΔAD co-expressed with HA-cyclin B1* (C) or HA-cyclin A1* (D). Lysate were treated with λ-PP as indicated. Myc-Otx2ΔAD and HA-cyclin B1* or HA-cyclin A1* were detected with anti-Myc and anti-HA antibodies, respectively. Lysates were prepared from embryos at stage 8 (C) or stage 9 (D). White asterisks, cell cycle-arrested blastomeres. Scale bars, 500 μm.

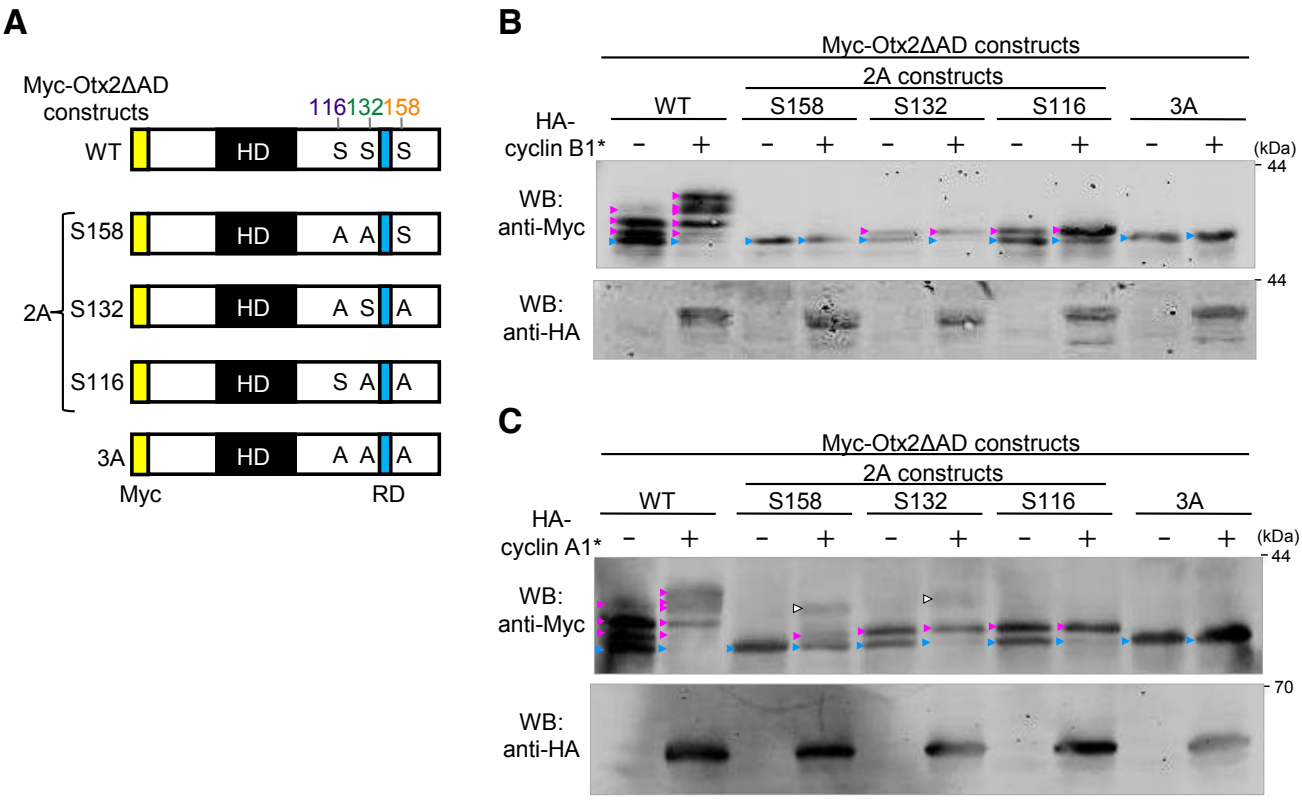

Fig. 18. Preference of cyclin B/Cdk and cyclin A/Cdks for Cdk sites of Otx2.

(A) Schematic presentation of Myc-Otx2ΔAD with double (2A) and triple alanine (3A) mutations at S116, S132 and S158. Yellow box, Myc-tag; black box, homeodomain (HD); blue box, repression domain (RD). In the 2A constructs, for example, the S158 construct indicates mutations at S116 and S132. S, serine phosphorylation sites (S116, S132, S158); A, alanine mutation. (B) Western blotting of Myc-Otx2ΔAD constructs (2A or 3A) co-expressed with (+) or without (-) HA-cyclin B1*. (C) Western blotting of Myc-Otx2ΔAD constructs (2A or 3A) co-expressed with (+) or without (-) HA-cyclin A1*. Blue arrowheads, nascent bands; magenta arrowheads, modified bands; white arrowheads, additional modified bands at sites other than S116, S132 and S158.

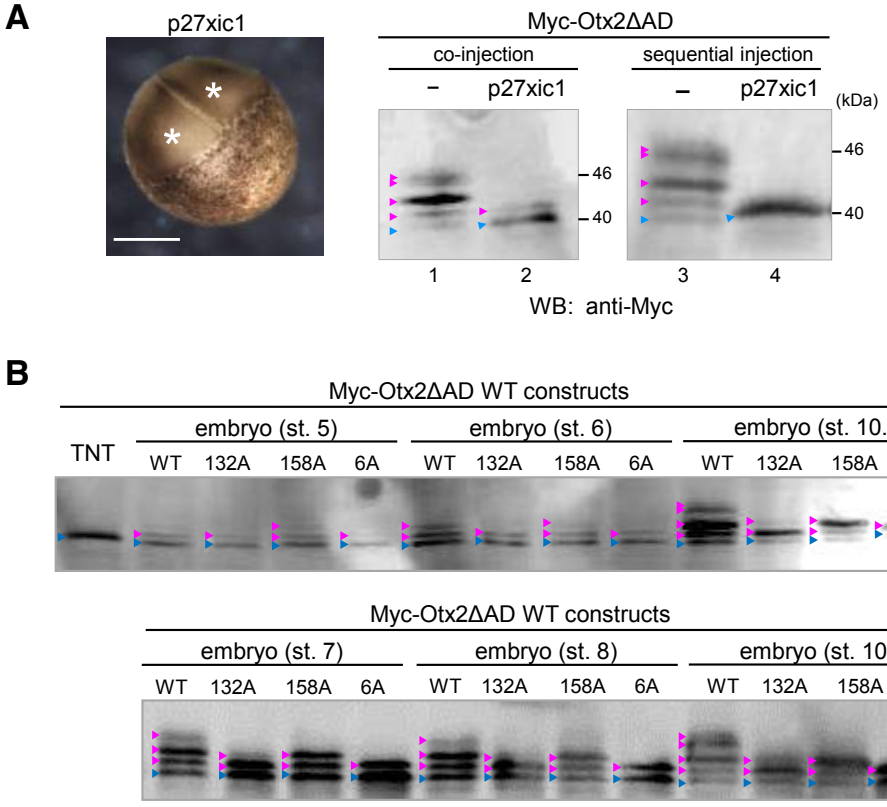

Fig. 19. Effects of p27xic1 to phosphorylation of Otx2 and developmental changes of phosphorylation of Otx2.

(A) Phenotype of p27xic1-overexpressing embryos (left) and western blotting of Myc-Otx2ΔAD co-expressed with p27xic1 (middle, right). Co-injection (middle): *Myc-Otx2ΔAD* mRNA (500 pg/embryo) was coinjected with (lane 2) or without (lane 1) *p27xic1* mRNA (2 ng/embryo) into one blastomere at the 2-cell stage. Sequential injection (right): *p27xic1* mRNA (1.5 ng/embryo) was injected into one blastomere at the 2-cell stage, then mRNAs for *Myc-Otx2ΔAD* (500 pg/embryo) and *p27xic1* (500 pg/embryo) were co-injected into the cleavage-arrested blastomeres at the 32-cell stage equivalent (lane 4). *Myc-Otx2ΔAD* mRNA was injected at the 2-cell stage as control (lane 3). Lysates were prepared from embryos at stage 9 (lanes 1 and 2) or stage 9.5 (lanes 3 and 4). White asterisks, cleavage-arrested blastomeres. Scale bars, 500 μm. (B) Developmental changes of phosphorylation of Otx2 as assayed by using Myc-Otx2ΔAD constructs. WT and alanine mutants of Otx2 in Myc-Otx2ΔAD constructs were analyzed from stages 5 to 10.5 as indicated. TNT, *in vitro* translation products; blue arrowheads, nascent bands; magenta arrowheads, modified bands.

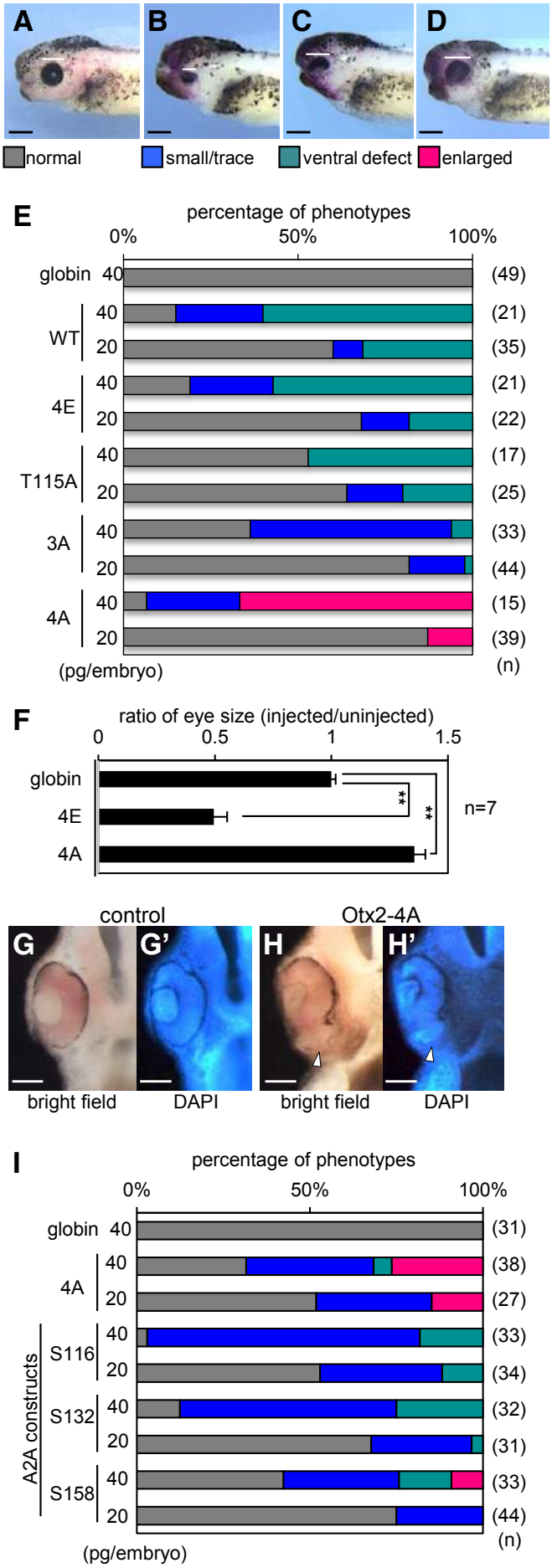

Fig. 20. Phosphomutants of Otx2 exhibit the distinct activity as assessed by developmental eye phenotype.

(A-D) Eye phenotypes of Otx2 mutant-expressing embryos (stages 38-42). mRNA for Otx2 constructs were co-injected with *nβ-gal* mRNA as a tracer. Representative phenotypes in injected embryos (A-D): normal looking (normal), trace eye (trace), normal eye diameter with pigmentation defect at the ventral side (ventral defect) and enlarged retinal diameter with pigmentation defect at the ventral side (enlarged). The white dashed lines indicate the diameter of the eye. Anterior to the left, dorsal is up. Scale bar, 500 μm. (E) Activity of Otx2 mutants for eye malformation phenotypes. The color bar (see panels A-D for color codes) indicates the percentages of the eye phenotype. Low-dose mRNA injection (20 pg/embryo) caused moderate phenotypes than high dose injection (40 pg/embryo). n, total number of injected embryos. (F) Quantitative assay for the ratio of the eye size in tailbud stage embryos (stages 38-42). $^{**}P<0.01$ (t-test); error bars, s.e.m.; n=7 samples. (G-H') Transverse hemisection observations. (G,G') Globin injected control. (H,H') The enlarged eye phenotype of 4A-expressing embryo. Bright field, G,H; DAPI staining, G',H'. Arrowheads, the retinal pigmentation defect at the ventral side. Scale bar, 100 μm.

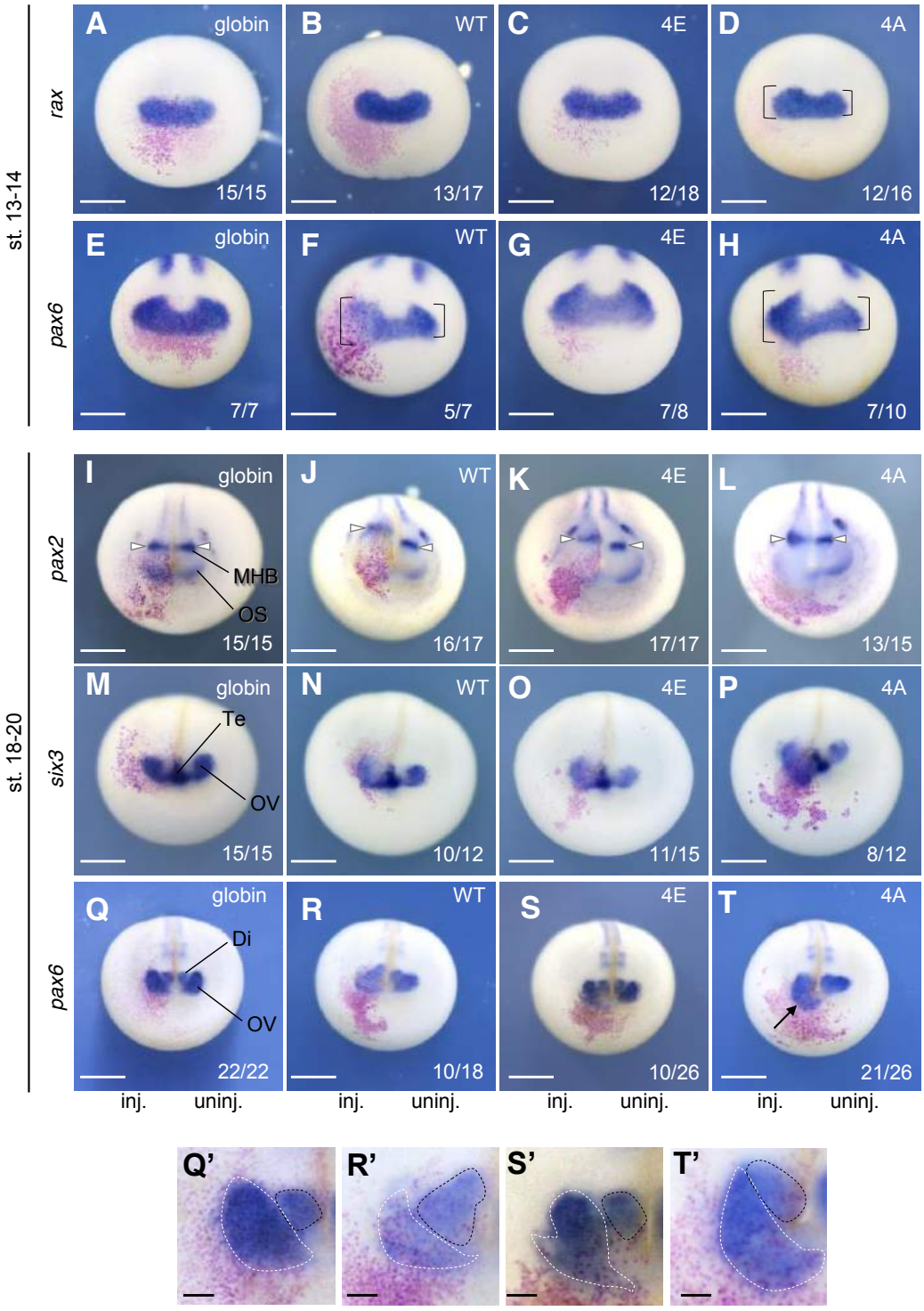

Fig. 21. Increased expression of eye marker genes by Otx2 mutant 4A.

(A-T) mRNA for globin, WT, 4E or 4A (20 pg/embryo) was injected with *nβ-gal* mRNA into the animal pole region of the dorsal-right blastomere at the 4-cell stage, and embryos were subjected to WISH at early neurula stages (stages 13-14) (A-H) and at late neurula stages (stages 18-20) (I-T). MHB, the midbrain-hindbrain boundary; OS, optic stalk; OV, optic vesicle; Te, telencephalon, Di, diencephalon. Arrowhead, the position of MHB; arrow, the expansion of *pax6* expression to the anterior region. Anterior view with dorsal up. Scale bar, 500 μm. (Q'-T') Enlarged images of Q-T. Black and white dash lines indicate diencephalon and optic vesicle regions, respectively, where *pax6* is expressed. Scale bar, 100 μm.

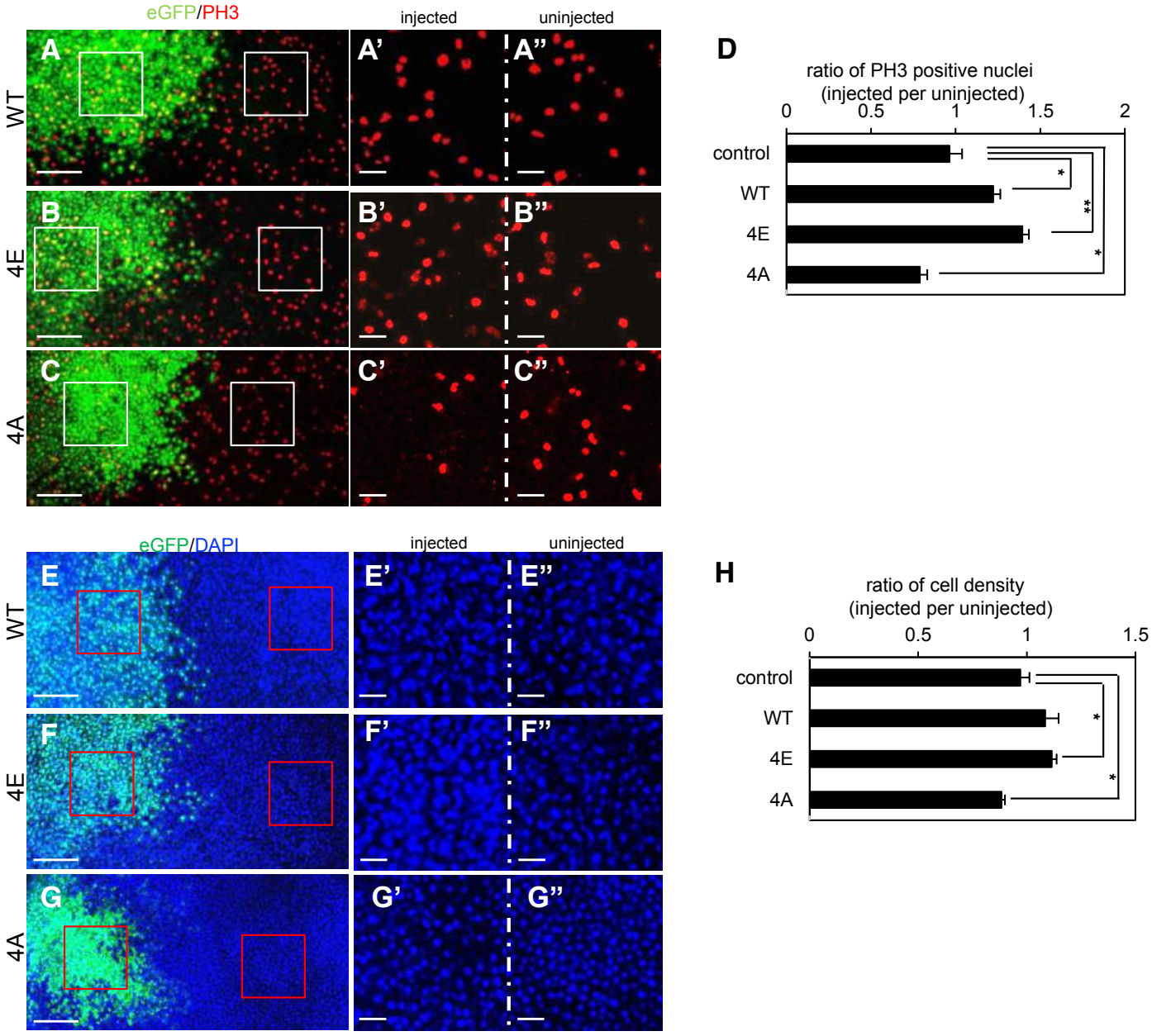

Fig. 22. Phosphomimetic Otx2 mutant 4E stimulates cell proliferation.

(A-C) mRNA for Otx2-WT (A), -4E (B) or -4A (C) together with that for eGFP as a tracer was injected in one blastomere at 2-cell stage. 4E and 4A are glutamate and alanine mutants, respectively, of full length Otx2 at T115, S116, S132 and S158. Embryos were immunostained with anti-phospho-Histone H3 (PH3) at the gastrula stage. The dorsoanterior region was observed. PH3-positive nuclei were shown in red, Otx2 mutant-expressing cells (expressing eGFP) were shown in green. White dash boxes in A-C correspond to enlarged area (A'-C"), respectively. Scale bar, 200 μm. (D) Quantitative assay for the ratio of PH3-positive nuclei. (E-G) Representative images of DAPI-stained nuclei in Otx2-WT (E) or -4E (F) or -4A (G) expressing gastrula embryos. The dorsoanterior region was observed. Nuclei were shown in blue, Otx2 mutant-expressing cells (expressing eGFP) were shown in green. Red boxes in E, F and G correspond to enlarged area (E'-G"), respectively. Scale bar, 200 μm (E-G); 50 μm (E'-G"). (H) Quantitative analysis for cell numbers. More than 500 total nuclei were counted in one embryos, and 5 to 7 embryos were analysed for calculating the mean ratio (and s.e.m.) of the number of nuclei in injected versus uninjected areas. $^{**}P<0.01$ (t-test), $^{*}P<0.05$ (t-test); error bars, s.e.m. (D,H).

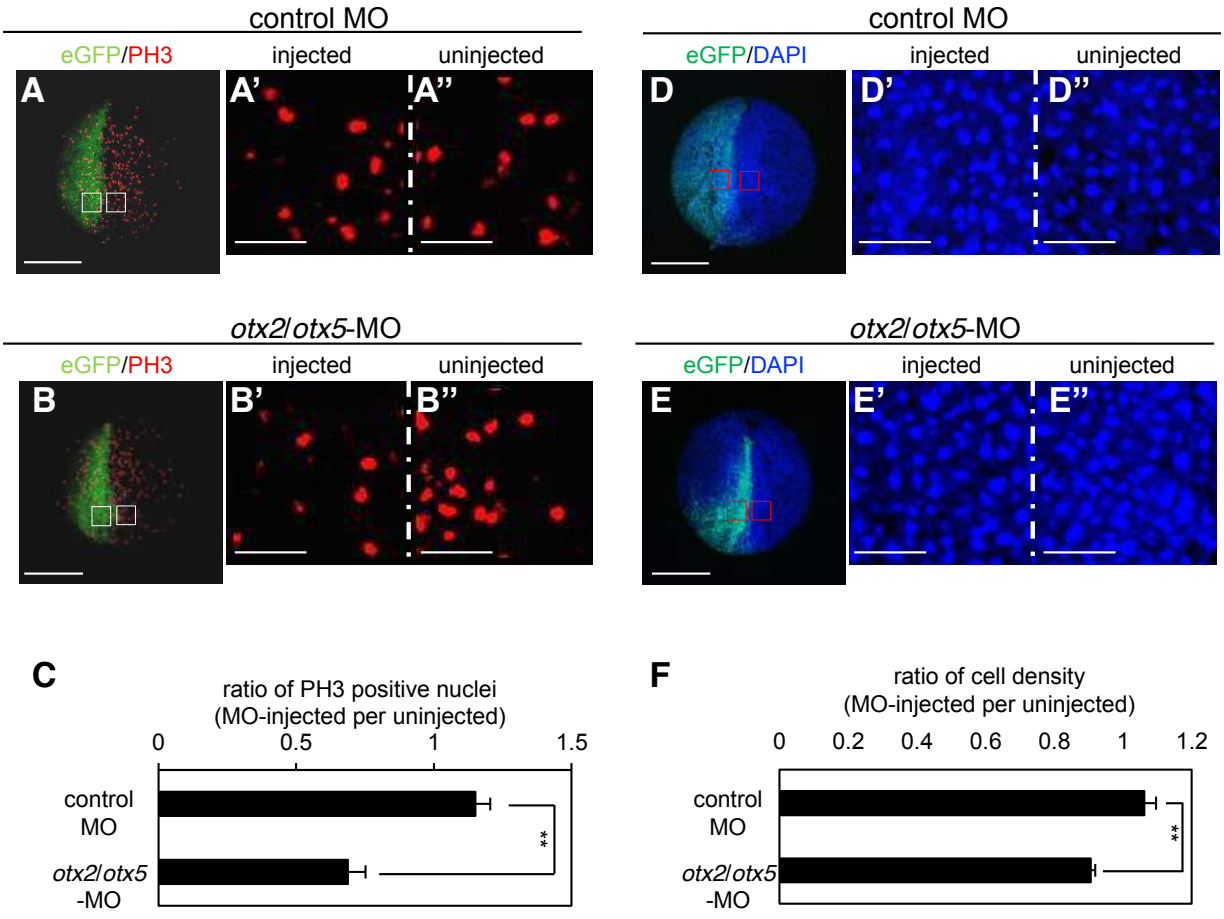

Fig. 23. Reduction of cell proliferation by otx2/otx5 knockdown in Xenopus tropicalis *embryos.*

Knockdown experiments were performed using *Xenopus tropicalis*. (A,B) Effects of *otx2*/*otx5*-MO injection on mitotically active cells. White boxes, enlarged area (A'-B"). (C) Quantitative analysis for the ratio of PH3-positive nuclei. PH3-positive nuclei in an injected or uninjected area (0.072 mm^2) in each embryo were counted (more than 60 nuclei in each area) with 9 embryos, and the ratio of the numbers of injected versus uninjected area was calculated for each embryo to obtain mean ± s.e.m. from 9 embryos. The ratio of PH3-positive nuclei in control MO-injected embryos was 1.15 ± 0.055 (mean ± s.e.m.), whereas that in *otx2*/*otx5*-MOs-injected embryos was 0.688±0.063, which significantly differed from the control (p = 4.95E-05). (D,E) Effects of *otx2*/*otx5*-MO on cell density. Red boxes, enlarged area (D'-E"). (F) Quantitative analysis for the ratio of cell densities. More than 500 total nuclei in each area (0.072 mm^2) were counted in one embryo, and 9 embryos were analysed. The ratio of cell density in control MO-injected embryos was 1.063 ± 0.034 (mean ± s.e.m.), whereas that in *otx2*/*otx5*-MOs-injected embryos was 0.906 ± 0.013, which differed from the control (p = 0.0015). **P<0.01 (t-test); error bars, s.e.m. (C,F). Scale bar, 500 μm (A,B,D,E); 50 μm (A'-B",D'-E",). The amount of injected MO (pmol/embryo): control MO, 1; *otx2*/*otx5*, 0.5 each.

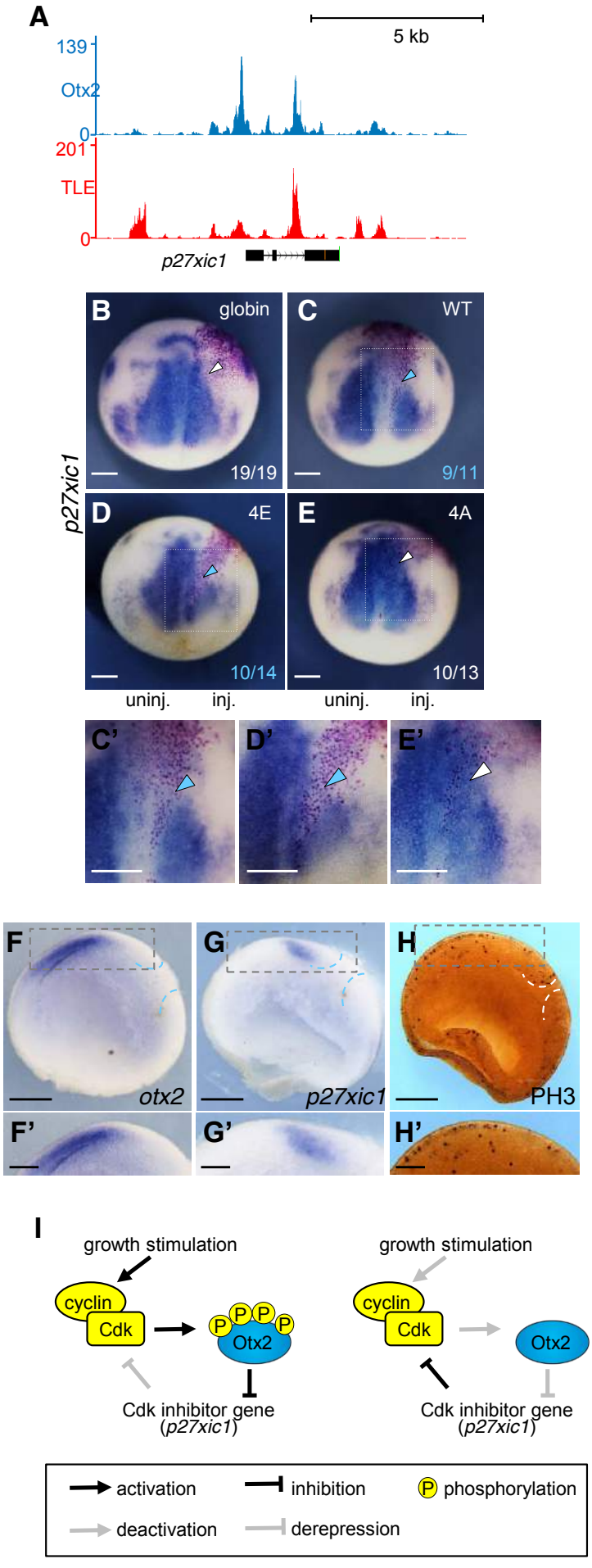

Fig. 24. Phosphomimetic Otx2-4E mutant negatively regulates p27xic1 *expression.*

(A) Genome browser representation showing occupancies of Otx2 and Tle1 in *Xenopus tropicalis* gastrula embryos for the *p27xic1* gene. (B-E) The WISH assay shows the expression of *p27xic1* in Otx2 mutant-expressing embryos. mRNA (30 pg each) for globin (B), WT (C), 4E (D), or 4A (E) was injected with *n*β-*gal* mRNA as a tracer into the animal pole region of the dorsal-left blastomere at the 4-cell stage. The fractions indicate the proportion of the presented phenotype per total number. Dorsal view with anterior up. inj., injected side; uninj., uninjected side. (C',D',E') Enlarged image of C, D and E (white dashed box). Colors of arrowheads: white, normal expression; blue, downregulation (B-E). The regional correlation between the domain where *otx2* and *p27xic1* are expressed. Cross hemisections show the expression of *otx2* (F) and *p27xic1* (G) visualized by WISH, and mitotically active cells by the immunostaining of PH3 (H). Lateral view with dorsal up, and anterior is left. (F',G',H') Enlarged image of F, G and H (gray dashed box). White dashed lines indicate the position of the blastopore. Scale bar, 500 μm (B-H); 250 μm (C'-H'). (I) A schematic model of feedback loops involving Cdk, Otx2, and p27xic in cell-proliferation (left) and non-proliferation states (right). Left, upon growth stimulation, (i) activation of Cdk causes phosphorylation of Otx2, (ii) phosphorylated Otx2 downregulates *p27xic1*, and (iii) the reduction of p27xic1 increases Cdk activity, thereby enhancing both cell proliferation and a phosphorylation state of Otx2. Right, upon the reduction of growth stimulation, (i) reduced Cdk activity causes the reduction of phosphorylation of Otx2, (ii) the reduction of phosphorylated Otx2 derepresses *p27xic1*, and (iii) increased p27xic1 inhibits Cdk activity, thereby reducing both cell proliferation and a phosphorylation state of Otx2.

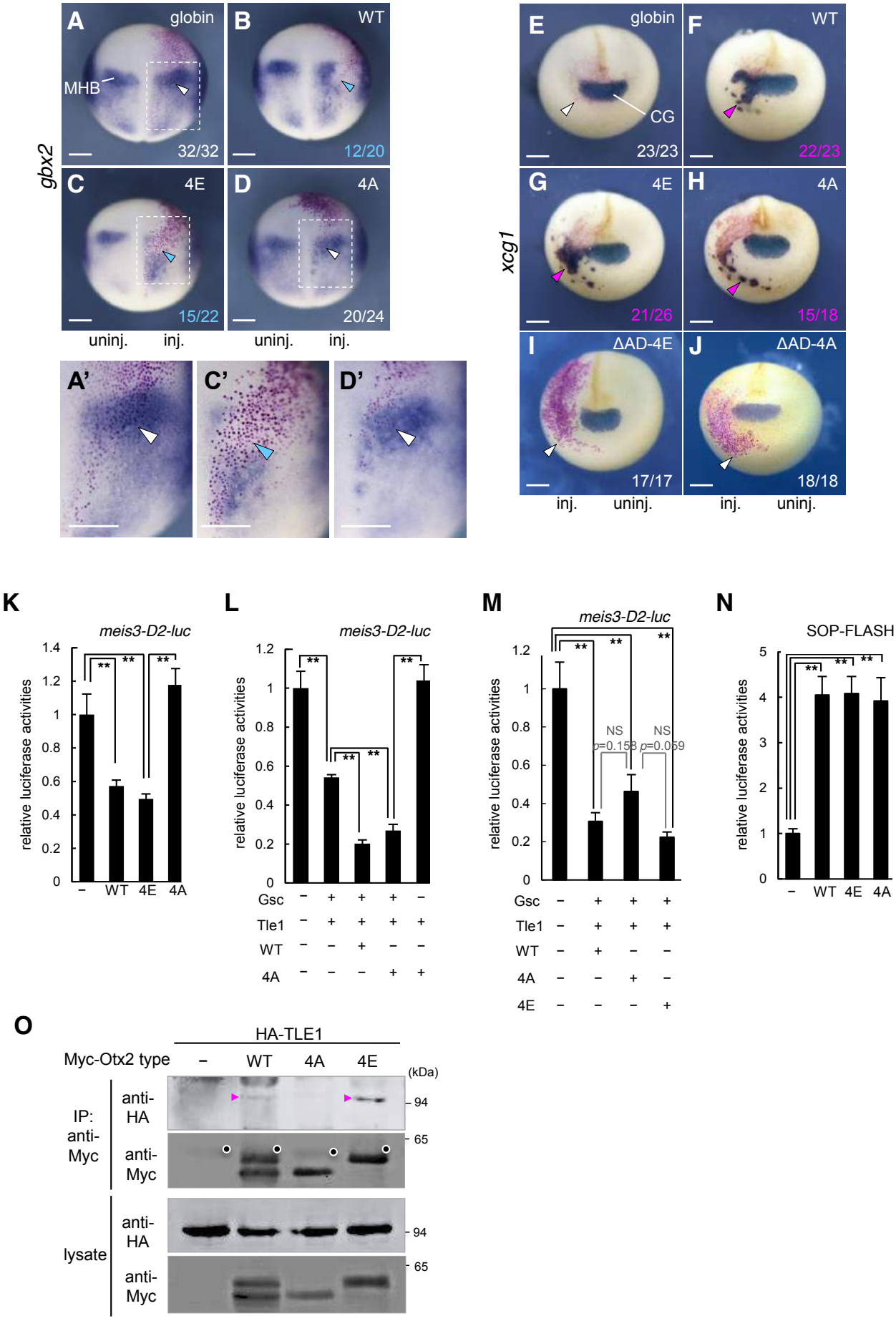

Fig. 25. The repressor activity of Otx2 depends on its phosphorylation.

(A-D) Repression of *gbx2* by 4E. mRNA (30 pg each) for globin (A), WT (B), 4E (C), or 4A (D) was injected with *nβ-gal* mRNA into the animal pole region of a dorsal-right blastomere at the 4-cell stage. Embryos were analysed by WISH at the late gastrula to early neurula stage (stages 12.5-13). Dorsal view with anterior up. (A',C',D') Enlarged images of A, C, and D (white dashed box). MHB, the midbrain and hindbrain boundary. (E-J) Activation of *xcg1* by 4E and 4A. mRNA (30 pg each) for globin (E), WT (F), 4E (G), 4A (H), ΔAD-4E (I), ΔAD-4A (J) was injected with *nβ-gal* mRNA. Embryos were analysed by WISH at the late neurula stage (stages 18-20). Anterior view with dorsal up. CG, cement gland. Colors of arrowheads: white, normal expression; magenta, upregulation; blue, downregulation (A-J). Scale bar, 500 μm (A-J); 250 μm (A',C',D'). (K-N) Luciferase reporter assays. (K-M) *meis3*-D2-luc reporter DNA was co-injected with mRNA for Otx2-WT, -4E or -4A (50 pg/embryo) (K) or with combinations of mRNAs for Gsc (12.5 pg/embryo), Tle1 (12.5 pg/embryo), Otx2-WT and -4A (25 pg/embryo) as indicated (L,M). (N) SOP-FLASH reporter DNA construct was co-injected with mRNA for Otx2-WT, 4E or 4A (50 pg/embryo) (N). **P*<0.05, ***P*<0.01 (t-test); error bars, s.e.m.; n=5 samples (K-N), NS, not significant (M). (O) Physical interaction between Tle1 and Otx2 mutant as assayed by Co-IP. The amounts of expressed protein were verified by western blotting (lysate). Magenta arrowheads, co-immunoprecipitated bands; circles, heavy chains of IgG from the anti-Myc antibody.

Fig. 26については、5年以内に雑誌で刊行予定のため、非公開。

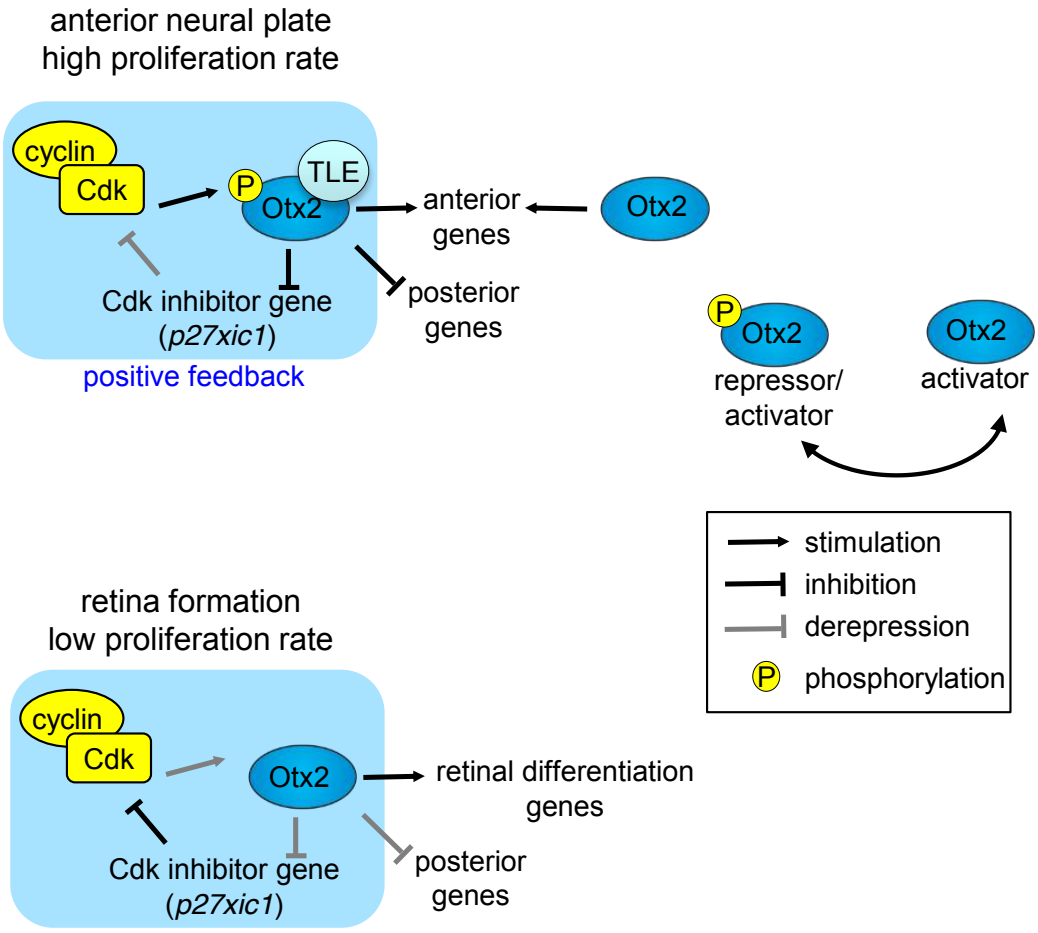

Fig. 27. Regulatory principles by Otx2 phosphorylation in the anterior neural plate and retina.

A schematic model of the regulatory mechanisms by Otx2 is shown. See the text for explanation.

Fig. 28については、5年以内に雑誌で刊行予定のため、非公開。

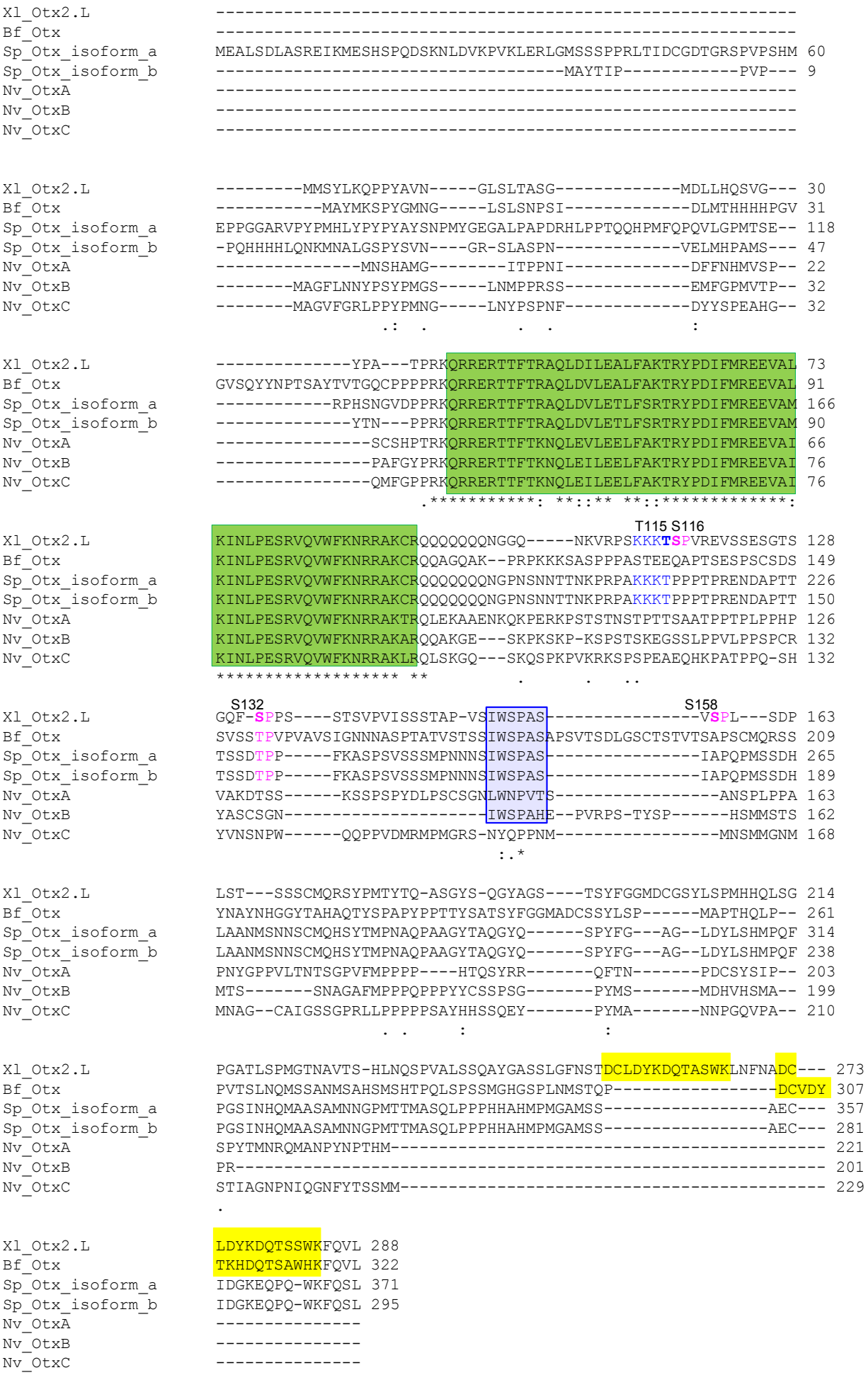

Fig. 29. Alignment of amino acid sequences of Xenopus *Otx2, and* Amphioxus *Otx,* Sea urchin *Otx* and Sea anemone *Otx*.

Abbreviations of species are *Xenopus laevis* (Xl), *Branchiostoma belcheri* (Bf), *Strongylocentrotus purpuratus* (Sp) and *Nematostella vectensis* (Nv). Protein sequences were obtained from the NCBI database: Xl_Otx2.L (NP_001084955), Bf_Otx (XP_019625651), Sp_Otx isoform a (NP_999753), Sp_Otx isoform b (NP_001027540), Nv_OtxA (AFJ11251), Nv_OtxB (AFJ11250) and Nv_OtxC (AC053863). Boxes coloured in green, homeodomain; blue, the conserved eh1 repression motif of Otx; yellow, Otx tail motif. Blue or magenta letters, consensus motifs for Akt and Cdks. Bold cases, putative phosphorylation sites of Otx2 in *Xenopus* as shown in this study.

References

Acampora, D., Postiglione, M. P. I. A., Avantaggiato, V., Bonito, M. D. I. and Simeone, A. (2000). The role of Otx and Otp genes in brain development. *Int. J. Dev. Biol.* **44**, 669–677.

Agoston, Z. and Schulte, D. (2009). Meis2 competes with the Groucho co-repressor Tle4 for binding to Otx2 and specifies tectal fate without induction of a secondary midbrain-hindbrain boundary organizer. *Development* **136**, 3311–3322.

Ali, F., Hindley, C., McDowell, G., Deibler, R., Jones, A., Kirschner, M., Guillemot, F. and Philpott, A. (2011). Cell cycle-regulated multi-site phosphorylation of Neurogenin 2 coordinates cell cycling with differentiation during neurogenesis. *Development* **138**, 4267–4277.

Andoniadou, C. L. and Martinez-Barbera, J. P. (2013). Developmental mechanisms directing early anterior forebrain specification in vertebrates. *Cell. Mol. Life Sci.*

Andreazzoli, M., Pannese, M. and Boncinelli, E. (1997). Activating and repressing signals in head development: the role of Xotx1 and Xotx2. *Development* **124**, 1733–1743.

Beby, F. and Lamonerie, T. (2013). The homeobox gene Otx2 in development and disease. *Exp. Eye Res.* **111**, 9–16.

Boyl, P. P., Signore, M., Acampora, D., Martinez-Barbera, J. P., Ilengo, C., Annino, A., Corte, G. and Simeone, A. (2001). Forebrain and midbrain development requires epiblast-restricted Otx2 translational control mediated by its 3' UTR. *Development* **128**, 2989–3000.

Brzezinski, J. A. and Reh, T. A. (2015). Photoreceptor cell fate specification in vertebrates. *Development*.

Bunt, J., Hasselt, N. E., Zwijnenburg, D. a., Hamdi, M., Koster, J., Versteeg, R. and Kool, M. (2012). OTX2 directly activates cell cycle genes and inhibits differentiation in medulloblastoma cells. *Int. J. Cancer* **131**,.

Cai, Y., Brophy, P. D., Levitan, I., Stifani, S. and Dressler, G. R. (2003). Groucho suppresses Pax2 transactivation by inhibition of JNK-mediated phosphorylation. *EMBO J.* **22**, 5522–5529.

Copley, R. R. (2005). The EH1 motif in metazoan transcription factors. *BMC Genomics*.

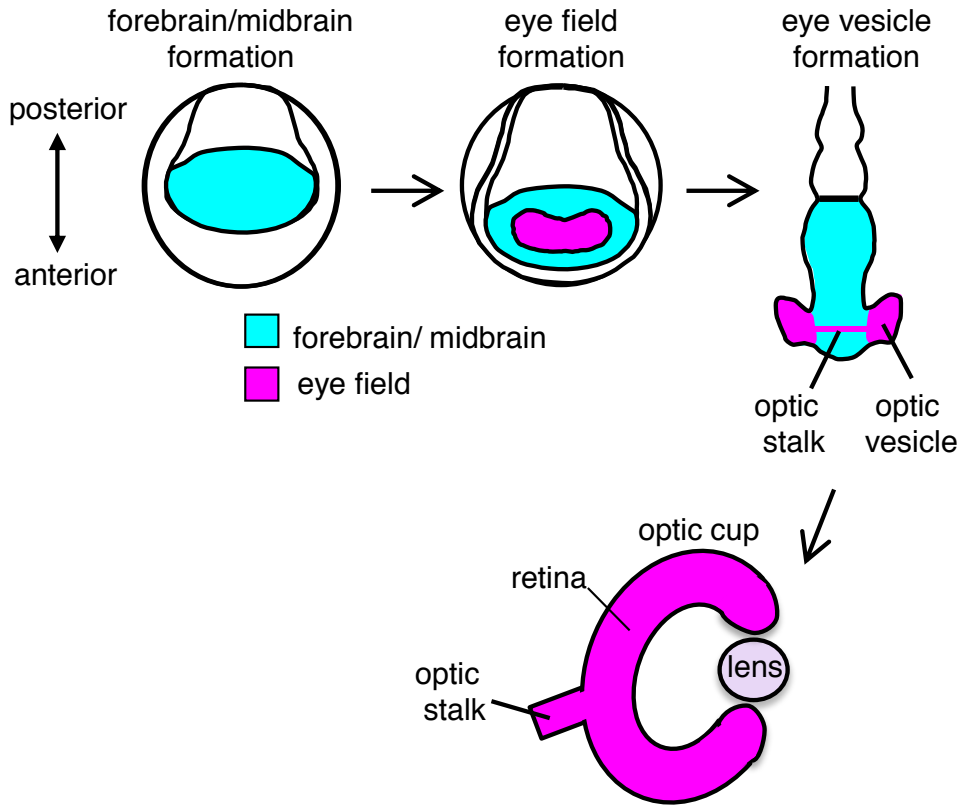

Fig. 1. Developmental processes of vertebrate eye.

In the neurula embryo, the neural plate is divided into the presumptive forebrain-midbrain region and hindbrain region, respectively, in terms of the anteroposterior position. As the first step of vertebrate eye development, the eye field, in which the eyes will be formed is specified in the center of the forebrain. The eye field is gradually separated into two bilateral regions to give rise to the optic vesicles, and subsequently the optic cup and retina are formed.

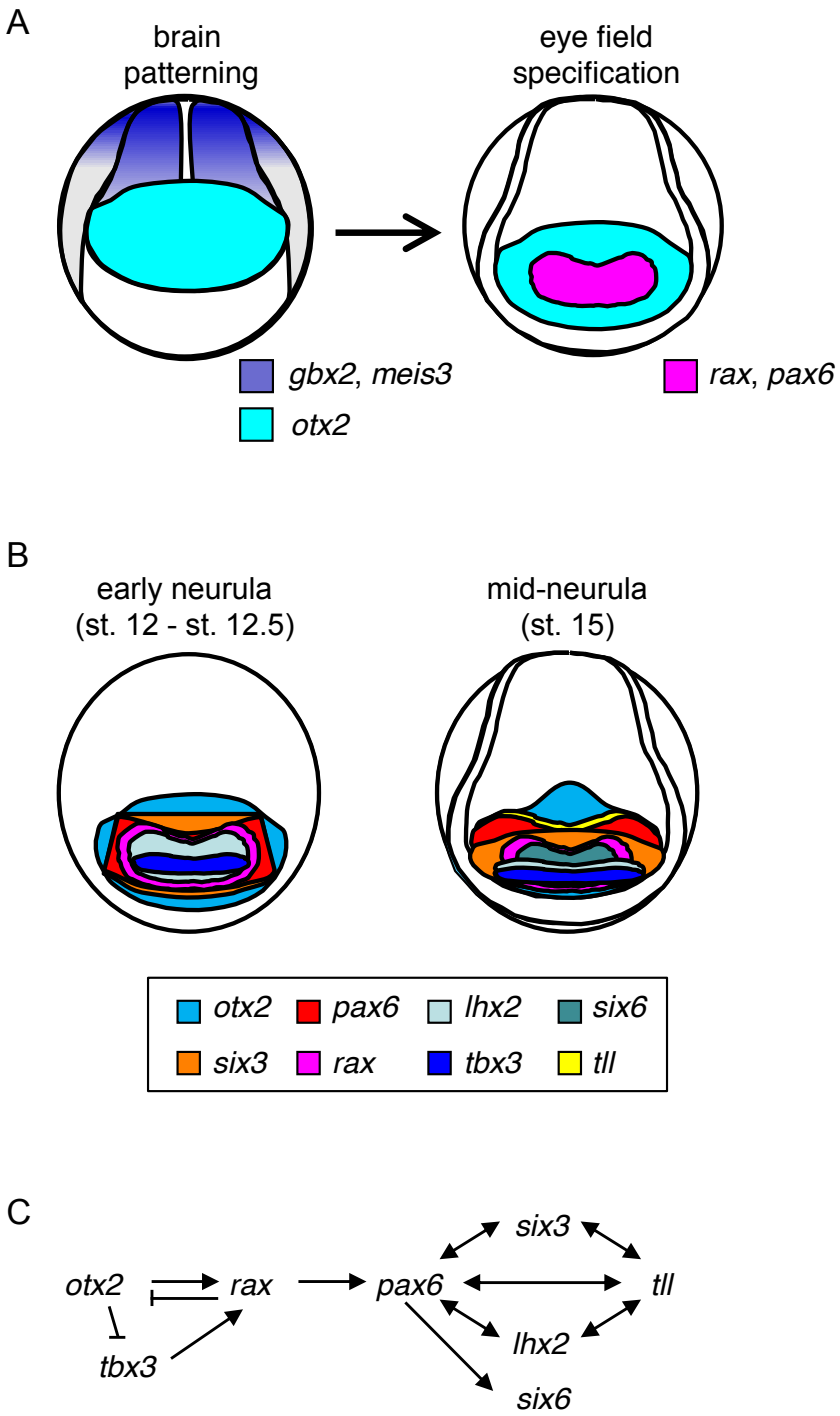

Fig. 2. A model of eye field formation in the anterior neural plate.

(A) Expression patterns of TFs *otx2* (forebrain and midbrain, light blue), *gbx2* and *meis3* (hindbrain, blue), *rax* and *pax6* (eye field, magenta) in early *Xenopus* neurula embryos. For the anteroposterior patterning in the neuroectoderm, *otx2* is expressed in the forebrain and midbrain, and *gbx2* and *meis3* are expressed in the hindbrain. During late gastrulation, EFTF genes, *rax* and *pax6*, are expressed in the center of the region where *otx2* is expressed. (B) A schematic model of gene expression patterns of known EFTFs in early neurula (stages 12-12.5, left) and mid-neurula (stage 15, right) embryos. (C) A gene cascade of eye field specification. In the early step of eye field specification, *otx2* upregulates the expression of *rax* and subsequently the expression of *pax6* is activated, and *otx2* represses the expression of *tbx3*. During mid-step for eye field specification, *rax* in turn represses *otx2*, forming a negative feedback loop between *otx2* and *rax*. In addition, the expression of other EFTFs (*six3*, *lhx2*, *six6*, and *tll*) downstream of *pax6* starts to be expressed.

Fig. 3〜Fig. 12については、5年以内に雑誌で刊行予定のため、非公開。

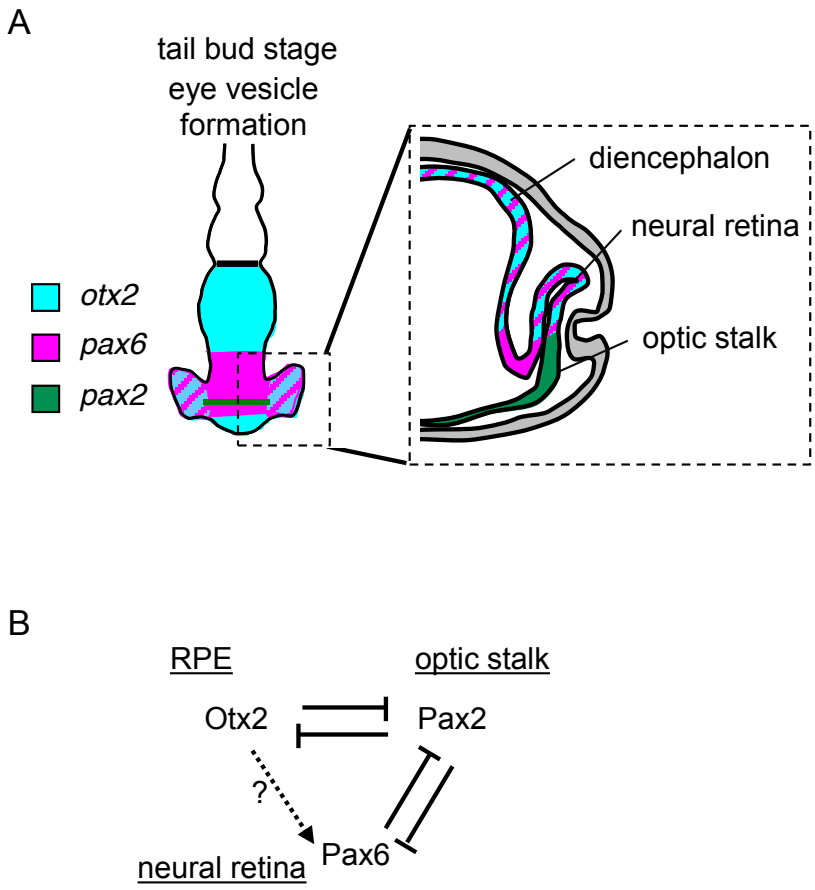

Fig. 13. Expression patterns and gene interactions involved in the patterning of eye vesicle.

(A) Expression patterns of *otx2*, *pax6* and *pax2* in the diencephalon, neural retina and optic stalk. (B) A model for gene interactions for the establishment of the territories of eye vesicle. The reciprocal repression of Otx2 and Pax2 determines the segregation of RPE (the retinal pigment epithelium)/OS (optic stalk), and the similar mechanism is proposed for Pax2 and Pax6 interaction in the establishment of RPE/NR (neural retina). It remains to be elucidated whether Otx2 contributes to the direct regulation of *pax6*.

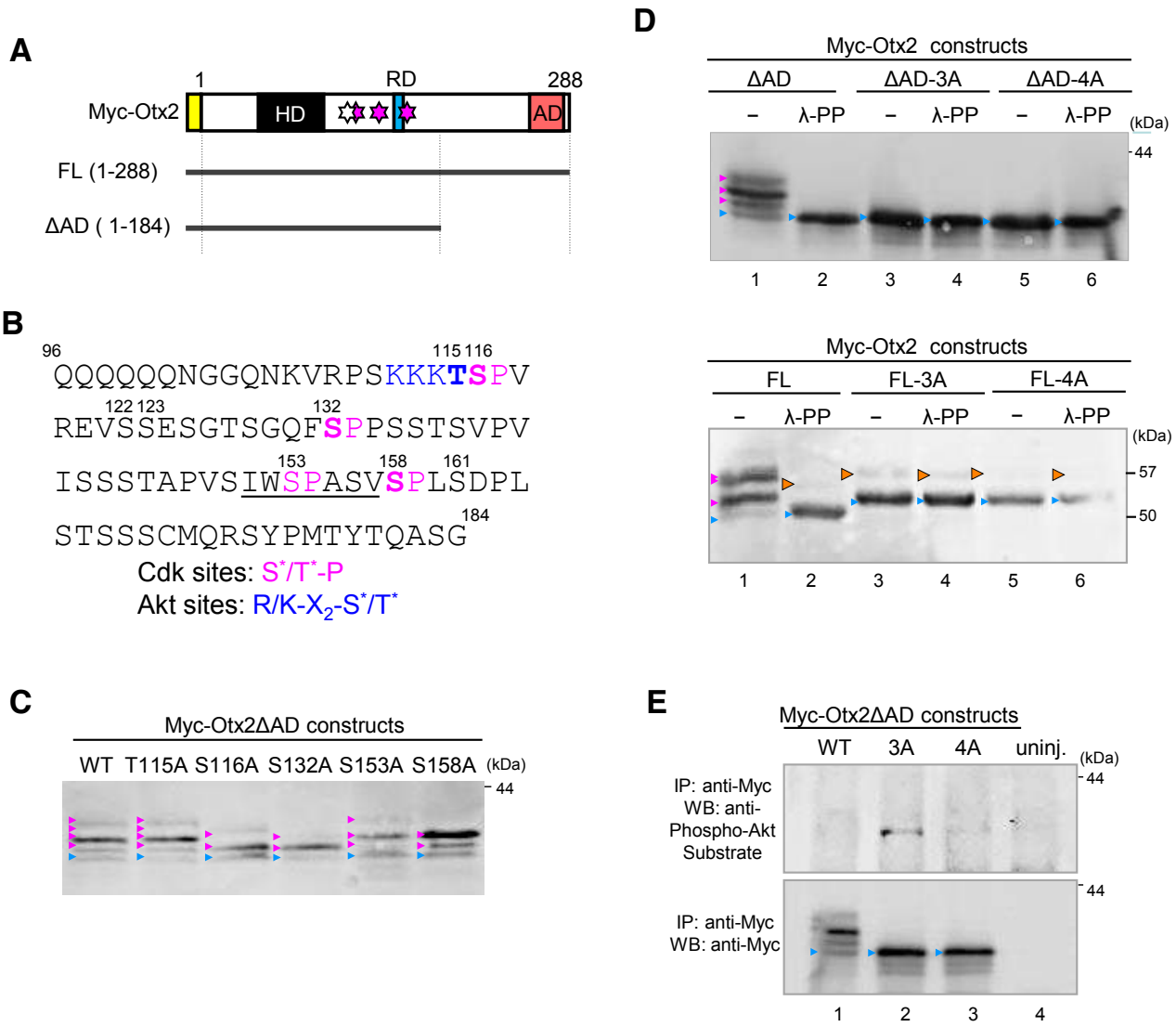

Fig. 14. Exogenous Otx2 is phosphorylated.

(A) Schematic structures of Myc-Otx2 and deletion constructs. The homeodomain (HD), repression domain (RD) and activation domain (AD) are indicated. A Myc-tag at the N-terminus is indicated as a yellow box. White star, Akt site; pink stars, Cdk sites. The regions of Otx2 constructs are indicated by thick lines and positions of amino acid residues are indicated in parentheses. (B) Amino acid sequences around the repression domain. Colored cases indicate the consensus motif for Cdks (magenta) and Akt kinase (blue). Bold cases indicate modified serine and threonine residues that were suggested in the experimental process (T115, S116, S132 and S158). Under line, the eh1 motif of the repression domain. Consensus motifs for Cdk and Akt are indicated at the bottom. *, phosphorylated serine/threonine residues. (C) Western blotting of Myc-Otx2ΔAD constructs, WT and alanine mutants at T115 (T115A), S116 (S116A), S132 (S132A), S153 (S153A) and S158 (S158A). (D) Western blotting of Myc-Otx2ΔAD (upper) and Myc-Otx2FL constructs (lower), WT, 3A and 4A with or without λ-protein phosphatase (λ-PP) treatment. (E) IP-western assay. Myc-Otx2ΔAD was immunoprecipitated with anti-Myc antibody, and subjected to western blotting with the anti-Phospho-Akt substrate antibody (upper) or anti-Myc antibody (lower). 3A, alanine mutant at S116, S132 and S158; 4A, alanine mutant at T115, S116, S132 and S158; uninj., uninjected control; orange arrowheads, bands resistant to λ-PP. FL, full length; WT, wild type; blue arrowheads, nascent proteins; magenta arrowheads, modified proteins. Size markers (kDa) are indicated on the right of panels (C,D,E).

Fig. 15. Alignment of amino acid sequences of Otx2 and Otx5/Crx among vertebrates.

Abbreviations of species are *Xenopus laevis* (Xl), *Xenopus tropicalis* (Xt), *Danio rerio* (Dr), *Gallus gallus* (Gg), *Mus musculus* (Mm) and *Homo sapiens* (Hs). Protein sequences were obtained from the NCBI database: Xl_Otx2.L (NP_001084955), Xl_Otx5.L (NP_001081916), Xt_Otx2 (NP_001016177), Xt_Otx5 (NP_001016021), Dr_Otx2 (NP_571326), Dr_Otx5 (NP_851848), Gg_Otx2 (NP_989851), Gg_Otx5 (NP_001288716), Mm_Otx2 (NP_001273412), Mm_Crx (NP_031796), Hs_Otx2 (NP_001257453), Hs_Crx (AAH53672). Boxes coloured in green, homeodomain; blue, SIWSPAS motif; yellow, repeated Otx tail motif; red, Otx2 mutation sites (P133 and P134) that were reportedly associated with human ocular malformation. Blue or magenta letters, consensus motifs for Akt and Cdks. Bold cases, putative phosphorylation sites of Otx2 as shown in this study.

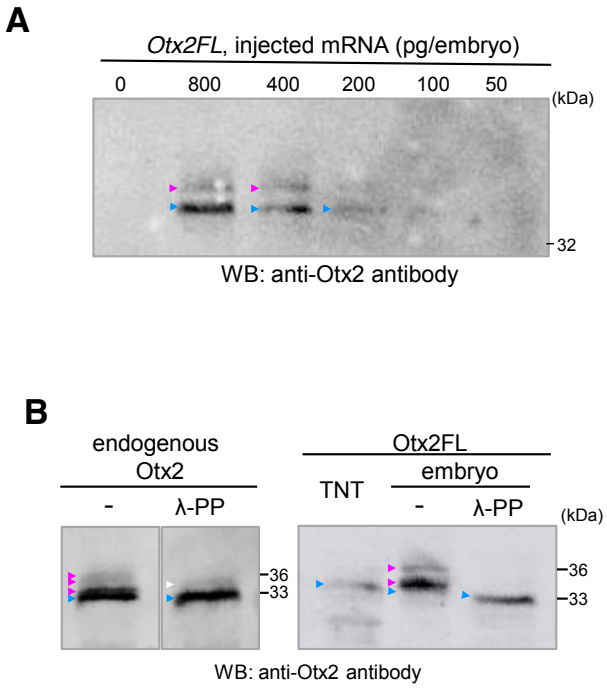

Fig. 16. The detection limit of Otx2FL and phosphorylation of endogenous Otx2 by western blotting.

(A) Embryos were injected with *Otx2FL* mRNA at various doses as indicated. Modified bands of Otx2FL was clearly detected when *Otx2FL* mRNAs were exogenously injected with greater than 400 pg per embryo, but not less than 200 per embryo. Embryonic lysate of 0.42 embryo equivalent was loaded per lane. (B) Western blotting of endogenous Otx2 (left panel) and exogenous Otx2FL construct (right panel) with or without λ-PP treatment. Otx2FL and endogenous Otx2 was detected with anti-Otx2 antibodies (A,B). Blue arrowheads, nascent proteins; magenta arrowheads, modified proteins.

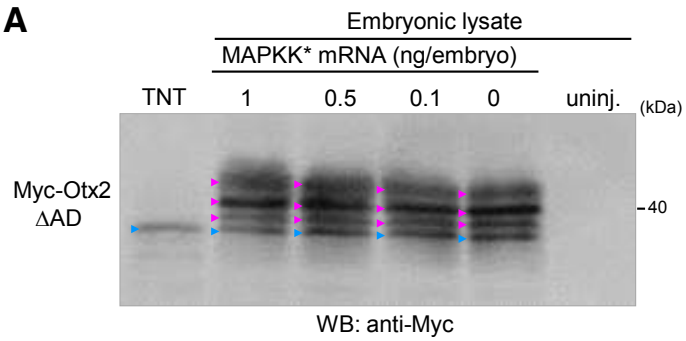

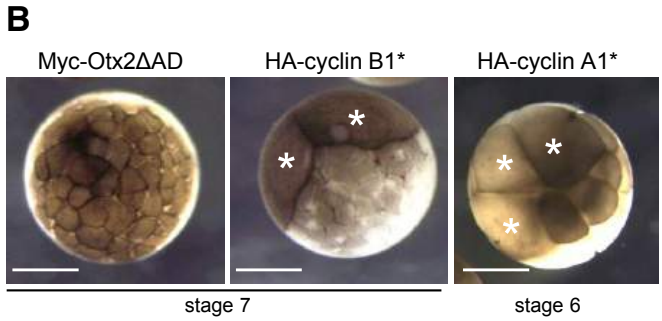

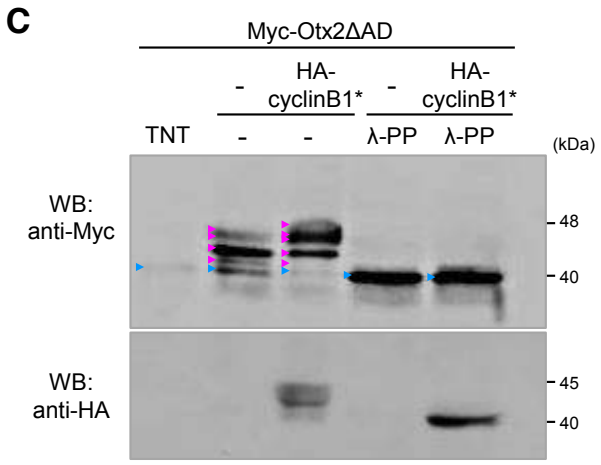

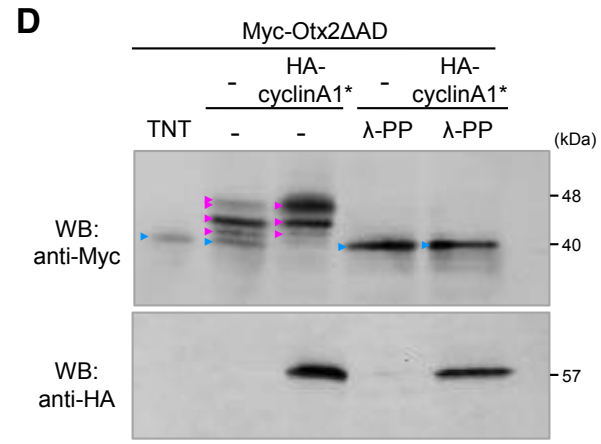

Fig. 17. Effects of MAPK and Cdk on modifications of exogenous Otx2.

(A) No effect of constitutively active mutant of MAPKK (MAPKK*) on modifications of Otx2. Western blotting of Myc-Otx2ΔAD co-expressed with MAPKK*. The amounts of injected *MAPKK*** mRNA were as indicated. mRNAs were injected into the animal pole region of both blastomeres at the 2-cell stage. (B) Phenotypes of Myc-Otx2ΔAD, HA-cyclin B1* (stable mutants of cyclin B1), and HA-cyclin A1* (stable mutants of cyclin A1) overexpressing embryos. Embryos were observed at the early blastula stage (animal pole view). (C,D) Western blotting of Myc-Otx2ΔAD co-expressed with HA-cyclin B1* (C) or HA-cyclin A1* (D). Lysate were treated with λ-PP as indicated. Myc-Otx2ΔAD and HA-cyclin B1* or HA-cyclin A1* were detected with anti-Myc and anti-HA antibodies, respectively. Lysates were prepared from embryos at stage 8 (C) or stage 9 (D). White asterisks, cell cycle-arrested blastomeres. Scale bars, 500 μm.

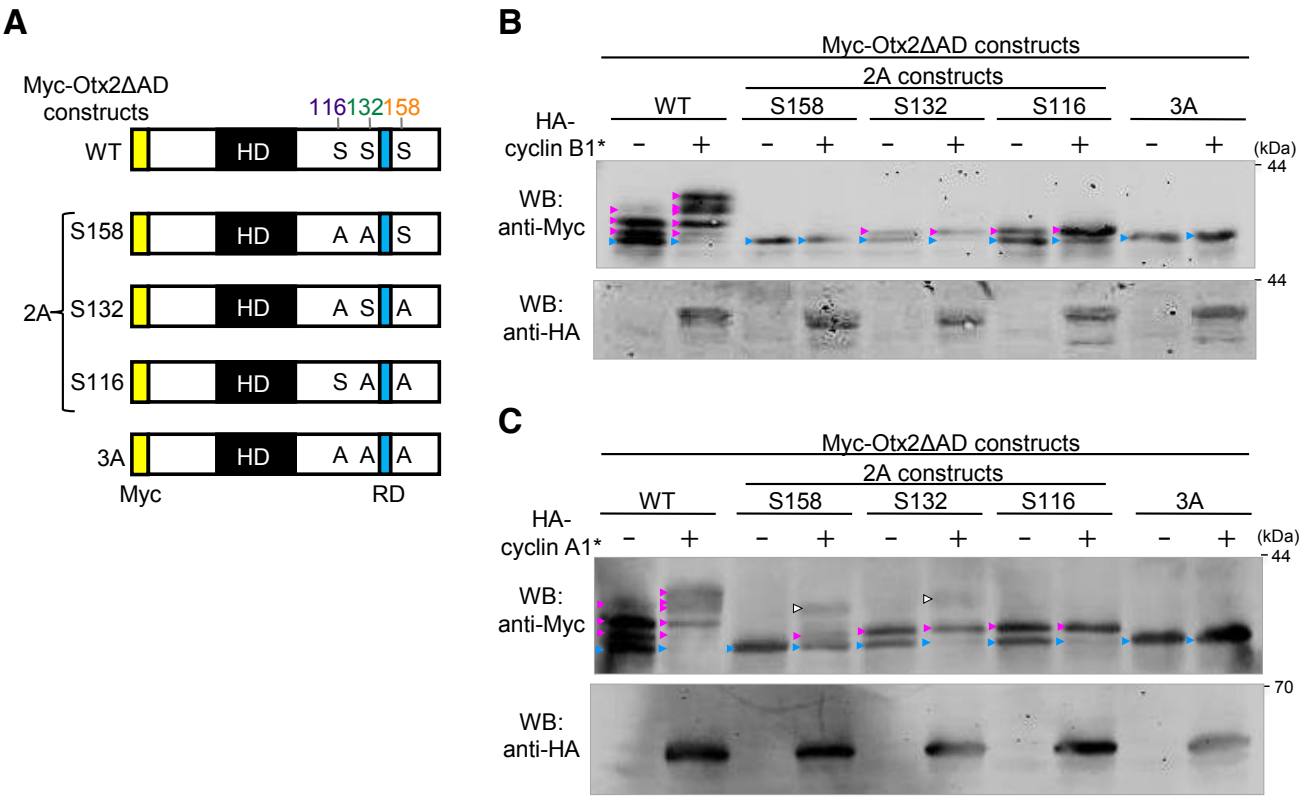

Fig. 18. Preference of cyclin B/Cdk and cyclin A/Cdks for Cdk sites of Otx2.

(A) Schematic presentation of Myc-Otx2ΔAD with double (2A) and triple alanine (3A) mutations at S116, S132 and S158. Yellow box, Myc-tag; black box, homeodomain (HD); blue box, repression domain (RD). In the 2A constructs, for example, the S158 construct indicates mutations at S116 and S132. S, serine phosphorylation sites (S116, S132, S158); A, alanine mutation. (B) Western blotting of Myc-Otx2ΔAD constructs (2A or 3A) co-expressed with (+) or without (-) HA-cyclin B1*. (C) Western blotting of Myc-Otx2ΔAD constructs (2A or 3A) co-expressed with (+) or without (-) HA-cyclin A1*. Blue arrowheads, nascent bands; magenta arrowheads, modified bands; white arrowheads, additional modified bands at sites other than S116, S132 and S158.

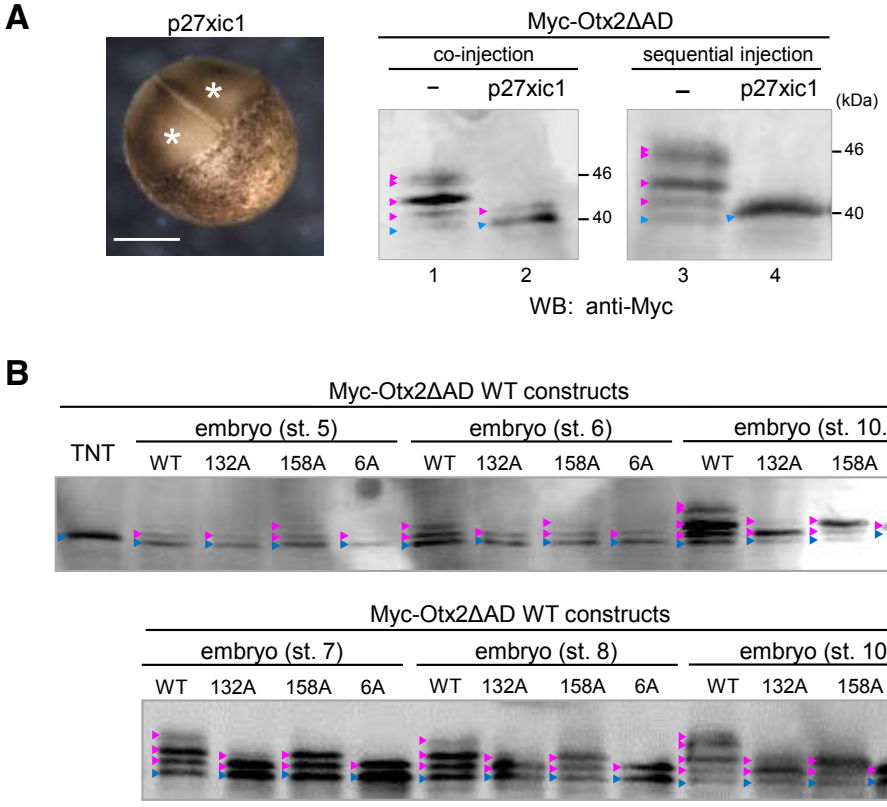

Fig. 19. Effects of p27xic1 to phosphorylation of Otx2 and developmental changes of phosphorylation of Otx2.

(A) Phenotype of p27xic1-overexpressing embryos (left) and western blotting of Myc-Otx2ΔAD co-expressed with p27xic1 (middle, right). Co-injection (middle): *Myc-Otx2ΔAD* mRNA (500 pg/embryo) was coinjected with (lane 2) or without (lane 1) *p27xic1* mRNA (2 ng/embryo) into one blastomere at the 2-cell stage. Sequential injection (right): *p27xic1* mRNA (1.5 ng/embryo) was injected into one blastomere at the 2-cell stage, then mRNAs for *Myc-Otx2ΔAD* (500 pg/embryo) and *p27xic1* (500 pg/embryo) were co-injected into the cleavage-arrested blastomeres at the 32-cell stage equivalent (lane 4). *Myc-Otx2ΔAD* mRNA was injected at the 2-cell stage as control (lane 3). Lysates were prepared from embryos at stage 9 (lanes 1 and 2) or stage 9.5 (lanes 3 and 4). White asterisks, cleavage-arrested blastomeres. Scale bars, 500 μm. (B) Developmental changes of phosphorylation of Otx2 as assayed by using Myc-Otx2ΔAD constructs. WT and alanine mutants of Otx2 in Myc-Otx2ΔAD constructs were analyzed from stages 5 to 10.5 as indicated. TNT, *in vitro* translation products; blue arrowheads, nascent bands; magenta arrowheads, modified bands.

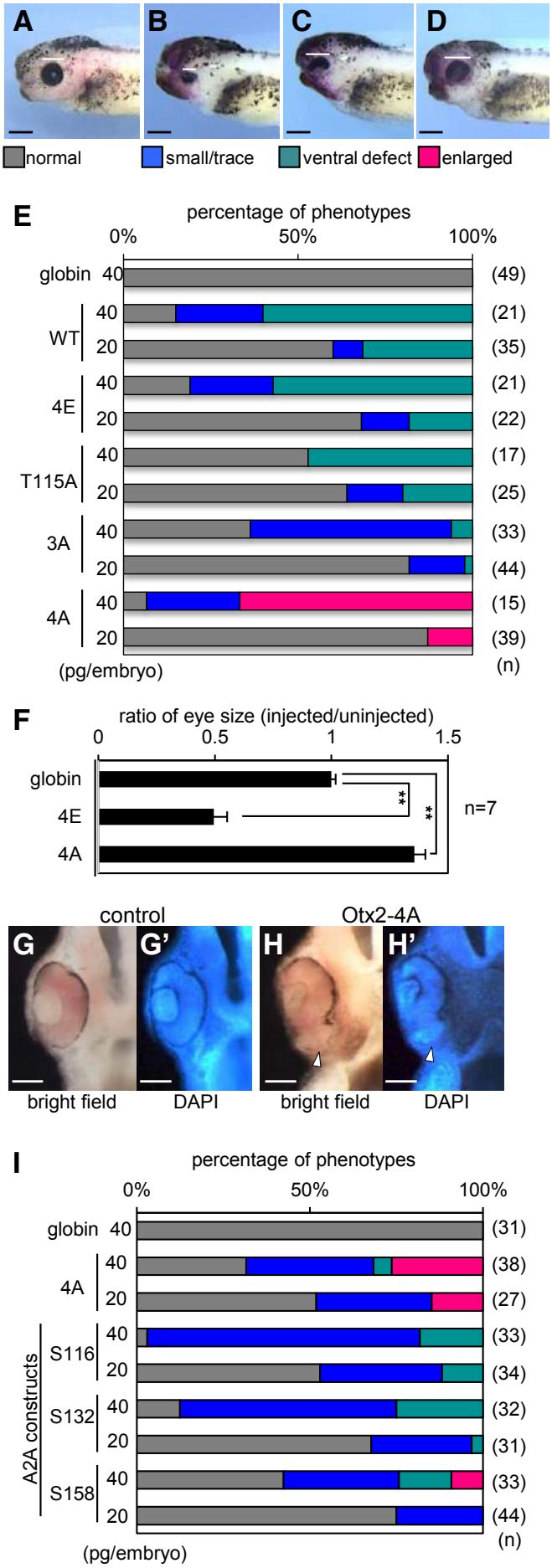

Fig. 20. Phosphomutants of Otx2 exhibit the distinct activity as assessed by developmental eye phenotype.

(A-D) Eye phenotypes of Otx2 mutant-expressing embryos (stages 38-42). mRNA for Otx2 constructs were co-injected with *nβ-gal* mRNA as a tracer. Representative phenotypes in injected embryos (A-D): normal looking (normal), trace eye (trace), normal eye diameter with pigmentation defect at the ventral side (ventral defect) and enlarged retinal diameter with pigmentation defect at the ventral side (enlarged). The white dashed lines indicate the diameter of the eye. Anterior to the left, dorsal is up. Scale bar, 500 μm. (E) Activity of Otx2 mutants for eye malformation phenotypes. The color bar (see panels A-D for color codes) indicates the percentages of the eye phenotype. Low-dose mRNA injection (20 pg/embryo) caused moderate phenotypes than high dose injection (40 pg/embryo). n, total number of injected embryos. (F) Quantitative assay for the ratio of the eye size in tailbud stage embryos (stages 38-42). $^{**}P<0.01$ (t-test); error bars, s.e.m.; n=7 samples. (G-H') Transverse hemisection observations. (G,G') Globin injected control. (H,H') The enlarged eye phenotype of 4A-expressing embryo. Bright field, G,H; DAPI staining, G',H'. Arrowheads, the retinal pigmentation defect at the ventral side. Scale bar, 100 μm.

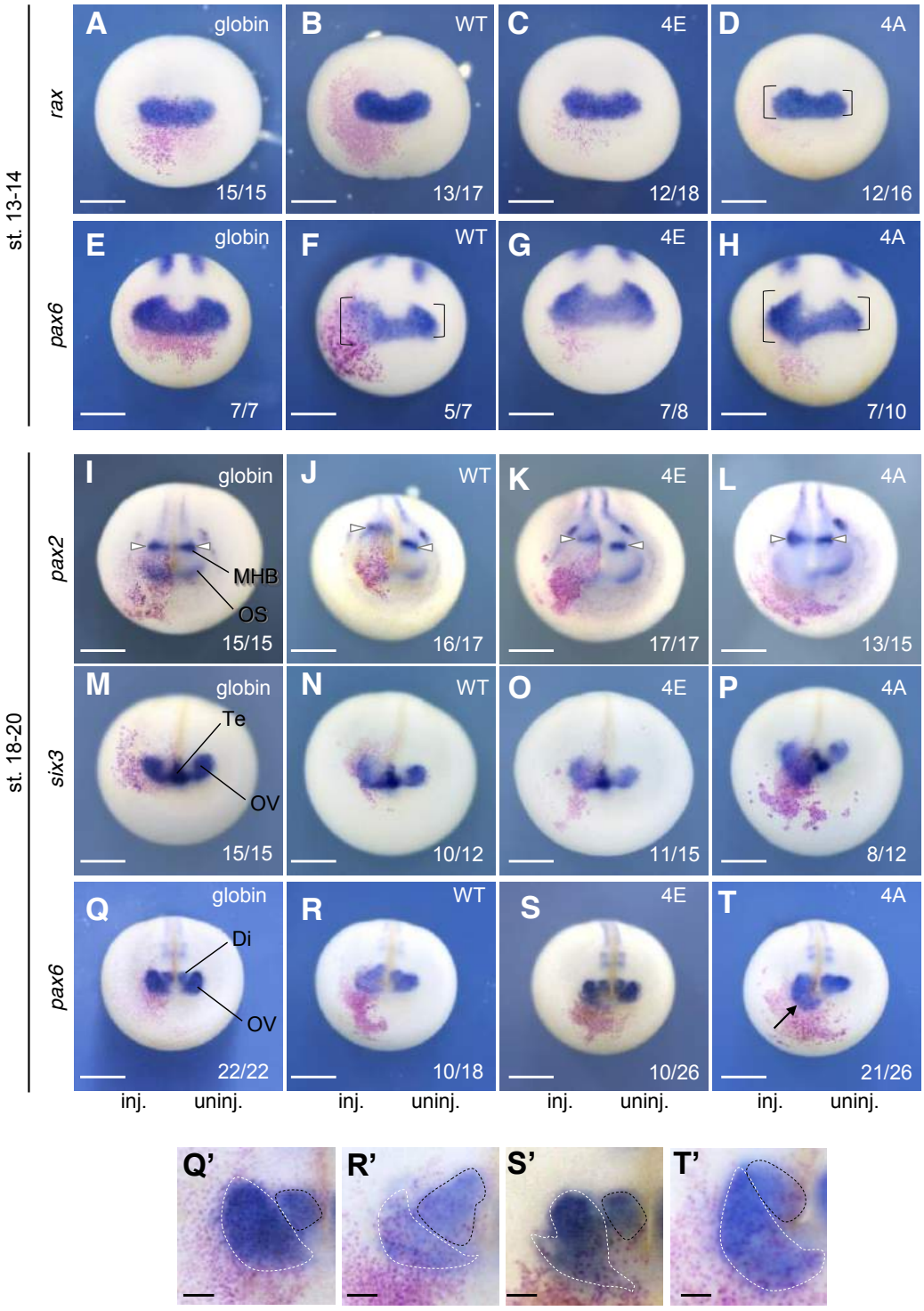

Fig. 21. Increased expression of eye marker genes by Otx2 mutant 4A.

(A-T) mRNA for globin, WT, 4E or 4A (20 pg/embryo) was injected with *nβ-gal* mRNA into the animal pole region of the dorsal-right blastomere at the 4-cell stage, and embryos were subjected to WISH at early neurula stages (stages 13-14) (A-H) and at late neurula stages (stages 18-20) (I-T). MHB, the midbrain-hindbrain boundary; OS, optic stalk; OV, optic vesicle; Te, telencephalon, Di, diencephalon. Arrowhead, the position of MHB; arrow, the expansion of *pax6* expression to the anterior region. Anterior view with dorsal up. Scale bar, 500 μm. (Q'-T') Enlarged images of Q-T. Black and white dash lines indicate diencephalon and optic vesicle regions, respectively, where *pax6* is expressed. Scale bar, 100 μm.

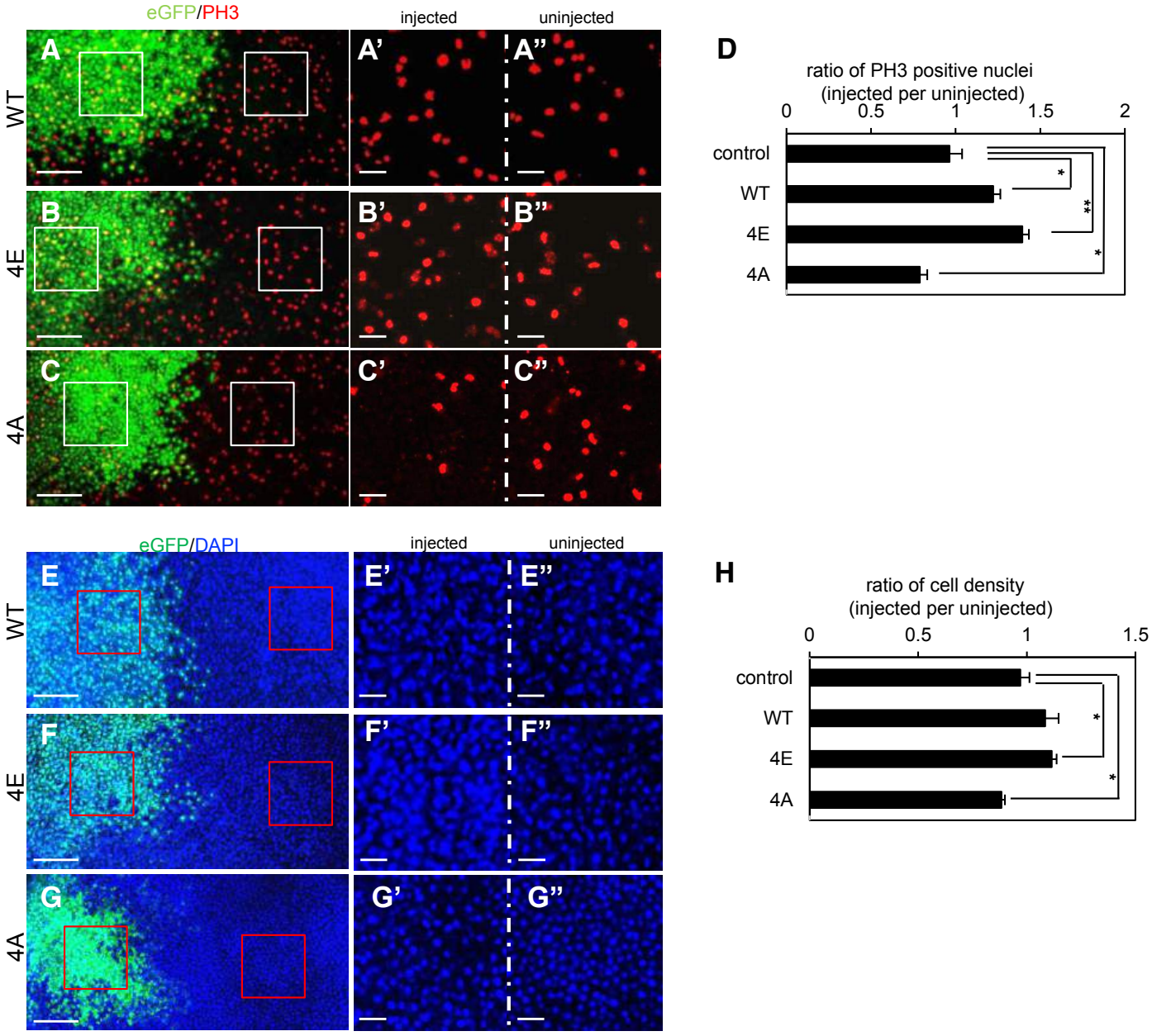

Fig. 22. Phosphomimetic Otx2 mutant 4E stimulates cell proliferation.

(A-C) mRNA for Otx2-WT (A), -4E (B) or -4A (C) together with that for eGFP as a tracer was injected in one blastomere at 2-cell stage. 4E and 4A are glutamate and alanine mutants, respectively, of full length Otx2 at T115, S116, S132 and S158. Embryos were immunostained with anti-phospho-Histone H3 (PH3) at the gastrula stage. The dorsoanterior region was observed. PH3-positive nuclei were shown in red, Otx2 mutant-expressing cells (expressing eGFP) were shown in green. White dash boxes in A-C correspond to enlarged area (A'-C"), respectively. Scale bar, 200 μm. (D) Quantitative assay for the ratio of PH3-positive nuclei. (E-G) Representative images of DAPI-stained nuclei in Otx2-WT (E) or -4E (F) or -4A (G) expressing gastrula embryos. The dorsoanterior region was observed. Nuclei were shown in blue, Otx2 mutant-expressing cells (expressing eGFP) were shown in green. Red boxes in E, F and G correspond to enlarged area (E'-G"), respectively. Scale bar, 200 μm (E-G); 50 μm (E'-G"). (H) Quantitative analysis for cell numbers. More than 500 total nuclei were counted in one embryos, and 5 to 7 embryos were analysed for calculating the mean ratio (and s.e.m.) of the number of nuclei in injected versus uninjected areas. $^{**}P<0.01$ (t-test), $^{*}P<0.05$ (t-test); error bars, s.e.m. (D,H).

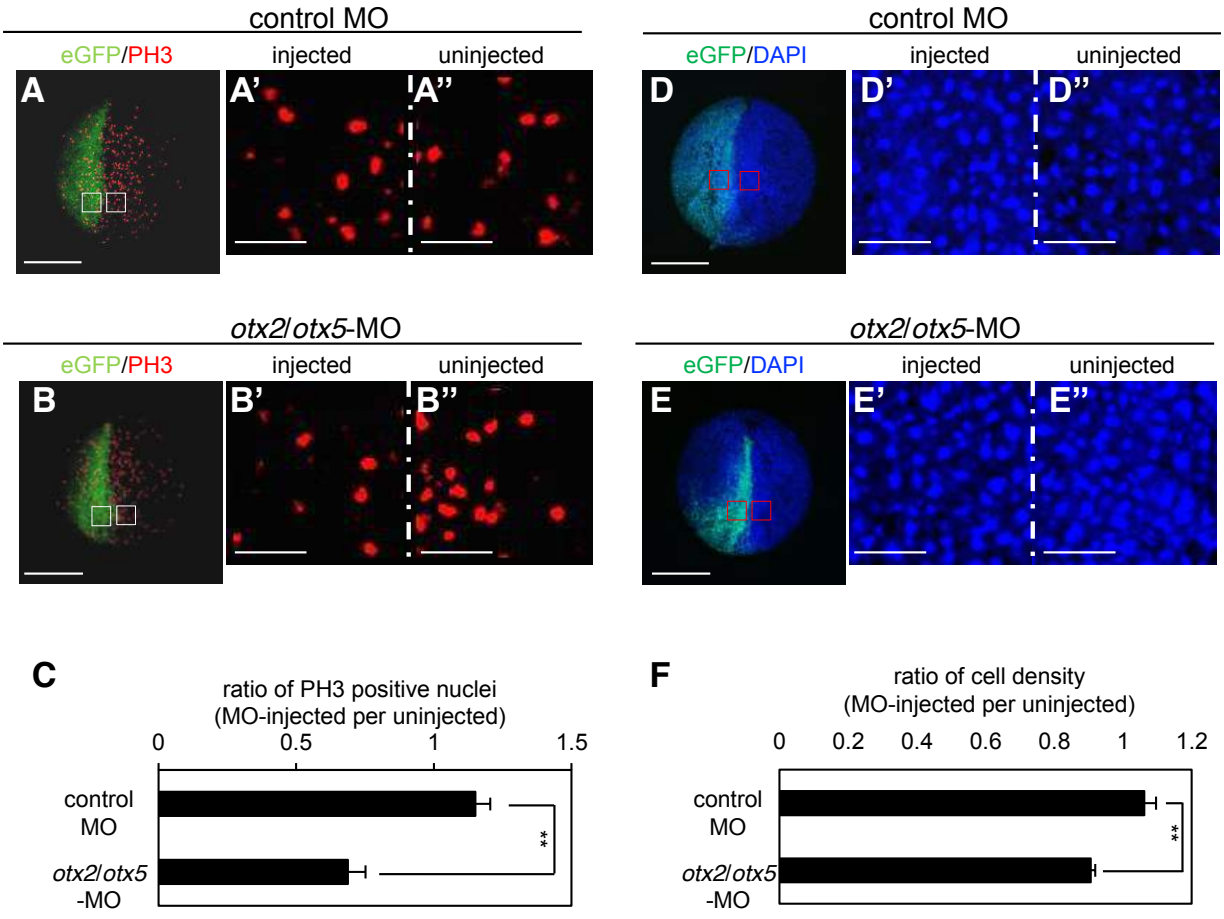

Fig. 23. Reduction of cell proliferation by otx2/otx5 knockdown in Xenopus tropicalis *embryos.*

Knockdown experiments were performed using *Xenopus tropicalis*. (A,B) Effects of *otx2*/*otx5*-MO injection on mitotically active cells. White boxes, enlarged area (A'-B"). (C) Quantitative analysis for the ratio of PH3-positive nuclei. PH3-positive nuclei in an injected or uninjected area (0.072 mm^2) in each embryo were counted (more than 60 nuclei in each area) with 9 embryos, and the ratio of the numbers of injected versus uninjected area was calculated for each embryo to obtain mean ± s.e.m. from 9 embryos. The ratio of PH3-positive nuclei in control MO-injected embryos was 1.15 ± 0.055 (mean ± s.e.m.), whereas that in *otx2*/*otx5*-MOs-injected embryos was 0.688±0.063, which significantly differed from the control (p = 4.95E-05). (D,E) Effects of *otx2*/*otx5*-MO on cell density. Red boxes, enlarged area (D'-E"). (F) Quantitative analysis for the ratio of cell densities. More than 500 total nuclei in each area (0.072 mm^2) were counted in one embryo, and 9 embryos were analysed. The ratio of cell density in control MO-injected embryos was 1.063 ± 0.034 (mean ± s.e.m.), whereas that in *otx2*/*otx5*-MOs-injected embryos was 0.906 ± 0.013, which differed from the control (p = 0.0015). **P<0.01 (t-test); error bars, s.e.m. (C,F). Scale bar, 500 μm (A,B,D,E); 50 μm (A'-B",D'-E",). The amount of injected MO (pmol/embryo): control MO, 1; *otx2*/*otx5*, 0.5 each.

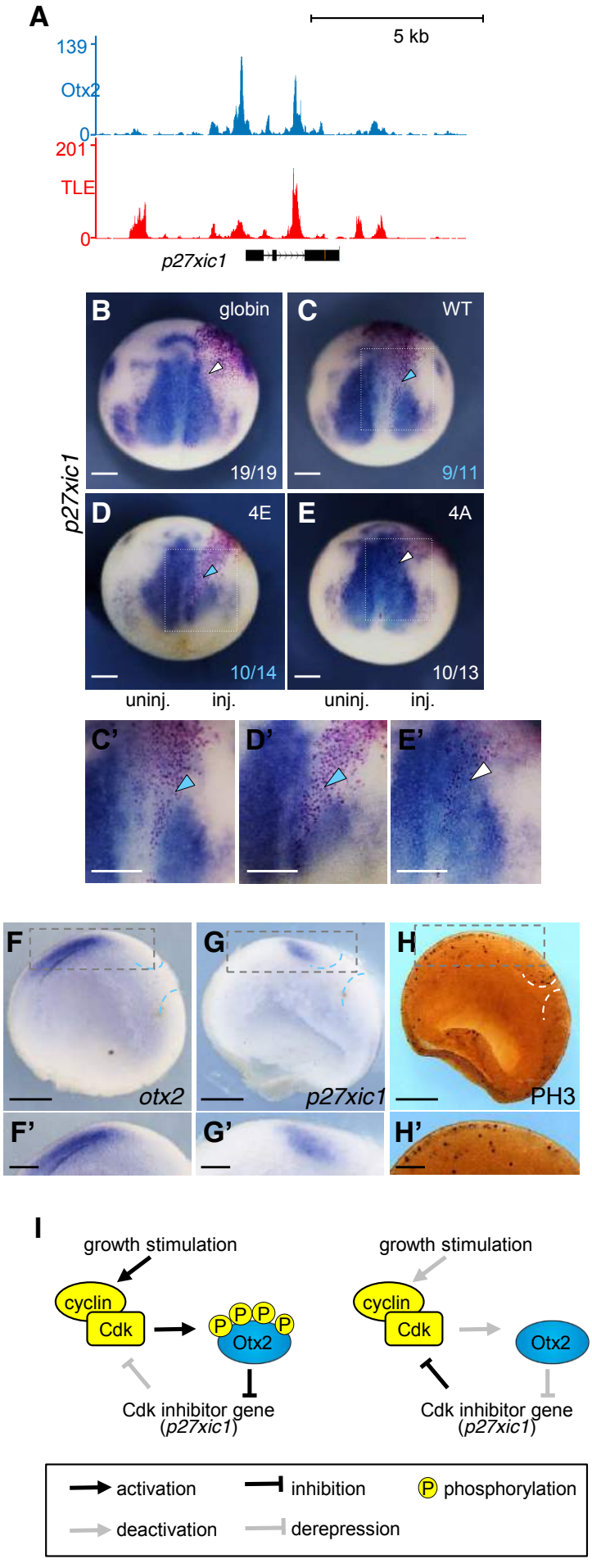

Fig. 24. Phosphomimetic Otx2-4E mutant negatively regulates p27xic1 *expression.*

(A) Genome browser representation showing occupancies of Otx2 and Tle1 in *Xenopus tropicalis* gastrula embryos for the *p27xic1* gene. (B-E) The WISH assay shows the expression of *p27xic1* in Otx2 mutant-expressing embryos. mRNA (30 pg each) for globin (B), WT (C), 4E (D), or 4A (E) was injected with *n*β-*gal* mRNA as a tracer into the animal pole region of the dorsal-left blastomere at the 4-cell stage. The fractions indicate the proportion of the presented phenotype per total number. Dorsal view with anterior up. inj., injected side; uninj., uninjected side. (C',D',E') Enlarged image of C, D and E (white dashed box). Colors of arrowheads: white, normal expression; blue, downregulation (B-E). The regional correlation between the domain where *otx2* and *p27xic1* are expressed. Cross hemisections show the expression of *otx2* (F) and *p27xic1* (G) visualized by WISH, and mitotically active cells by the immunostaining of PH3 (H). Lateral view with dorsal up, and anterior is left. (F',G',H') Enlarged image of F, G and H (gray dashed box). White dashed lines indicate the position of the blastopore. Scale bar, 500 μm (B-H); 250 μm (C'-H'). (I) A schematic model of feedback loops involving Cdk, Otx2, and p27xic in cell-proliferation (left) and non-proliferation states (right). Left, upon growth stimulation, (i) activation of Cdk causes phosphorylation of Otx2, (ii) phosphorylated Otx2 downregulates *p27xic1*, and (iii) the reduction of p27xic1 increases Cdk activity, thereby enhancing both cell proliferation and a phosphorylation state of Otx2. Right, upon the reduction of growth stimulation, (i) reduced Cdk activity causes the reduction of phosphorylation of Otx2, (ii) the reduction of phosphorylated Otx2 derepresses *p27xic1*, and (iii) increased p27xic1 inhibits Cdk activity, thereby reducing both cell proliferation and a phosphorylation state of Otx2.

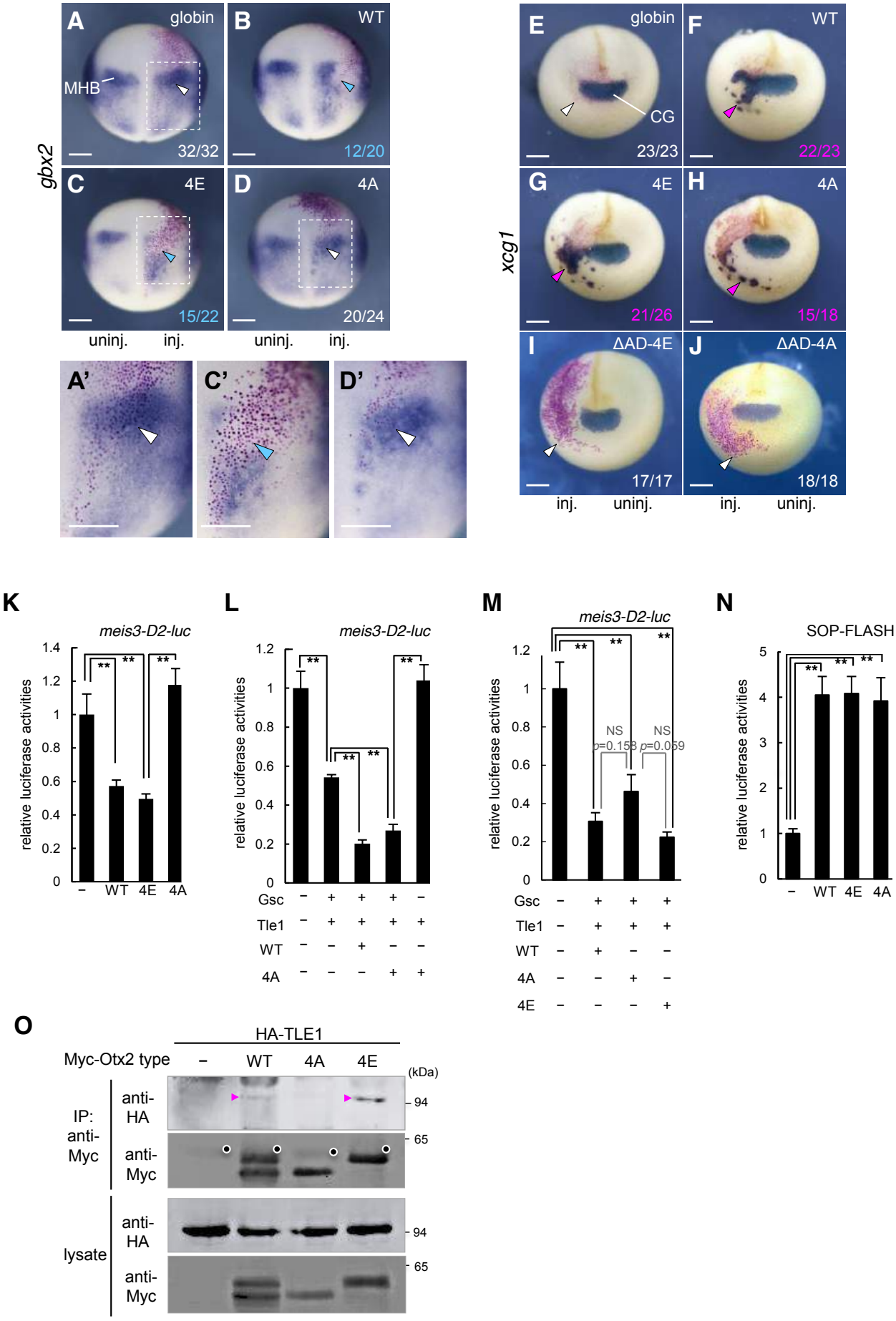

Fig. 25. The repressor activity of Otx2 depends on its phosphorylation.

(A-D) Repression of *gbx2* by 4E. mRNA (30 pg each) for globin (A), WT (B), 4E (C), or 4A (D) was injected with *nβ-gal* mRNA into the animal pole region of a dorsal-right blastomere at the 4-cell stage. Embryos were analysed by WISH at the late gastrula to early neurula stage (stages 12.5-13). Dorsal view with anterior up. (A',C',D') Enlarged images of A, C, and D (white dashed box). MHB, the midbrain and hindbrain boundary. (E-J) Activation of *xcg1* by 4E and 4A. mRNA (30 pg each) for globin (E), WT (F), 4E (G), 4A (H), ΔAD-4E (I), ΔAD-4A (J) was injected with *nβ-gal* mRNA. Embryos were analysed by WISH at the late neurula stage (stages 18-20). Anterior view with dorsal up. CG, cement gland. Colors of arrowheads: white, normal expression; magenta, upregulation; blue, downregulation (A-J). Scale bar, 500 μm (A-J); 250 μm (A',C',D'). (K-N) Luciferase reporter assays. (K-M) *meis3*-D2-luc reporter DNA was co-injected with mRNA for Otx2-WT, -4E or -4A (50 pg/embryo) (K) or with combinations of mRNAs for Gsc (12.5 pg/embryo), Tle1 (12.5 pg/embryo), Otx2-WT and -4A (25 pg/embryo) as indicated (L,M). (N) SOP-FLASH reporter DNA construct was co-injected with mRNA for Otx2-WT, 4E or 4A (50 pg/embryo) (N). **P*<0.05, ***P*<0.01 (t-test); error bars, s.e.m.; n=5 samples (K-N), NS, not significant (M). (O) Physical interaction between Tle1 and Otx2 mutant as assayed by Co-IP. The amounts of expressed protein were verified by western blotting (lysate). Magenta arrowheads, co-immunoprecipitated bands; circles, heavy chains of IgG from the anti-Myc antibody.

Fig. 26については、5年以内に雑誌で刊行予定のため、非公開。

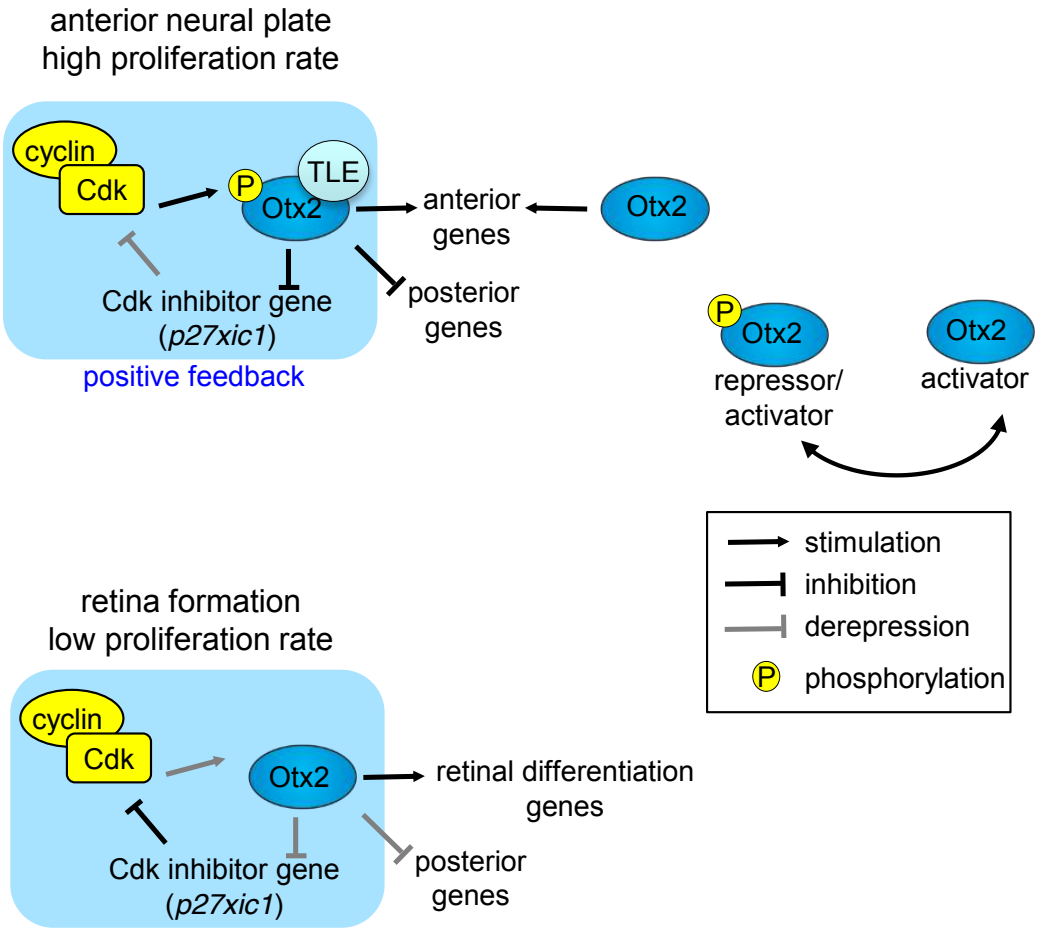

Fig. 27. Regulatory principles by Otx2 phosphorylation in the anterior neural plate and retina.

A schematic model of the regulatory mechanisms by Otx2 is shown. See the text for explanation.

Fig. 28については、5年以内に雑誌で刊行予定のため、非公開。

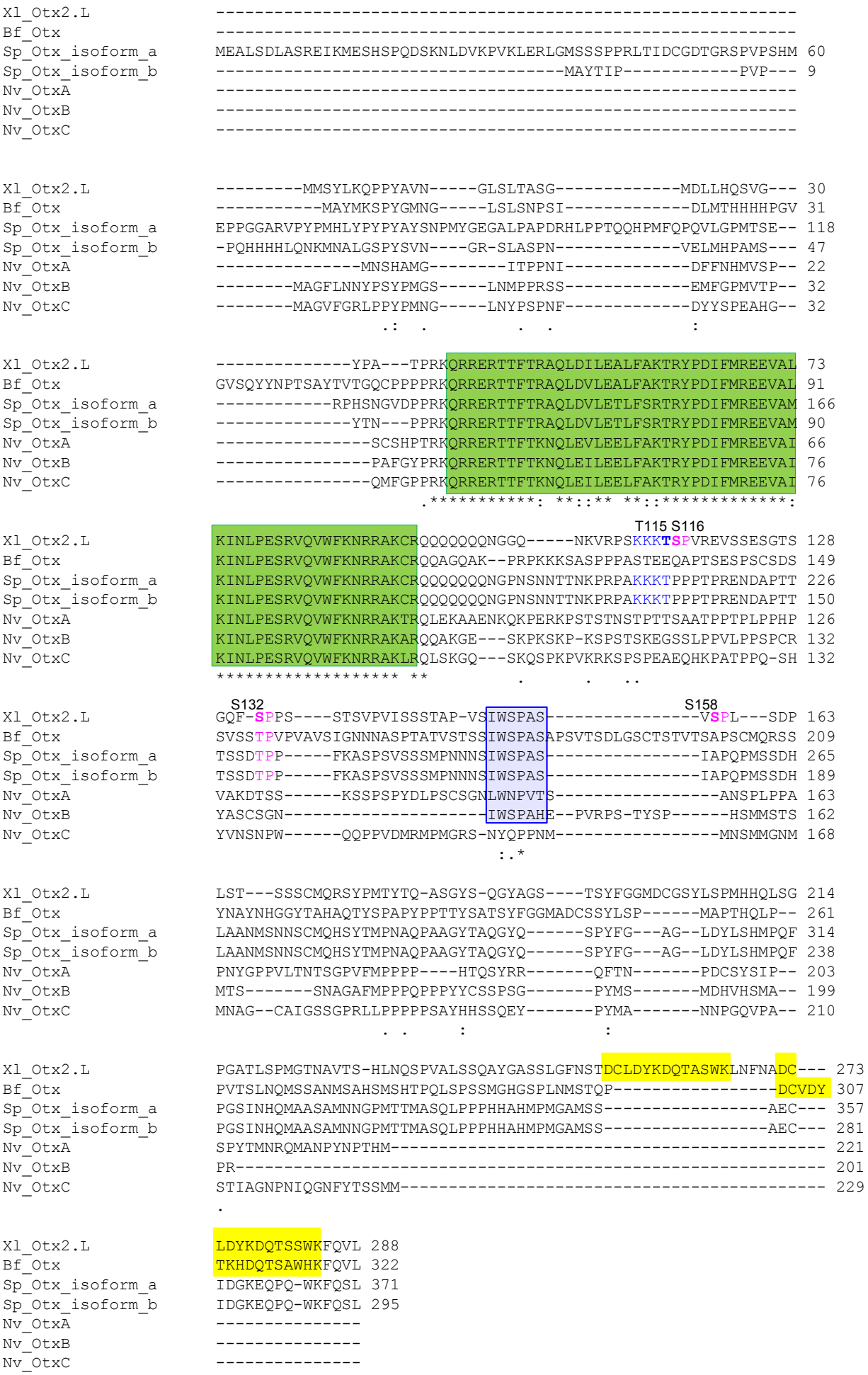

Fig. 29. Alignment of amino acid sequences of Xenopus *Otx2, and* Amphioxus *Otx,* Sea urchin *Otx* and Sea anemone *Otx*.

Abbreviations of species are *Xenopus laevis* (Xl), *Branchiostoma belcheri* (Bf), *Strongylocentrotus purpuratus* (Sp) and *Nematostella vectensis* (Nv). Protein sequences were obtained from the NCBI database: Xl_Otx2.L (NP_001084955), Bf_Otx (XP_019625651), Sp_Otx isoform a (NP_999753), Sp_Otx isoform b (NP_001027540), Nv_OtxA (AFJ11251), Nv_OtxB (AFJ11250) and Nv_OtxC (AC053863). Boxes coloured in green, homeodomain; blue, the conserved eh1 repression motif of Otx; yellow, Otx tail motif. Blue or magenta letters, consensus motifs for Akt and Cdks. Bold cases, putative phosphorylation sites of Otx2 in *Xenopus* as shown in this study.

Cordenonsi, M., Dupont, S., Maretto, S., Insinga, A., Imbriano, C. and Piccolo, S. (2003). Links between tumor suppressors: p53 is required for TGF-β gene responses by cooperating with Smads. *Cell* **113**, 301–314.

Danno, H., Michiue, T., Hitachi, K., Yukita, A., Ishiura, S. and Asashima, M. (2008). Molecular links among the causative genes for ocular malformation: Otx2 and Sox2 coregulate Rax expression. *Proc. Natl. Acad. Sci.* **105**, 5408–5413.

De Robertis, E. M., Larraín, J., Oelgeschläger, M. and Wessely, O. (2000). The establishment of Spemann's organizer and patterning of the vertebrate embryo. *Nat. Rev. Genet.* **1**, 171–181.

Decembrini, S., Andreazzoli, M., Vignali, R., Barsacchi, G. and Cremisi, F. (2006). Timing the generation of distinct retinal cells by homeobox proteins. *PLoS Biol.* **4**, 1562–1571.

Gammill, L. S. and Sive, H. (1997). Identification of otx2 target genes and restrictions in ectodermal competence during Xenopus cement gland formation. *Development* **124**, 471–81.

Gammill, L. S. and Sive, H. (2001). otx2 expression in the ectoderm activates anterior neural determination and is required for Xenopus cement gland formation. *Dev. Biol.* **240**, 223–236.

Geley, S., Kramer, E., Gieffers, C., Gannon, J., Peters, J. M. and Hunt, T. (2001). Anaphase-promoting complex/cyclosome-dependent proteolysis of human cyclin A starts at the beginning of mitosis and is not subject to the spindle assembly checkpoint. *J. Cell Biol.* **153**, 137–147.

Graw, J. (2010). Eye development. *Curr. Top. Dev. Biol.* **90**, 343–386.

Harland, R. M. (1991). Appendix G: In Situ Hybridization: An Improved Whole-Mount Method for Xenopus Embryos BT - Methods in cell biology. In *Methods in cell biology*, pp. 685–695.

Heimbucher, T., Murko, C., Bajoghli, B., Aghaallaei, N., Huber, A., Stebegg, R., Eberhard, D., Fink, M., Simeone, A. and Czerny, T. (2007). Gbx2 and Otx2 interact with the WD40 domain of Groucho/Tle corepressors. *Mol. Cell. Biol.* **27**, 340–351.

Hindley, C., Ali, F., McDowell, G., Cheng, K., Jones, A., Guillemot, F. and Philpott, A. (2012). Post-translational modification of Ngn2 differentially affects transcription of distinct targets to regulate the balance between progenitor

maintenance and differentiation. *Development* **139**, 1718–1723.

Hörmanseder, E., Tischer, T. and Mayer, T. U. (2013). Modulation of cell cycle control during oocyte-to-embryo transitions. *EMBO J*.

Hu, R., Peng, G., Dai, H., Breuer, E. K., Stemke-Hale, K., Li, K., Gonzalez-Angulo, A. M., Mills, G. B. and Lin, S. Y. (2011). ZNF668 functions as a tumor suppressor by regulating p53 stability and function in breast cancer. *Cancer Res*. **71**, 6524–6534.

Hu, R., Wang, E., Peng, G., Dai, H. and Lin, S. Y. (2013). Zinc finger protein 668 interacts with Tip60 to promote H2AX acetylation after DNA damage. *Cell Cycle* **12**, 2033–2041.

Isaacs, H. V., Andreazzoli, M. and Slack, J. M. W. (1999). Anteroposterior patterning by mutual repression of orthodenticle and caudal-type transcription factors. *Evol. Dev*. **1**, 143–152.

Iwabuchi, M., Ohsumi, K., Yamamoto, T. M. and Kishimoto, T. (2002). Coordinated regulation of M phase exit and S phase entry by the Cdc2 activity level in the early embryonic cell cycle. *Dev. Biol*. **243**, 34–43.

Katahira, T., Sato, T., Sugiyama, S., Okafuji, T., Araki, I., Funahashi, J. I. and Nakamura, H. (2000). Interaction between Otx2 and Gbx2 defines the organizing center for the optic tectum. *Mech. Dev*. **91**, 43–52.

Keightley, M. C., Carradice, D. P., Layton, J. E., Pase, L., Bertrand, J. Y., Wittig, J. G., Dakic, A., Badrock, A. P., Cole, N. J., Traver, D., et al. (2017). The Pu.1 target gene Zbtb11 regulates neutrophil development through its integrase-like HHCC zinc finger. *Nat. Commun*.

Kitzmann, M., Vandromme, M., Schaeffer, V., Carnac, G., Labbé, J. C., Lamb, N. and Fernandez, A. (1999). cdk1- and cdk2-mediated phosphorylation of MyoD Ser200 in growing C2 myoblasts: role in modulating MyoD half-life and myogenic activity. *Mol. Cell. Biol*. **19**, 3167–76.

Kosako, H., Nishida, E. and Gotoh, Y. (1993). cDNA cloning of MAP kinase kinase reveals kinase cascade pathways in yeasts to vertebrates. *EMBO J*. **12**, 787–94.

Lake, B. B. and Kao, K. R. (2003). Early head specification in Xenopus laevis. *ScientificWorldJournal*. **3**, 655–76.

Lee, S. U. and Maeda, T. (2012). POK/ZBTB proteins: An emerging family of proteins that regulate lymphoid development and function. *Immunol. Rev*. **247**, 107–119.

Lee, P. C., Taylor-Jaffe, K. M., Nordin, K. M., Prasad, M. S., Lander, R. M. and

LaBonne, C. (2012). SUMOylated SoxE factors recruit Grg4 and function as transcriptional repressors in the neural crest. *J. Cell Biol.* **198**, 799–813.

Li, X., Peng, H., Schultz, D. C., Lopez-Guisa, J. M., Rauscher, F. J. and Marmorstein, R. (1999). Structure-function studies of the BTB/POZ transcriptional repression domain from the promyelocytic leukemia zinc finger oncoprotein. *Cancer Res.*

Liu, P., Kao, T. P. and Huang, H. (2008). CDK1 promotes cell proliferation and survival via phosphorylation and inhibition of FOXO1 transcription factor. *Oncogene* **27**, 4733–44.

Major, M. L., Lepe, R. and Costa, R. H. (2004). Forkhead box M1B transcriptional activity requires binding of Cdk-cyclin complexes for phosphorylation-dependent recruitment of p300/CBP coactivators. *Mol. Cell. Biol.* **24**, 2649–61.

Mallamaci, A., Di Blas, E., Briata, P., Boncinelli, E. and Corte, G. (1996). OTX2 homeoprotein in the developing central nervous system and migratory cells of the olfactory area. *Mech. Dev.*

Martinez-Morales, J. R., Signore, M., Acampora, D., Simeone, a and Bovolenta, P. (2001). Otx genes are required for tissue specification in the developing eye. *Development* **128**, 2019–2030.

Mii, Y. and Taira, M. (2009). Secreted Frizzled-related proteins enhance the diffusion of Wnt ligands and expand their signalling range. *Development* **136**, 4083–4088.

Mizuseki, K., Kishi, M., Matsui, M., Nakanishi, S. and Sasai, Y. (1998). Xenopus Zic-related-1 and Sox-2, two factors induced by chordin, have distinct activities in the initiation of neural induction. *Development* **125**, 579–587.

Mori, H., Miyazaki, Y., Morita, T. and Nitta, H. (1994). Different spatio-temporal expressions of three otx homeoprotein transcripts during zebrafish embryogenesis. *Mol. Brain Res.* **27**, 221–231.

Nakamura, H., Katahira, T., Matsunaga, E. and Sato, T. (2005). Isthmus organizer for midbrain and hindbrain development. *Brain Res. Rev.* **49**, 120–126.

Niehrs, C. (2004). Regionally specific induction by the Spemann-Mangold organizer. *Nat. Rev. Genet.* **5**, 425–434.

Nishihara, D., Yajima, I., Tabata, H., Nakai, M., Tsukiji, N., Katahira, T., Takeda, K., Shibahara, S., Nakamura, H. and Yamamoto, H. (2012). Otx2 Is Involved in the Regional Specification of the Developing Retinal Pigment Epithelium by Preventing the Expression of Sox2 and Fgf8, Factors That Induce Neural Retina

Differentiation. *PLoS One* **7**, 1–12.

Nowling, T. K., Johnson, L. R., Wiebe, M. S. and Rizzino, A. (2000). Identification of the transactivation domain of the transcription factor Sox-2 and an associated co-activator. *J. Biol. Chem.*

Ohnuma, S. I., Philpott, A., Wang, K., Holt, C. E. and Harris, W. A. (1999). p27Xic1, a Cdk inhibitor, promotes the determination of glial cells in Xenopus retina. *Cell* **99**, 499–510.

Omodei, D., Acampora, D., Mancuso, P., Prakash, N., Di Giovannantonio, L. G., Wurst, W. and Simeone, A. (2008). Anterior-posterior graded response to Otx2 controls proliferation and differentiation of dopaminergic progenitors in the ventral mesencephalon. *Development* **135**, 3459–3470.

Owens, N. D. L., Blitz, I. L., Lane, M. A., Patrushev, I., Overton, J. D., Gilchrist, M. J., Cho, K. W. Y. and Khokha, M. K. (2016). Measuring Absolute RNA Copy Numbers at High Temporal Resolution Reveals Transcriptome Kinetics in Development. *Cell Rep.* **14**, 632–647.

Pannese, M., Polo, C., Andreazzoli, M., Vignali, R., Kablar, B., Barsacchi, G. and Boncinelli, E. (1995). The Xenopus homologue of Otx2 is a maternal homeobox gene that demarcates and specifies anterior body regions. *Development* **121**, 707–720.

Park, J. Il, Kim, S. W., Lyons, J. P., Ji, H., Nguyen, T. T., Cho, K., Barton, M. C., Deroo, T., Vleminckx, K. and McCrea, P. D. (2005). Kaiso/p120-Catenin and TCF/β-Catenin complexes coordinately regulate canonical Wnt gene targets. *Dev. Cell* **8**, 843–854.

Park, H. J., Wang, Z., Costa, R. H., Tyner, A., Lau, L. F. and Raychaudhuri, P. (2008). An N-terminal inhibitory domain modulates activity of FoxM1 during cell cycle. *Oncogene* **27**, 1696–1704.

Peng, G., Chun-Jen Lin, C., Mo, W., Dai, H., Park, Y.-Y., Kim, S. M., Peng, Y., Mo, Q., Siwko, S., Hu, R., et al. (2014). Genome-wide transcriptome profiling of homologous recombination DNA repair. *Nat. Commun.* **5**, 1–11.

Pickles, L. M., Roe, S. M., Hemingway, E. J., Stifani, S. and Pearl, L. H. (2002). Crystal structure of the C-terminal WD40 repeat domain of the human Groucho/TLE1 transcriptional corepressor. *Structure* **10**, 751–761.

Pilo, P., Signore, M., Annino, A., Pedro, J., Barbera, M., Acampora, D. and Simeone,

A. (2001). Otx genes in the development and evolution of the vertebrate brain. *Int. J. Neurosci.* **19**, 353–363.

Saka, Y. and Smith, J. C. (2001). Spatial and temporal patterns of cell division during early Xenopus embryogenesis. *Dev. Biol.* **229**, 307–318.

Schuff, M., Siegel, D., Bardine, N., Oswald, F., Donow, C. and Knöchel, W. (2010). FoxO genes are dispensable during gastrulation but required for late embryogenesis in Xenopus laevis. *Dev. Biol.* **337**, 259–273.

Shibano, T., Mamada, H., Hakuno, F., Takahashi, S. I. and Taira, M. (2015). The inner nuclear membrane protein Nemp1 is a new type of RanGTP-binding protein in eukaryotes. *PLoS One* **10**, 1–21.

Stahl, M., Dijkers, P. F., Kops, G. J. P. L. and Medema, R. H. (2002). The Forkhead Transcription Factor FoxO Regulates Transcription of p27 Kip1 and Bim in Response to IL-2. *J. Immunol.* **168**, 5024–5031.

Stead, M. A., Trinh, C. H., Garnett, J. A., Carr, S. B., Baron, A. J., Edwards, T. A. and Wright, S. C. (2007). A Beta-Sheet Interaction Interface Directs the Tetramerisation of the Miz-1 POZ Domain. *J. Mol. Biol.*

Sudou, N., Yamamoto, S., Ogino, H. and Taira, M. (2012). Dynamic in vivo binding of transcription factors to cis-regulatory modules of cer and gsc in the stepwise formation of the Spemann-Mangold organizer. *Development* **139**, 1651–1661.

Takahashi, N., Tochimoto, N., Ohmori, S. Y., Mamada, H., Itoh, M., Inamori, M., Shinga, J., Osada, S. I. and Taira, M. (2005). Systematic screening for genes specifically expressed in the anterior neuroectoderm during early Xenopus development. *Int. J. Dev. Biol.* **49**, 939–951.

Takebayashi-Suzuki, K., Funami, J., Tokumori, D., Saito, A., Watabe, T., Miyazono, K., Kanda, A. and Suzuki, A. (2003). Interplay between the tumor suppressor p53 and TGF beta signaling shapes embryonic body axes in Xenopus. *Development* **130**, 3929–3939.

van Roy, F. M. and McCrea, P. D. (2005). A role for Kaiso-p120ctn complexes in cancer? *Nat. Rev. Cancer* **5**, 956–964.

Vernay, B., Koch, M., Vaccarino, F., Briscoe, J., Simeone, A., Kageyama, R. and Ang, S.-L. (2005). Otx2 regulates subtype specification and neurogenesis in the midbrain. *J. Neurosci.* **25**, 4856–4867.

Vernon, A. E. (2003). A single cdk inhibitor, p27Xic1, functions beyond cell cycle

regulation to promote muscle differentiation in Xenopus. *Development*.

Vernon, A. E. and Philpott, A. (2003). The developmental expression of cell cycle regulators in Xenopus laevis. *Gene Expr. Patterns* **3**, 179–192.

Viczian, A. S., Vignali, R., Zuber, M. E., Barsacchi, G. and Harris, W. a (2003). XOtx5b and XOtx2 regulate photoreceptor and bipolar fates in the Xenopus retina. *Development* **130**, 1281–1294.

Wang, J. C. C. and Harris, W. A. (2005). The role of combinational coding by homeodomain and bHLH transcription factors in retinal cell fate specification. *Dev. Biol*. **285**, 101–115.

Wang, Q., Zou, Y., Nowotschin, S., Kim, S. Y., Li, Q. V., Soh, C. L., Su, J., Zhang, C., Shu, W., Xi, Q., et al. (2017). The p53 Family Coordinates Wnt and Nodal Inputs in Mesendodermal Differentiation of Embryonic Stem Cells. *Cell Stem Cell*.

Williams, N. A. and Holland, P. W. H. (1998). Gene and Domain Duplication in the Chordate Otx Gene Family : Insights from Amphioxus Otx. *Mol. Biol. Evol*. **15 (5)**, 600–607.

Wortham, M., Jin, G., Sun, J. L., Bigner, D. D., He, Y. and Yan, H. (2012). Aberrant Otx2 expression enhances migration and induces ectopic proliferation of hindbrain neuronal progenitor cells. *PLoS One* **7**, 2–9.

Yaffe, M. B. and Elia, A. E. H. (2001). Phosphoserine/threonine-binding domains. *Curr. Opin. Cell Biol*. **13**, 131–138.

Yamamoto, S., Hikasa, H., Ono, H. and Taira, M. (2003). Molecular link in the sequential induction of the Spemann organizer: Direct activation of the cerberus gene by Xlim-1, Xotx2, Mix.1, and Siamois, immediately downstream from Nodal and Wnt signaling. *Dev. Biol*. **257**, 190–204.

Yamano, H., Gannon, J., Mahbubani, H. and Hunt, T. (2004). Cell Cycle-Regulated Recognition of the Destruction Box of Cyclin B by the APC/C in Xenopus Egg Extracts. *Mol. Cell* **13**, 137–147.

Yasuoka, Y. and Taira, M. (2018). The molecular basis of the gastrula organizer in amphibians and cnidarians. In *Reproductive and Developmental Strategies* (ed. Kobayashi, K., Kitano, T., Iwao, Y., and Kondo, M.) in press. Animal Diversity and Generality series, Springer Japan.

Yasuoka, Y., Suzuki, Y., Takahashi, S., Someya, H., Sudou, N., Haramoto, Y., Cho, K. W., Asashima, M., Sugano, S. and Taira, M. (2014). Occupancy of tissue-

specific cis-regulatory modules by Otx2 and TLE/Groucho for embryonic head specification. *Nat. Commun.* **5**, 4322.

Zhang, X., Jiang, G., Wu, J., Zhou, H., Zhang, Y., Miao, Y., Feng, Y. and Yu, J. (2018). Zinc finger protein 668 suppresses non-small cell lung cancer invasion and migration by downregulating Snail and upregulating E-cadherin and zonula occludens-1. *Oncol. Lett.* 3806–3813.

Zuber, M. E. (2010). *Eye field specification in Xenopus laevis*.

Zuber, M. E., Gestri, G., Viczian, A. S., Barsacchi, G. and Harris, W. A (2003). Specification of the vertebrate eye by a network of eye field transcription factors. *Development* **130**, 5155–5167.

Acknowledgements

I thank Dr. Masanori Taira for conducting my research as the supervisor. I also thank Drs. Shuji Takahashi and Makoto Asashima for *X. tropicalis* experiments as collaborators; Mr. Noriyuki Takahashi and Dr. Hiroshi Mamada for cloning *xxxx* and *yyyy*; Dr. Norihiro Sudou for teaching whole-mount in situ hybridization and how to make hemisections of *Xenopus* embryos; Ms. Erina Hosono, Mr. Kohei Minami and Mr. Hajime Okada for cloning several mutant constructs of Otx2 and performing western blotting analysis; Dr. Yuuri Yasuoka for MO injection using *X. tropicalis* embryos, ChIP-seq data and reviewing the manuscript; Dr. Keita Ohsumi for providing pGEX-GST-ΔN106cyclin B1 (a stable mutant of cyclin B1); Dr. Nobuaki Furuno for providing pGEM-Δcyclin A (a stable mutant of cyclin A1) before the publications; Dr. Yukiko Gotoh for providing pSP64T-MAPKK*; Dr. Hidetoshi Saiga and Dr. Mariko Kondo for critical reading of the manuscript; Dr. Toshiaki Tanaka for discussing about cell cycle. I also thank Dr. Takashi Shibano for helping initial experiments and supporting my work including conducting the experiments and reviewing the manuscript; other members of Taira's laboratory for giving helpful comments and discussion. Male and female frogs of *X. tropicalis* were obtained from the National Bioresource Project (Amphibian Research Center, Hiroshima University). Finally, I am deeply grateful to my husband Hironori for always supporting and encouraging me, and my parents Shoki and Sekiko for always loving and pushing me to do the best.